

CONSEIL INTERNATIONAL DES UNIONS SCIENTIFIQUES

UNION GÉODESIQUE ET GÉOPHYSIQUE INTERNATIONALE

ASSOCIATION DE SÉISMOLOGIE  
ET DE  
PHYSIQUE DE L'INTÉRIEUR DE LA TERRE

PUBLICATIONS DU BUREAU CENTRAL SÉISMOLOGIQUE INTERNATIONAL

Sous la direction de J. P. ROTHÉ

SECRÉTAIRE DE L'ASSOCIATION DE SÉISMOLOGIE ET DE PHYSIQUE DE L'INTÉRIEUR DE LA TERRE

SÉRIE A  
TRAVAUX SCIENTIFIQUES

Fascicule 21

Assemblée Générale d'Helsinki 1960

ONDES SÉISMIQUES



Publié avec le concours financier de l'U. N. E. S. C. O.

TOULOUSE  
ÉDOUARD PRIVAT & C<sup>e</sup> Libraire-Éditeur  
14, RUE DES ARTS, 14

—  
1961



## AVERTISSEMENT

---

Parmi les nombreuses communications scientifiques qui ont été présentées au cours de l'Assemblée Générale d'Helsinki (25 juillet-6 août 1960) l'Association Internationale de Séismologie et de Physique de l'Intérieur de la Terre a décidé de publier dans la série des « Travaux Scientifiques » celles qui se rapportent à des sujets particulièrement importants.

Dans le présent fascicule (fascicule 21) on trouvera le texte des mémoires consacrés à l'étude de la propagation des ondes séismiques. Le fascicule suivant (fascicule 22) sera réservé aux problèmes de la structure des continents et des arcs insulaires.

Les autres communications sont destinées à être publiées dans différents périodiques scientifiques. On en trouvera les références bibliographiques dans les Comptes Rendus n° 13, Association de Séismologie et de Physique de l'Intérieur de la Terre, Comptes rendus des séances de la XII<sup>e</sup> conférence, réunie à Helsinki du 25 juillet au 6 août 1960, Strasbourg 1961.

J.-P. ROTHE,  
*Secrétaire général*  
*de l'Association Internationale de Séismologie*  
*et de Physique de l'Intérieur de la Terre.*

*Strasbourg, 31 mars 1961.*



ASSEMBLEE GENERALE D'HELSINKI

(25 juillet au 6 août 1960)

SYMPORIUM  
SUR LA  
PROPAGATION DES ONDES SÉISMIQUES

TABLE DES MATIÈRES

	PAGES
K.E. BULLEN, Seismic travel-times and velocity distributions .....	7
S.D. KOGAN, Travel times of body waves from surface focus .....	15
A.M. YEPINATYEVA, On dynamic relations of reflected and head waves beyond initial point .....	23
I.P. KOSMINSKAYA and R.M. KRAKSHINA, On supercritical reflections from the Mohorovicic discontinuity .....	39
B.F. HOWELL, Jr., Absorption of seismic waves in Rock .....	55
I.S. BERZON, Methods and some results of interpretation of data of seismic waves' spectrum analysis .....	65
C.H. DIX, The seismic head pulse .....	79
L.M. BALAKINA, H.I. SHIROKOVA and A.V. VVEDENSKAYA, Double refraction in aeolotropic layers and some peculiarities of low velocity layer in Earth's mantle .....	87
M. LAVERGNE, Recherches expérimentales sur modèles séismiques.	99



# SEISMIC TRAVEL-TIMES AND VELOCITY DISTRIBUTIONS

by K. E. BULLEN  
University of Sydney (Australia)

Let  $v$  be the (P or S) seismic velocity at distance  $r$  from the centre of a (spherically symmetrical) Earth, and let  $\eta$  and  $\alpha$  be defined by

$$\eta = r/v, \quad (1)$$

$$\alpha = 2d \log r/d \log \eta. \quad (2)$$

This paper extends earlier work (Bullen 1945, 1954, 1955, 1959, 1960) on uses of the variables  $\eta$  and  $\alpha$  in problems of travel-times and associated velocity distributions. The paper is mainly theoretical, but the later part contains a preliminary account of certain numerical applications to problems of the upper mantle.

## 1. A new method of deriving velocity distributions from travel-time data.

For a given family of rays, all terminating at both ends at a given level  $r = r_0$ , let  $\Delta$  and  $t$  denote the angular length and travel-time, and let  $p = dt/d\Delta$ , as usual. The subscript zero relates to the level  $r_0$ , and  $\Delta$  to the lowest point of the ray of length  $\Delta$ .

Introduce  $\theta$ , where

$$\theta = \frac{d\Delta}{dp} + \frac{\alpha_0}{\sqrt{(r_0^2 - p^2)}}. \quad (3)$$

It can then be shown (Bullen, 1960) that

$$\theta = \int_{\alpha_\Delta}^{\alpha_0} \frac{d\alpha}{\sqrt{(r_0^2 - p^2)}}. \quad (4)$$

If  $\alpha$  is constant, equal to  $\alpha_0$  say, in the region  $r_1 \leq r \leq r_0$ , then, by (4),  $\theta$  is zero in this range. For this case (Bullen, 1959), (3) leads to the very simple relations

$$t = \alpha_0 \eta_0 \sin(\Delta/\alpha_0), \quad (5)$$

$$v = v_0 x \zeta_0, \quad (6)$$

where  $x = r/r_0$  and  $\zeta = 1 - 2/\alpha$ .

There are regions of the Earth where (5) and (6) represent the relevant seismic observations well. Where this is not the case, (5) and (6) can in general be used as a first approximation, and the necessary corrections fairly readily derived as follows. The procedure is powerful when the first approximation is fairly good.

By a method somewhat analogous to that used in the classical

Herglotz method, it can be shown (Bullen, 1960) that (subject to the usual condition  $dv/dr < v/r$ )

$$\frac{1}{2} \pi (\alpha_0 - \alpha_1) = \int_0^{\theta_1} (p^2 - \eta_1^2)^{\frac{1}{2}} d\theta, \quad (7)$$

where the subscript 1 relates to an arbitrarily assigned level  $r_1$ .

Now by (3), with  $p = dt/d\Delta$ ,  $\theta$  is readily computed as a function of  $\Delta$  or  $p$  for a given or assigned  $t - \Delta$  relation. Then (7) gives  $\alpha_0 - \alpha_1$  for an assigned  $\eta_1$ , and so gives, for the level  $r_1$ , the correction to the first — approximation value  $\alpha_0$  of  $\alpha$ . When  $\alpha_0$  is already a good approximation, the needed correction is small and can be rapidly computed.

By way of illustration, the method has been applied (Bullen, 1960) to determining the P velocity distribution for the entire region E of the Earth, taking the Jeffreys-Bullen travel-times as data.

## 2. Amplitudes in triplicated travel-times.

The previous Section is most readily applicable to 'ordinary' regions of the Earth, stripped if necessary. In the present Section some departures from ordinary behaviour are considered.

When there are sudden changes in  $v$  or its derivatives with respect to  $r$ , the corresponding travel-times,  $t$ , as functions of  $\Delta$ , may be triplicated and the graphs have two cusps. The character of such cusps will now be discussed, again with the help of  $\eta$  and  $\alpha$ .

Where  $v$  increases discontinuously with depth,  $\eta$  decreases discontinuously; and where the gradient ( $-dv/dr$ ) increases discontinuously (the so-called 'second-order' discontinuity),  $\alpha$  decreases discontinuously.

For the purpose of a first model, let L be an outer layer for which  $r_1 \leq r \leq r_0$ , overlying a layer N for which  $r \leq r_1$ . Let  $\alpha$  have the constant values  $\alpha_0$ ,  $k\alpha_0$ , where  $k < 1$ , in L, N respectively. In this model, let  $v$  and therefore  $\eta$  be continuous throughout.

Then, corresponding to (5), we have (Bullen, 1959) for rays entirely in L

$$\Delta = \alpha_0 \cos^{-1} (p/\eta_0), \quad (8)$$

$$t = \alpha_0 (\eta_0^2 - p^2)^{\frac{1}{2}}, \quad (9)$$

and

$$d\Delta/dp = -\alpha_0 (\eta_0^2 - p^2)^{-\frac{1}{2}}. \quad (10)$$

It can be deduced (Bullen, 1960a) that, for rays penetrating N,

$$\Delta = \alpha_0 \{ \cos^{-1} (p/\eta_0) - (1 - k) \cos^{-1} (p/\eta_1) \}, \quad (11)$$

$$t = \alpha_0 \{(\eta_0^2 - p^2)^{\frac{1}{2}} - (1 - k)(\eta_1^2 - p^2)^{\frac{1}{2}}\}, \quad (12)$$

$$d\Delta/dp = \alpha_0 \{-(\eta_0^2 - p^2)^{-\frac{1}{2}} + (1 - k)(\eta_1^2 - p^2)^{-\frac{1}{2}}\}. \quad (13)$$

Consider variations as  $p$  decreases continuously from the value  $\eta_0$  (for which  $\Delta = 0$ ). At  $p = \eta_0$ ,  $d\Delta/dp$  is by (10) equal to  $-\infty$ . At  $p = \eta_1$ ,  $d\Delta/dp$  has increased to a moderate negative value, and then by (13) jumps discontinuously to  $+\infty$ . As  $p$  further decreases,  $d\Delta/dp$  decreases continuously from  $+\infty$ , and by (13) in general passes through a zero where  $p = \eta'$ , say.

Corresponding to each of the values  $p = \eta_1$ ,  $\eta'$ , there is a cusp on the  $t - \Delta$  curve, which exhibits the well-known triplication; (8), (9), (11) and (12) show that  $t$  and  $\Delta$  are both continuous at  $p = \eta_1$  and  $p = \eta'$ ). But there is a vital difference in the character of the two cusps in that  $\Delta$ , as a function of  $p$ , has at  $p = \eta_1$  a node-point maximum at which  $d\Delta/dp$  is not in general zero, whereas  $p = \eta'$  corresponds to an ordinary minimum at which  $d\Delta/dp$  is zero.

Since  $p$  is proportional to  $\cos e$  (Bullen, 1959), where  $e$  is the angle of emergence, the condition for abnormally large wave amplitudes is  $d\Delta/dp = 0$ . It follows that, with the present model, large amplitudes are expected to be associated with the cusp with the smaller value of  $\Delta$ , but not with the more distant cusp.

Cases of models in which  $v$  itself changes discontinuously from L to N can be similarly investigated. When the change in  $v$  is an increase, it can be shown that again there is in general triplication of the time curve, but that abnormal amplitudes are to be expected at *neither* cusp. When the change in  $v$  is a decrease, there is a discontinuity in both  $t$  and  $\Delta$ , and there is a single cusp associated in general with large amplitudes (as with PKP waves near  $\Delta = 142^\circ$ ).

Next, if there lies between L and N an intermediate layer M in which  $\alpha$  decreases continuously from the value  $\alpha_0$  in L to the value  $k\alpha_0$  in N, and if  $\eta$  is continuous throughout L, M and N, then there exists a wide class of cases in which the time-curve is triplicated, with large amplitudes associated with both cusps.

The analytical details of these various cases are being set down elsewhere (Bullen, 1960a, 1961). It is shown that use of  $\eta$  and  $\alpha$  enables quantitative detail to be carried a long way, with consequent gain in treating "difficult" regions of the Earth, such as the upper mantle.

An important point is that the occurrence of large wave amplitudes can depend on changes in the second (or higher) derivative of  $v$  with respect to  $r$ . The analysis underlines the caution needed

in seeking to draw inferences on velocity distributions from amplitude data.

### 3. *Preliminary application to P waves in the upper mantle.*

Following is an outline of provisional results emerging from numerical application of the foregoing theory to P wave data in the upper mantle. The results in this Section are subject to revision and extension.

The data used were the revised travel-times of Jeffreys (1958) for the Earth stripped to the Mohorovičić discontinuity. An attempt was made to represent the region below the crust in terms of models having the form of the first model of Section 2.

It was found possible to fit the Jeffreys times up to  $15^\circ$  within the uncertainties by letting  $\alpha$  have any constant value greater than about unity throughout the outer layer L. (With  $\eta_0 = 790$  sec and  $\alpha = 1$ , the largest residuals are  $-0.5$  sec at  $8^\circ$  and  $+0.5$  sec at  $15^\circ$ . With  $5 \leq \alpha \leq \infty$ , the times can be fitted to 0.1 sec by selecting  $\eta_0$  suitably.)

It can be shown that (details will be published in a later paper) when the law (6) applies, the energy per unit surface area reaching the surface is approximately proportional to  $\Delta^{-2}$  for values of  $\Delta$  up to a moderate fraction of a radian. This law can account for some of the observed amplitude diminution with increasing  $\Delta$ , but not for the sharp fall in P amplitudes which many writers refer to near  $5^\circ$  or  $6^\circ$ . It is usually stated that the amplitudes are low between about  $6^\circ$  and  $15^\circ$ , after which there is a fairly sharp rise.

Such amplitude observations can be readily met by taking L to be mildly composite. A model in which L was taken to consist of an upper part L' in which  $\alpha = 2$  and a lower part L'' in which  $\alpha = 10$  gave the requisite amplitude fall near  $6^\circ$  when L' was taken to be 6 km thick. Consideration of this and other models led to the conclusion that all the observed amplitude variations could be met by making suitable minor adjustments in the velocity gradient in the outermost few km of L. It follows conversely that the amplitude observations can throw very little direct light on the structure of this part of the Earth.

The possibility of using the theory on amplitudes near a cusp on the time-curve was next considered. The amplitude data suggest that any cusps associated with abnormally large amplitudes lie outside the range  $6^\circ \leq \Delta \leq 15^\circ$ . The theory indicates that unless such a cusp should arise from a 'third' (or higher) order discon-

tinuity in  $v$ , it will be the nearer cusp alone that is involved. Let  $\Delta'$  be the angular distance to this nearer cusp.

Four models were then constructed on the following assumptions : —

- (i)  $\alpha = 10$  in L ;  $\Delta'$  slightly less than  $6^\circ$ .
- (ii)  $\alpha = 1$  in L ;  $\Delta'$  slightly less than  $6^\circ$ .
- (iii)  $\alpha = 10$  in L ;  $\Delta'$  between  $15^\circ$  and  $16^\circ$ .
- (iv)  $\alpha = 1$  in L ;  $\Delta'$  between  $15^\circ$  and  $16^\circ$ .

From these assumptions, using the value of  $\eta_0$  deduced from the Jeffreys times, and taking the time given by Jeffreys for  $\Delta = 16^\circ$  to apply to a ray which has penetrated the region N, it is possible to deduce (inter alia) the thickness ( $d$ , say) of L and the value ( $\alpha_1$ , say) of  $\alpha$  in N. The results were : —

Model	$d$	$\alpha_1$
(i)	11 km	0.7
(ii)	19 km	0.7
(iii)	111 km	0.5
(iv)	174 km	0.5

The cases (i) and (iii), for which  $\alpha = 10$  in L, correspond to an outer layer (below the crust) in which the P velocity  $v$  decreases moderately with increase of depth. (Taking  $10 < \alpha < \infty$  would not lead to significantly different results;  $\alpha = \infty$  corresponds to  $dv/dr = v/r$ .) The cases (ii) and (iv), for which  $\alpha = 1$  in L, correspond to a moderate increase of  $v$  with depth in L, near the greatest increase compatible with the Jeffreys times.

The results in the table therefore indicate that, on the hypothesis that no large amplitudes occur between  $6^\circ$  and  $16^\circ$ , the thickness of the first significant layer L below the crust is either less than 20 km or greater than 110 km. It could be as little as 11 km or as great as 174 km, but probably not much greater. (It is being here assumed that the condition  $dv/dr < v/r$  is not violated.)

The result in the case (iv) is in good agreement with a solution of Jeffreys (1958a) in which the assumptions happen to be approximately equivalent to those in (iv), although Jeffreys brought to bear certain data of Lehmann (not used here) to locate the further cusp. In addition, the result (iv) agrees within 20 km or so with estimates made independently by Lehmann (1959) and Gutenberg (1959) of the depth at which  $v$  or its gradient changes markedly.

A necessary further step is to adjust the models so far as necessary to fit the Jeffreys times for  $\Delta > 16^\circ$ . Provisional calculations suggest that only small adjustments may be required; these may involve a small discontinuous change in  $v$  at the boundary between L and N, a second discontinuous reduction in  $\alpha$  somewhere below this boundary, or a velocity gradient in the outer part of N slightly exceeding that associated with a constant value of  $\alpha$ . Further calculations are being made.

At the present (incomplete) stage of the work, it would appear that the observed complications in P travel-times up to  $20^\circ$  or so could conceivably all arise from vagaries in the velocity variation in the immediate 20 km or so below the Mohorovičić discontinuity. Should it transpire that the condition  $dv/dr < v/r$  is violated in this part of the Earth, it is also conceivable that the complications really arise from a "high-velocity" layer some 20 km thick just below the Mohorovičić discontinuity.

From travel-time data for surface foci alone, it does not seem possible to discriminate between a number of widely different alternatives, largely because of the great difficulty (on the theory of Section 2) of locating with precision the more distant cusp, if it exists. Quite slight changes in the velocity gradient assumed for the region L can in some circumstances displace the position of the cusp by ten degrees and more.

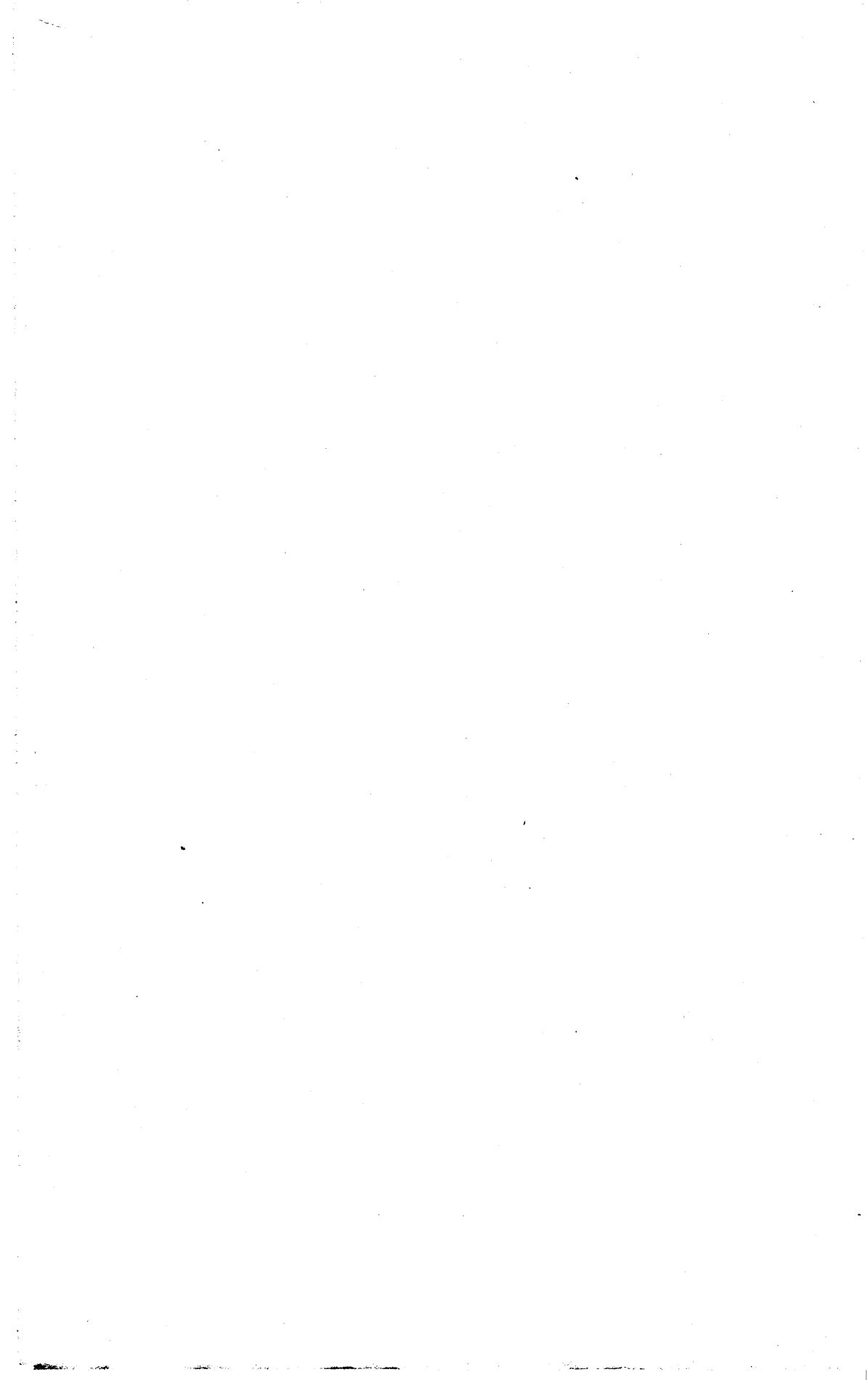
With the use of travel-time data corresponding to foci below the surface, it may just prove possible to decide on the existence of the further cusp and to locate it with some definiteness. The procedures of this paper are to be extended to investigate this point. Lehmann has lately brought data from deep-focus earthquakes to bear in her discussions. Her work to date makes it rather likely that the complications in the P velocity distribution extend to the order of 200 km rather than 20 km depth below the Mohorovičić discontinuity.

The problem of the velocity distributions in the upper mantle is obviously still far from solved. It is hoped that the approach of the present paper will, however, through its capacity to yield quantitative detail with the minimum of effort, lead to a useful narrowing of the possibilities. But a wide variety of models has yet to be examined.

#### REFERENCES

- BULLEN (K. E.), 1945. « Features of the travel-time curve of seismic rays »,  
*Mon. Not. Roy. Astr. Soc., Geophys. Suppl.*, 5, 91-98.  
BULLEN (K. E.), 1954. *Seismology*, Methuen.

- BULLEN (K. E.), 1955. « Features of seismic  $pP$  and  $PP$  rays », *Mon. Not. Roy. Astr. Soc., Geophys. Suppl.*, 7, 49-59.
- BULLEN (K. E.), 1959. *Introduction to the Theory of Seismology*, 2nd edn., reprinted (with revisions), Cambridge University Press.
- BULLEN (K. E.), 1960. « A new method of deriving seismic velocity distributions from travel-time data », *Geophys. J., Roy. Astr. Soc.*, 3, 258-269.
- BULLEN (K. E.), 1960a. « Note on cusps in seismic travel-time curves », *Geophys. J., Roy. Astr. Soc.*, 4, in course of publication.
- BULLEN (K. E.), 1961. « Seismic ray theory », *Geophys. J., Roy. Astr. Soc.*, Sir Harold Jeffreys birthday volume, in course of publication.
- GUTENBERG (B.), 1959. *Physics of the Earth's Interior*, Academic Press, New York and London, p. 84.
- JEFFREYS (Sir Harold), 1958. « The times of  $P$  up to  $30^\circ$  (second paper) », *Geophys. J., Roy. Astr. Soc.*, 7, 154-161.
- JEFFREYS (Sir Harold), 1958a. « On the interpretation of  $Pd$  », *Geophys. J., Roy. Astr. Soc.*, 1, 191-197.
- LEHMANN (I.), 1959. « Velocities of longitudinal waves in the upper part of the Earth's mantle », *Ann. de Géophys.*, 15, 93-118.



## TRAVEL TIMES OF BODY WAVES FROM SURFACE FOCUS

by S. D. KOGAN

Institute of Earth's Physics, Academy of Sciences, USSR

---

Seismic records of nuclear explosions conducted by the USA in the region of the Marshall islands were used for the determination of the real travel times of seismic waves in a great interval of epicentral distances and for their comparison with the data of the Jeffreys-Bullen curve [1] for a surface focus. This verification of the curve is important not only for the improvement of the accuracy of the determination of the earthquakes epicentres' coordinates but for the study of the physics of the earth as well since the curve is the source of our knowledge about the propagation of seismic waves inside the Earth which in its turn serves the basis of our conception about the inner structure of the Earth.

The basic material for the present paper were the records of the USSR seismic stations and seismic bulletins of foreign countries. Data published in papers of Gutenberg B. [2], Burke-Gaffney T. N., and Bullen K. E. [3], Garder D. and Bailey L. [4], Ritzema A. [5], Labrouste I. [6] were also partly used. Coordinates of epicentres and explosions times were taken according to the data of the USA National Academy of Sciences [7], [8].

The obtained results are based on the observations of 1946 to 1956 of the 8 explosions in the region of the Bikini atoll and 1 explosion in the region of the Enivetok atoll (Table 1). From these explosions the following body waves were recorded by USSR seismic stations : P, PP, P<sub>c</sub>P, S, SKS.

The values of the observed travel times were allowed for the ellipticity of the Earth and the altitude of the station above the sea level and then they are compared with the corresponding travel times according to the Jeffreys-Bullen curve.

The most complete data about the deviation of the experimental travel times from the Jeffreys-Bullen travel time curve are obtained for the P wave. These residuals  $\delta t_p$ , as is well seen from the curve (*fig. 1*), depend neither on the azimuth nor on the epicentral distance. True, no observations were obtained for a considerable interval of azimuths (unshaded areas on the diagram in the right top corner of *fig. 1*).

The fact that for stations situated in the heart of the continent (USSR) and on the shore of the Pacific ocean (USA) the residuals  $\delta t_p$  are the same for the same epicentral distances confirms the

existing conception of the homogeneity of the structure of the mantle under continents and oceans.

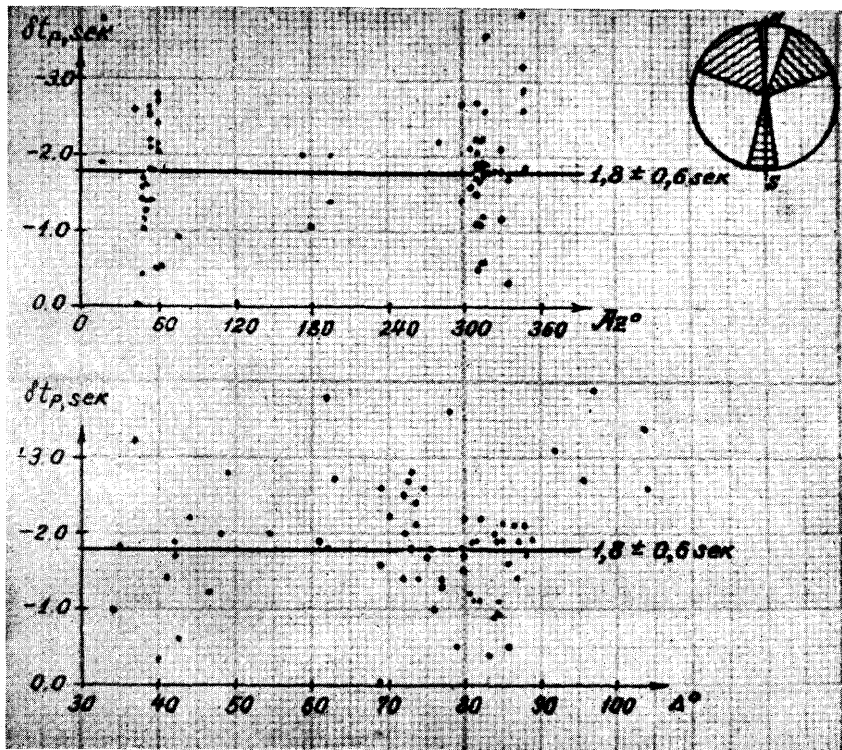


FIG. 1. —  $\delta t_p$ , sec as a function of the azimuth and the epicentral distance  $\Delta^{\circ}$ .

The absence of the dependence of  $\delta t_p$  on the epicentral distance seems to indicate that the Jeffreys-Bullen curve gives a correct dependence of the variation of the longitudinal wave velocity with depth.

Assuming that the scatter of values  $\delta t_p$  is connected only with the difference of the geological conditions under stations and with the errors of observations the mean value of the residual of the observed travel times for 232 arrivals of the P wave from the Jeffreys-Bullen curve was calculated : the mean  $\delta t_p = -1.8 \pm 0.6$  sec.

Thus the experimental curve of the P wave for a surface source in the Western Pacific reduced to the standard sphere is parallel to the Jeffreys-Bullen curve in the interval of the epicentral distances from  $30^{\circ}$  to  $104^{\circ}$  but is approximately 2 sec lower. This result completely coincides with the data of Gutenberg [2] and Bullen [3] who consider that the decrease of the travel time of the P wave can be explained by the absence of the granitic layer in the

region of the epicentre. Such explanation is confirmed by three facts :

1) According to the data of D. Carder and L. Bailey [4] for seismic stations situated on the Pacific ocean islands the value of  $\delta t_p$  is about 4 sec.

2) The travel time of the PP wave with the reflection point in an oceanic region is about 5 sec less than according to the curve. This will be discussed in detail lower.

3) The travel time of the P wave recorded from the underground nuclear explosions in Nevada (USA) coincides with the Jeffreys-Bullen curve [9] within the accuracy of the observations.

For each station we can write that  $\delta t_p = -1.8 \pm \delta S$  sec. The station correction  $\delta S$  must characterize the peculiarities of the crustal structure and the thickness of sediments in the region of a given station. However, it is rather difficult to make any conclusions from the available observations due to a small number of observations at a separate station. The value  $\delta S$  may also depend on the azimuth.

The wave PP is recorded 28 times at 21 stations. The arrivals of this waves are not very sharp, which is the cause of a greater scatter of data as compared with P wave. If to exclude the correction for the P wave from the travel time of PP wave the value of the difference  $(\delta t_{pp} - \delta t_p)$  will characterize the peculiarities of the crustal structure in the reflection point (fig. 2). At it was men-

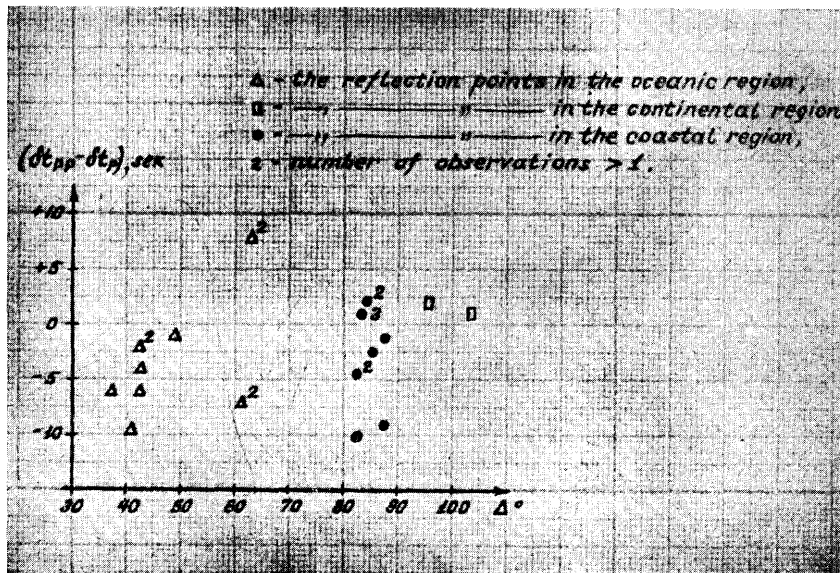


FIG. 2. —  $(\delta t_{pp} - \delta t_p)$  sec as a function of the epicentral distance  $\Delta^\circ$ .

tioned above the reflection in the oceanic region gives  $(\delta t_{pp} - \delta t_r) = -5$  sec. The exception is Irkutsk for which  $(\delta t_{pp} - \delta t_r) = +8$  sec with the reflection point located  $36^\circ$  N;  $144^\circ$  E.

For the continental region data for only two reflection points are available; according to the data of Ashkhabad and Goris  $(\delta t_{pp} - \delta t_p) = +2$  sec. Stations Erevan, Ksara and Tamanrasset can not be used due to the absence of the P wave, and Uppsala gives (we know it beforehand) a too late arrival of the PP wave  $(\delta t_{pp} = -17$  sec).

In cases when the reflection points are in the region of seas and the coast of Eastern Asia corrections of different signs are obtained.

For the investigation of the PcP travel time observations of the explosions of June 28 and July 12, 1958 (Table I) were used besides the observations of 1954 to 1956.

The total of 12 arrivals of this wave was considered for which the travel time is on the average 3 sec less in comparison with the travel time curve (table 2). This is 1 sec greater than the mean value  $\delta t_p$ .

The curve of the PcP wave with which it was compared was calculated by Jeffreys for the earth's core radius  $r = 0.5480$ ,  $R \pm 0.0004 R = 3473 \pm 2.5$  km. Such value of the core radius was obtained by Gutenberg and Richter and then by Jeffreys from the travel times of the PcP and ScS waves for several earthquakes. In one of the papers by Jeffreys of 1939 [10] the curves of the PcP wave calculated for the values of the core radius from  $0.52 R$  to  $0.56 R$  are given. The observed travel times of the PcP wave seem to better coincide with the curve calculated for  $r = 0.550 R = 3486$  km. As is well seen from fig. 3 all differences  $(\delta t_{pcp} - \delta t_p)$  for  $r = 0.548 R$  are negative and are generally greater than the corresponding values  $(\delta t_{pcp} - \delta t_p)$  for  $r = 0.550 R$ ; the differences  $(\delta t_{pcp} - \delta t_p)$  for  $r = 0.550 R$  are negative and positive.

Thus one of the possible explanations of the presence of the PcP wave travel time residual of 1 sec may be an underestimated (by about 10 km) value of the earth's core radius.

The transverse wave is recorded at 14 stations 21 times for the interval of the epicentral distances from  $34^\circ$  to  $87^\circ$ . At epicentral distances greater than  $80^\circ$  the transverse wave was interpreted as the S wave or the SKS wave depending on the absolute value of the residual from the curve. As a result the travel time of the S and SKS waves turned to be greater than the corresponding values according to the curve. The mean values for  $\delta t_s = +4 \pm 1$  sec

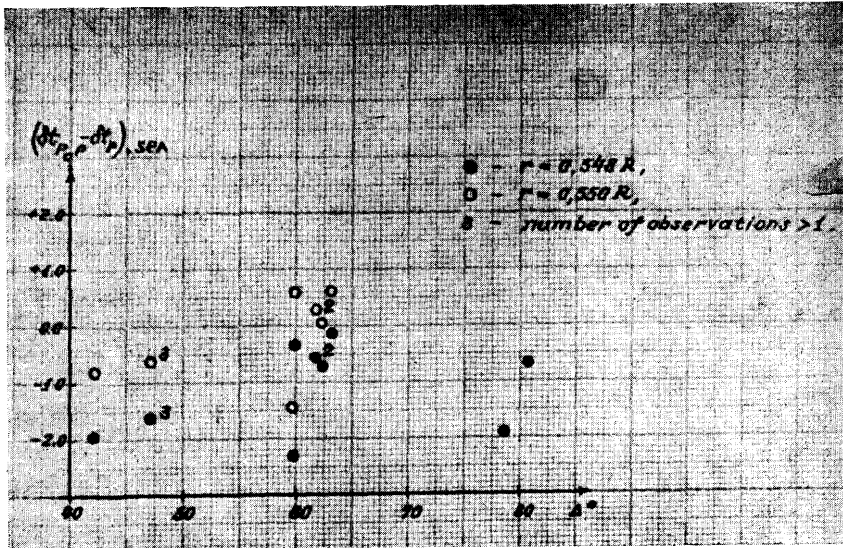


FIG. 3. —  $(\delta t_{p\text{cp}} - \delta t_p)$  sec as a function of the core radius  $r$  and the epicentral distance  $\Delta^\circ$ .

and for  $\delta t_{\text{SKS}} = +5 \pm 2$  sec are practically the same (fig. 4). The only exception is Semipalatinsk for which  $\delta t_s = -11$  sec.

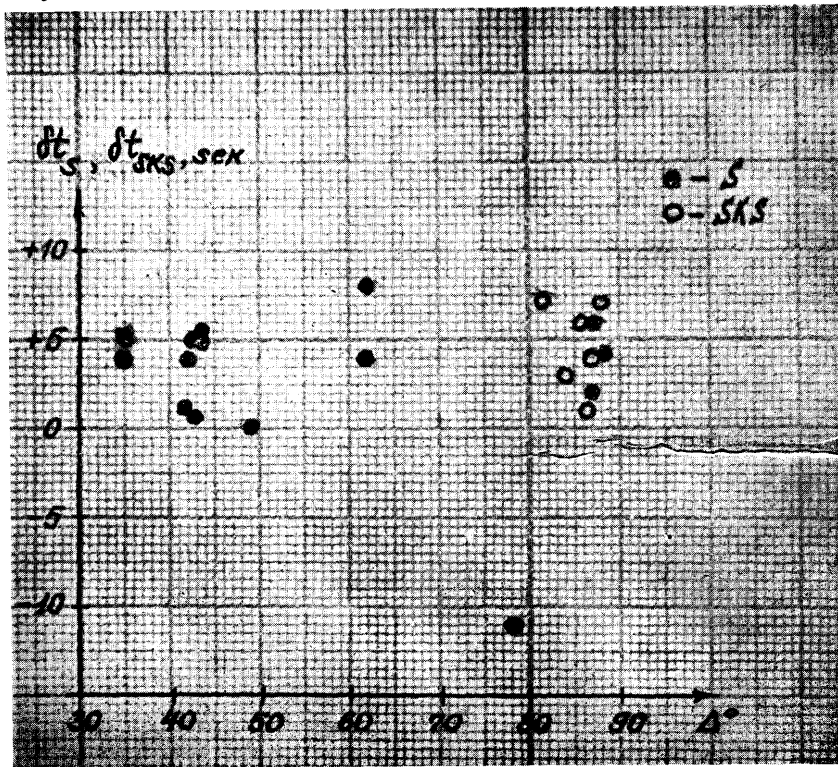


FIG. 4. —  $\delta t_s$  and  $\delta t_{\text{SKS}}$  as functions of the epicentral distance  $\Delta^\circ$ .

None of the known papers dealing with the recording of distant nuclear explosions does not contain any data of transverse waves as yet. All the observations used are obtained for near values of the azimuth therefore we can nothing say about the dependence of  $\delta t$  on the azimuth for the transverse wave as yet.

If the residuals from the curve for the P wave are connected with the absence of the granitic layer in the region of the epicentre then for the transverse wave the surface Jeffreys-Bullen curve gives a still more underestimated travel time, i.e. a somewhat overestimated propagation velocity.

The absence of a considerable variation of  $\delta t$  for the transverse wave with the epicentral distance allows to assume that the velocity of the transverse wave must be somewhat less than the accepted values for the upper mantle. It must be certainly borne in mind that the existing scatter of observations can screen a weak dependence of  $\delta t$  on  $\Delta$  if it does exist.

It is interesting to note a number of dynamic peculiarities of seismic records of explosions conducted on the earth's surface. On all the available records the P wave corresponds to the compressional wave. The Pcp wave also corresponds to the compressional wave in the interval of distances from  $42^\circ$  to  $80^\circ$  where it is sufficiently clear.

The fact that along with the longitudinal waves transverse waves are recorded for which the component SV is greater than the component SH permits to consider the explosions near the earth's surface as a vertical shock.

In conclusion I would like to note a surprising accuracy with which Jeffreys and Bullen compiled the « Seismic Tables » over 20 years ago and which we use at present.

#### REFERENCES

- [1] JEFFREYS (H.), BULLEN (K. E.), Seismological Tables, 1940.
- [2] GUTENBERG (B.), Travel Times of Longitudinal Waves from Surface Foci. Proc. Sci. Un. States, V. 39, N. 8, 1953.
- [3] BURKE-GAFFNEY (T. N.), BULLEN (K. E.), On the Seismological Aspects of the 1954 Hydrogen Bomb Explosions. Austr. J. Phys., V. 11, N. 3, 1958.
- [4] CARDER (D. S.), BAILEY (L. F.), Seismic Wave Travel Times from Nuclear Explosions. Bull. Seism. Soc. Am., V. 48, N. 4, 1958.
- [5] LABROUSTE (I.), Enregistrement séismique d'explosions nucléaires. Madjalahilmu alam untuk Indonesia, 113, 1957.
- [6] LABROUSTE (I.), Enregistrement séismique d'explosions nucléaires. Compt. rend. hebdomadaires des séances de l'Académie des Sciences, 247, N. 3, Paris, 1958.

- [7] BULLETIN OF THE SEISMOLOGICAL SOCIETY OF AMERICA, V. 48, N. 3, 1958.
- [8] EARTHQUAKE NOTES, Eastern Section, Seism. Soc.; of Am. V. XXIX, N. 4, 1958.
- [9] PASSECHNIK (I. P.), KOGAN (S. D.), SULTANOV (D. D.), TZIBULSKY (V. I.), Results of the Observations of Underground Nuclear and TNT Explosions. Transactions of the Institute of Earth's Physics; Acad. Sci. USSR, N. 15 (182), 1960.
- [10] JEFFREYS (H.), Times of P, S and SKS and Velocities of P and S. Monthly Notices of the R. A. S. Geophys. Suppl., V. 4, N. 7, 1939.

TABLE 1.

Nº	Date	Location of epicentre		Conditions of explosion	Time of explosion (Greenwich)
		N	E		<sup>h</sup> <sup>m</sup> <sup>s</sup>
1.	24.VII.46	11° 35'	165° 30'	in water	21 34 59.76 ± 0.1
2.	28.II.54	11 47 27	165 16 25	on ground	18 45 00.0
3.	26.III.54	11 41 27	165 16 23	on barge	18 30 00.4
4.	25.IV.54	11 39 59	165 23 14	on ground	18 10 00.7
5.	4.V.54	11 39 56	165 23 13	on barge	18 10 00.1
6.	27.V.56	11 29 48	165 22 09	on ground	17 56 00.3
7.	8.VII.56	11 40 17	162 12 01	on barge	18 06 00.2
8.	10.VII.56	11 39 48	165 23 14	on barge	17 56 00.3
9.	20.VII.56	11 40 26	165 20 22	on barge	17 46 00.0
10.	28.VI.58	11 36 28	162 06 28	surface ZCU Hull	19 30 00.1
11.	12.VII.58	11 41 17	165 15 52	on barge	03 30 00.1

TABLE 2.

Nº	Station	Date	$\Delta$	$t_{pcp}$ experi- mental	$\eta_{pcp}$	$t_{pcp}$ 0.548 R	$t_{pcp}$ 0.550 R	$t_{pcp}$ 0.548 R	$t_{pcp}$ 0.550 R	$\frac{\delta t_{pcp}}{\delta t_p}$ 0.548 R	$\frac{\delta t_{pcp}}{\delta t_p}$ 0.550 R
1.	Uglegorsk	28.II.54	42°03'	09 <sup>m</sup> 47.0 <sup>s</sup>	— 0.2 <sup>s</sup>	09 <sup>m</sup> 50.4 <sup>s</sup>	09 <sup>m</sup> 49.3 <sup>s</sup>	— 3.6	— 2.5	— 1.9	— 0.8
2.	Temporary station	20.VII.56	46 41	10 03.8	— 0.3	10 06.4	10 05.4	— 2.9	— 1.9	— 2.1	— 1.1
3.	Temporary station	10.VII.56	46 43	04.0				— 2.7	— 1.7	— 1.5	— 0.5
4.	Temporary station	27.V.56	46 54	04.3		07.1	06.1	— 3.1	— 2.1	— 1.3	— 0.3
5.	Kyakohta	28.VI.58	59 30	50.6	— 0.1	54.6	53.7	— 4.7	— 3.8	— 2.3	— 1.4
6.	Kabansk	28.VI.58	59 59	53.7	— 0.1	56.6	55.7	— 3.0	— 2.1	— 0.3	0.6
7.	Kabansk	12.VII.58	61 45	11 00.9		11 03.8	11 03.1	— 3.0	— 2.3	— 0.2	0.5
8.	Kabansk	26.III.54	61 45	01.6				— 2.3	— 1.6	— 0.9	— 0.2
9.	College	10.VII.56	62 06	00.7	— 0.2	05.0	04.3	— 4.5	— 3.8	— 0.6	0.1
10.	Irkutsk	26.III.54	63 12	06.6	— 0.1	09.5	08.8	— 3.0	— 2.3	— 0.1	0.6
11.	Temporary station	28.VI.58	78 38	12 10.0	0.3	12 14.6		— 4.3		— 1.9	
12.	Temporary station	12.VII.58	80 32	19.5		22.8		— 3.0		— 0.6	

1.  $\eta_{pcp}$  — allowance for the ellipticity of the Earth and the altitude of the station above the sea level.

## ON DYNAMIC RELATIONS OF REFLECTED AND HEAD WAVES BEYOND INITIAL POINT

by A. M. YEPINATYEVA

---

At distances from the source equal or greater than the distance to the initial point of refracted waves reflected and refracted (head) waves corresponding to one and the same interface boundary can be observed simultaneously. In this distance range the angle of incidence of reflected waves to the interface boundary is equal or greater than the critical angle ( $i_{crit.} = \arcsin \frac{V_1}{V_2}$ ;  $V_1$  and  $V_2$  are the velocities above and below the interface boundary). The study of reflected and refracted waves in this distance range and the angles of incidence is necessary for the investigation of the peculiarities of wave propagation in real media for working out the criteria to distinguish waves recorder in the subsequent part of a seismogram, for working out the methods of interpretation based on the use of the dynamic characteristics of these waves, etc.

The solution of these tasks is important for seismic investigations in the most various frequency ranges : for seismic prospecting, the methods of deep seismic sounding and seismology.

We shall choose two points out of the great number of problems connected with the study of the dynamic of reflected and refracted waves when they are observed simultaneously :

1) The peculiarities of the dynamics of reflected waves at  $i > i_{crit.}$ , in particular, the possibility of the correlation of reflected waves at  $i > i_{crit.}$ .

2) The relation of the intensities of reflected and refracted waves.

Some results of the study of these problems by means of experiments in real media and partly by means of theoretical calculations [1, 2] are given in the present paper. Media with layers of great thicknesses are considered.

The experimental data of reflected and refracted waves beyond the beginning point are obtained for the interface boundary with various velocity and density differentiation lying at depths of different values and with different frequency response of the apparatus used. The inferences given in this paper are based on the experimental data obtained for the following interface boundaries corresponding to thick layers.

TABLE 1

N	Rocks above and below the boundary	$p = \frac{V_1}{V_r}$	H, m	Predominant wave
1.	Sand-clay - metamorphized	0.4	500	reflected
2.	Sand-clay - granites	0.565	250	refl. + refracted
3.	Sand-clay - gneiss	0.565	1650	refl. + refracted
4.	Sand-clay - limestone	0.71	800-1300	reflected
5.	Sand-clay	0.8	30	refracted
6.	Sand-clay	0.8	100	refracted
7.	Sand-clay	0.98	400	refracted
8.	Sand-clay	0.9	3500	refracted

Symbols :  $V_1$  — velocity in layers above the interface boundary;  $V_r$  — boundary velocity in rocks below the interface; H — depth of the interface boundary.

*Criteria for the Distinguishing of Reflected and Refracted Waves.*

At great distances from the source reflected and refracted waves may have close kinematic characteristics (arrival times, apparent velocities), and it may be difficult to distinguish these waves. When analysing the experimental data the following criteria are used for the determination of the types of waves (reflected and refracted).

1. Differences of the shape of the travel time curves. In the case of a plane interface boundary the plots of the reflected waves' travel times are curvilinear and of the refracted - rectilinear.

The criterion of the shape of the curve often does not give an unambiguous result since beyond the beginning point the curve of reflected waves little deviates from a straight line on a considerable part of its length and the apparent velocities determined by means of the reflected and refracted waves' curves may be close to each other.

2. The relation between the overlapping travel time curves. For refracted waves the overlapping curves should be parallel. For reflected waves the overlapping curves are not parallel, the curves that are overlapped having greater apparent velocities than the overlapping ones.

The relation between the overlapping curves is one of the reliable criterion for the determination of the types of waves recorded within the region of the initial point and beyond it.

3. Other kinematic criteria are based on the analysis of the form and position of the interface boundaries at the cross-sections that are constructed on the assumption that the recorded wave is a reflected one and then a refracted one, on the analysis of the values of effective velocities etc.

4. Near the (initial) point and the interference zone of reflected and refracted waves we can attempt to determine the type of the predominant wave as to its intensity. In this zone besides the kinematic criteria mentioned above the shape of the plots of the amplitude as a function of distance  $A = A(x)$  can be used. The clear extrema of the curves  $A = A(x)$  are characteristic for the interference motion with near values of the interference waves' amplitudes (the amplitude ratio is 1 - 3). The gradual decrease of amplitudes with distance is characteristic for the cases when one of the waves is predominant as to its intensity.

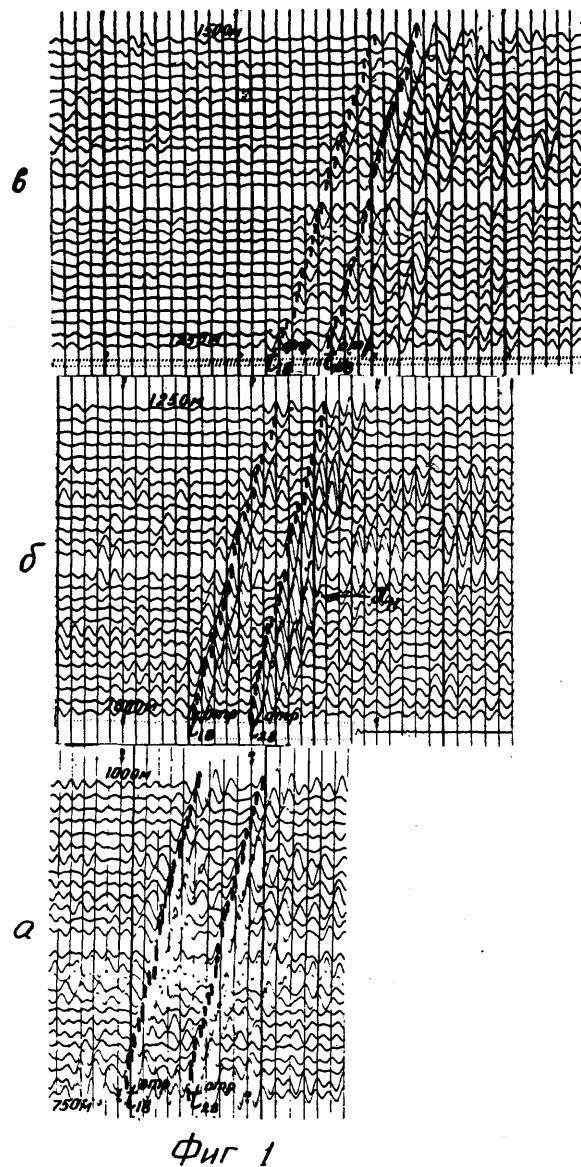
*Dynamic Peculiarities of Reflected Waves at  $i > i_{crit.}$*

*The shape of a reflected waves' record.* Experimental data show that the shape of a reflected wave at the angles more than critical one ( $i > i_{crit.}$ ) remains practically unchanged at great intervals. In a great number of cases a reflected wave is continuously identified beyond the critical angle ( $i = i_{crit.}$ ) as well (fig. 1).

According to the theoretical data at  $i \geq i_{crit.}$  the record shape of a reflected wave must change with distance due to the appearance of phase shifts [3]. However for the multi-phase impulses that are often recorded from experimental shots the change of the record shape of the central most intensive phases may be unnoticeable.

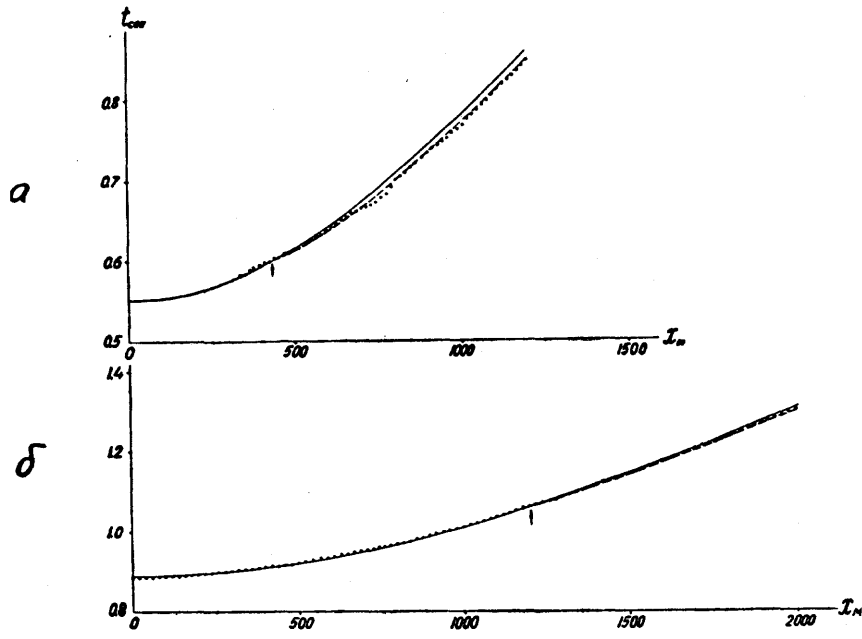
According to the theory the phase shifts changing with the angle of incidence must lead to the distortion of the shape of reflected waves' travel time curves. But the velocity differentiation  $\left(\frac{V_2}{V_1} \leq 1,8\right)$  being not too great and with the frequencies of the motion and the depths of the interface boundaries possible for an experimental shot these changes are also not too great and they are difficult to be noticed from the experimental data. The velocity differentiation being greater the change of the travel time curve due to the phase shift of a reflected wave is stronger and in some cases it can be noticed from the experimental data (fig. 2).

The change of the record shape of a reflected wave (accompanied by a sharp change of the amplitude) is observed only in the case of a very strong interface boundary ( $p = 0.4$ ) which has a second critical angle ( $b_2 > a_1$ ;  $b_2$  is the velocity of shear waves in the second medium,  $a_1$  is the velocity of longitudinal waves in the first medium;  $i_{2crit.} = \arcsin \frac{a_1}{b_2}$ ). Fig. 3 represents an example of record. These changes of the record shape occur at the angle of incidence somewhat less than  $i_{2crit.}$ . The indicated peculiarites of the record shape



Фиг. 1

FIG. 1. — Seismograms. In the region of the critical angle ( $i_{crit.} = \arcsin \frac{V_1}{V_2}$ ,  $x = x_H$ ) and at  $i > i_{crit.}$  the record shape of the reflected wave  $t_{\frac{1}{2}B}^{refl}$  ( $H = 800$  m;  $p = 0.7$ ) does not change.



Фиг 2

FIG. 2. — Experimental and theoretical travel time curves of reflected waves

- a)  $H = 500 \text{ m} \quad p = 0.4$
- b)  $H = 800 \text{ m} \quad p = 0.7$

Solid lines are theoretical travel time curves without the allowance for phase shifts; dashed lines with the allowance for phase shifts.

of a reflected wave at  $i \approx i_{crit.}$  are similar to the record shape that was observed earlier for the beginning points of refracted waves.

According to the theoretical data in this range of the angles of incidence ( $i \approx i_{crit.}$ ) the reflection coefficient as a function of the angle of incidence sharply changes. This can lead to sharp changes of the reflected waves' amplitude with the change of the distance from the shot point. At some distances a sharp increase of a reflected wave's amplitude can be noticed which may create an impression about the appearance of a new wave.

2. *Amplitudes of reflected waves.* The general character of the experimental plots of the reflected waves' amplitudes  $A = A(x)$

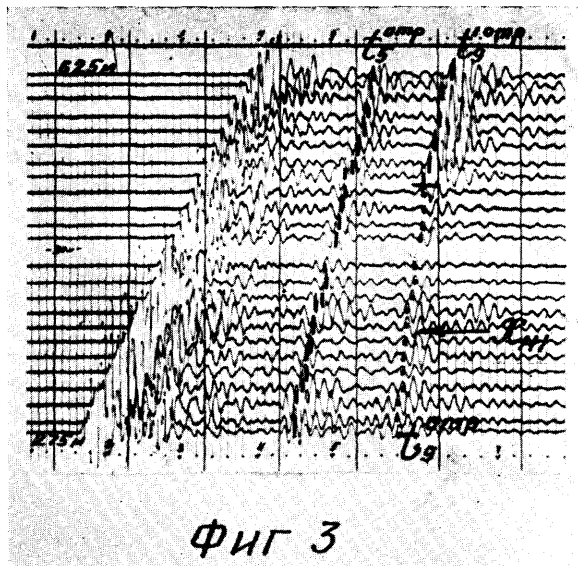


FIG. 3. — A seismogram. The reflected wave  $t_9^{\text{refl}}$  ( $H = 500$  m,  $p = 0.4$ ) undergoes sharp changes as to its amplitude and the record shape in the region of the angles of incidence somewhat less than  $i_{\text{crit.}}$  ( $i_{\text{crit.}} = \arcsin \frac{a_1}{b_2}$ )

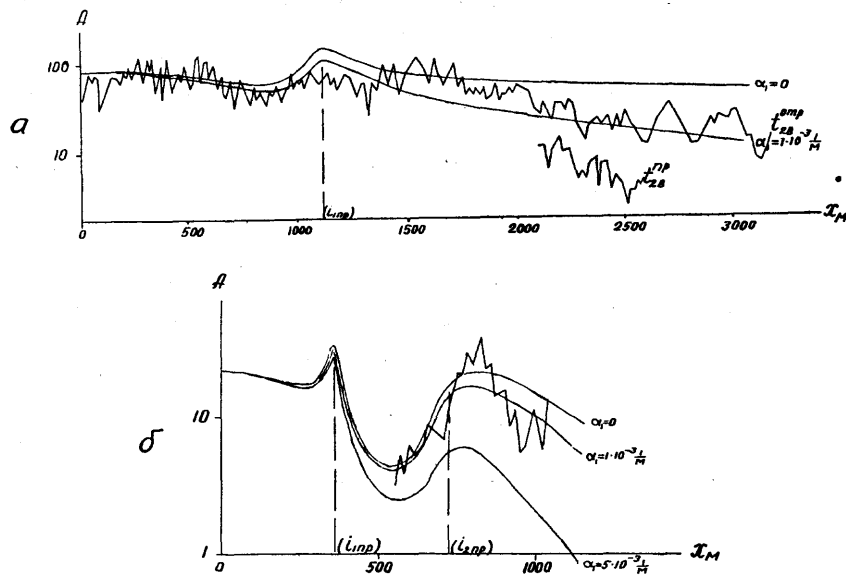
(excluding the region of the first critical angle) agrees with the theoretical calculations for absorbing media (fig. 4). A gradual decrease of the amplitude with distance is observed (when the second critical angle is absent).

In the majority of cases no amplitude maximum is noticed in the region of the first critical angle from the experimental data; beyond the critical angle the amplitude gradually decreases with distance. According to the theoretical data the reflection coefficient of plane waves must be maximum at  $i = i_1$ . The absence of the maximum according to the experimental data may be connected with the results of the interference of reflected and refracted waves [4].

The experimental and theoretical data obtained for very sharp interface boundaries (at  $b_2 > a_1$ ) in the region of great angles of incidence well agree. In these cases (fig. 4b) the amplitude maximum is observed beyond the second critical angle. The experimental data about the position of the maximum, its width and steepness of its slopes are close to the theoretical ones.

Thus at angles of incidence greater than critical reflected waves can have a steady shape of the record, the amplitude gradually

varying with distance and they are continuously identified at great distances. The presence of the phase shifts changing with the angle



ФИГ 4.

FIG. 4. — Plots of the amplitude as a function of distance : a) reflected wave  $t_{2B}^{\text{refl}}$  and refracted wave  $t_{2B}^{\text{imp}}$ . The amplitude of the wave  $t_{2B}^{\text{refl}}$  gradually decreases with distance; b) reflected wave  $t_{2B}^{\text{refl}}$  ( $p = 0.4$ ,  $H = 500$  m). The maximum of amplitudes is observed beyond the critical angle. Dashed lines are theoretical curves at different  $\alpha$ .

of incidence does not violate the correlation or lead to the disappearance of reflected waves with the form of impulses recorded in real media. The main cause of the appearance and the disappearance of reflected waves on records is not the phase shifts but the change of the relative intensity of reflected waves.

#### Intensity Relation of Reflected and Refracted Waves.

*Theoretical calculations.* The following conditions and simplifying assumptions are taken into consideration when making calculations to establish the general conception about the possible relations of the amplitudes of reflected and refracted waves in the range of distances greater than the distance to the beginning point of the refracted waves :

1. The calculations are made for a homogeneous overlying medium and a thick reflecting layer.

2. The minimum distances are assumed such for which the asymptotic formulas for refracted waves are valid, i.e. the region of the beginning point was excluded from consideration.

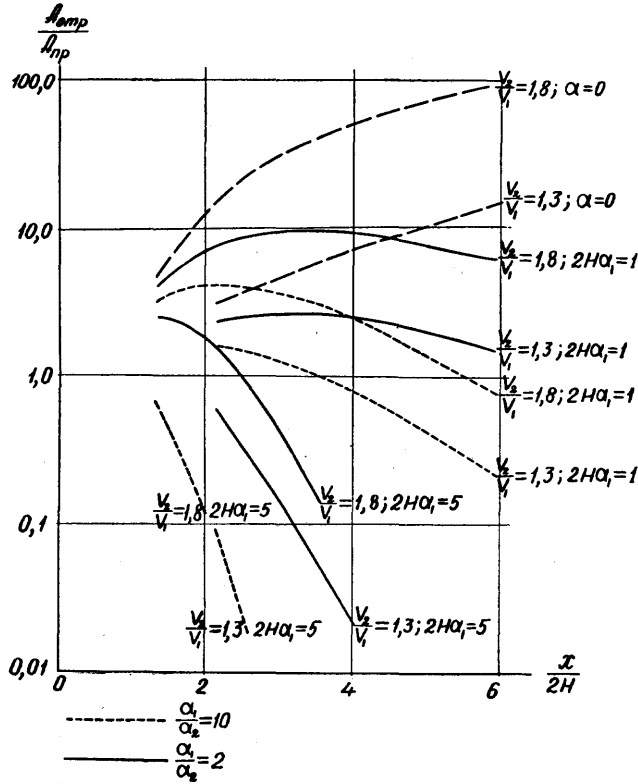
3. The reflection from the free surface was not taken into account.

4. In constructing the curves  $\frac{A_{\text{refl.}}}{A_{\text{refr.}}} = f(x)$  as a function of distance the phase shifts of reflected waves were not taken into account.

5. The allowance for the absorption is performed only approximately, by means of inserting the exponential factor into the formulas for elastic media.

The assumed simplifications do not distort the general rules in the behaviour of the relation  $\frac{A_{\text{refl.}}}{A_{\text{refr.}}}$  for media with thick layers.

Fig. 5 represents the curves  $\frac{A_{\text{refl.}}}{A_{\text{refr.}}} = f\left(\frac{x}{2H}\right)$  at  $\frac{H}{\lambda} = 10$  and different



ФИГ 5

FIG. 5. — Theoretical plots of  $\frac{A_{\text{refl.}}}{A_{\text{refr.}}}$  as a function of  $\frac{x}{2H}$  at  $\frac{H}{\lambda} = 10$ , parameters :  $p$ ,  $2H\alpha_i$  and  $\frac{\alpha_1}{\alpha_2}$ .

rent  $p$ . In fig. 6 the curves  $\frac{A_{refl.}}{A_{refr.}} = f\left(\frac{x}{2H}\right)$  at  $p = \frac{1}{1,3}$  and different  $\frac{H}{\lambda}$  are given.

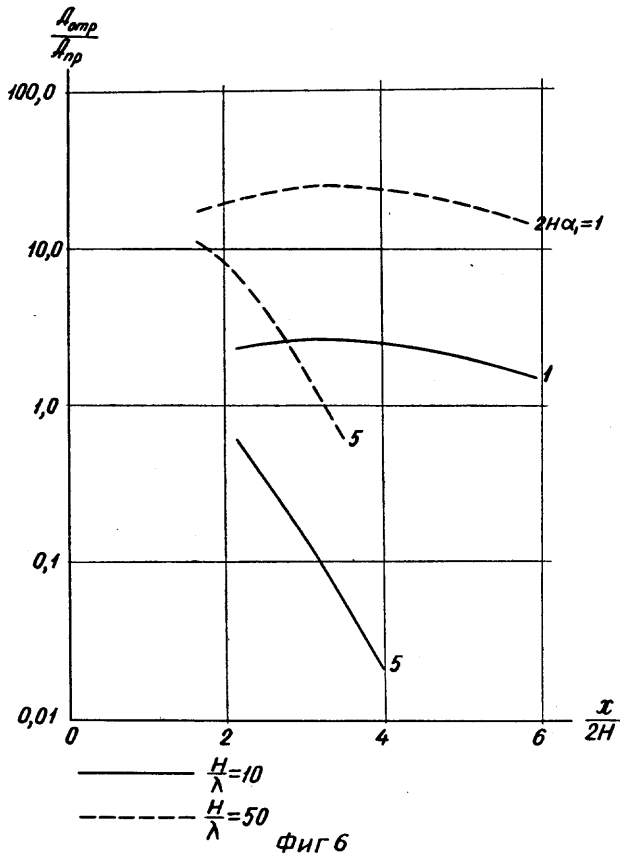


FIG. 6. — Theoretical plots of  $\frac{A_{refl.}}{A_{refr.}}$  as a function of  $\frac{x}{2H}$ ;  $p = \frac{1}{1,3}, \frac{\alpha_1}{\alpha_2} = 2$ ; parameters  $\frac{H}{\lambda}$  and  $2H\alpha_1$ .

The following dimensionless values are taken as parameters :  $p = \frac{V_1}{V_2}, \frac{H}{\lambda}, 2H\alpha_1$  and  $\frac{\alpha_1}{\alpha_2}$  ( $V_1$  and  $V_2$  are velocities in media overlying and underlying the interface boundary;  $H$  is the depth of the boundary,  $\lambda$  is the wave length,  $\alpha_1$  and  $\alpha_2$  are absorption coefficients in the media overlying and underlying the boundary). The accepted values  $2H\alpha_1$  and  $\frac{\alpha_1}{\alpha_2}$  cover the possible range of the quantities of

these values for seismic prospecting, deep seismic sounding and seismology.

Fig. 5 and 6 show that the value  $\frac{A_{refl.}}{A_{refr.}}$  is the greater the greater is  $p$  (the stronger is the velocity differentiation), the greater is  $\frac{H}{\lambda}$  (i.e. the greater is the depth and the less is the wave length), the less is  $2H\alpha_1$  ( $H$  being specified, the less is the absorption coefficient) and the less is the ratio  $\frac{\alpha_1}{\alpha_2}$ .

For elastic media beyond the interference zone the amplitudes of a reflected wave are greater than those of a refracted one and the ratio  $\frac{A_{refl.}}{A_{refr.}}$  increases with distance. The allowance for absorption relatively decreases the amplitude of a reflected wave. The absorption coefficient of the overlying medium being greater than that of the refracting one ( $\alpha_1 > \alpha_2$ ) the plots  $\frac{A_{refl.}}{A_{refr.}} = f\left(\frac{x}{2H}\right)$  have the maximum and beyond it the decrease of  $\frac{A_{refl.}}{A_{refr.}}$  with distance is noticed, and it is the sharper the greater are the absorption coefficients. For the values of the absorption coefficients characteristic for real media the ratio  $\frac{A_{refl.}}{A_{refr.}}$  may be less than unit.

The greater is  $2H\alpha_1$ , the ratio  $\frac{A_{refl.}}{A_{refr.}}$  becomes less than unit at less and less distances. For small  $2H\alpha_1$  in a great range of distances  $\frac{A_{refl.}}{A_{refr.}} > 1$ ; in this range the ratio  $\frac{A_{refl.}}{A_{refr.}}$  may amount to great values (for the parameters being accepted up to 10 to 100).

The performed calculations show that the use of higher frequencies leads to an increase of  $\frac{A_{refl.}}{A_{refr.}}$  in the vicinity of the beginning point and to a more rapid variation of  $\frac{A_{refl.}}{A_{refr.}}$  with distance.

The performed calculations show that the allowance for the absorption essentially changes the value  $\frac{A_{refl.}}{A_{refr.}}$ . Hence a conclusion can be made that for the calculations of  $\frac{A_{refl.}}{A_{refr.}}$  for certain media to compare them with the experimental data or to predict the intensity relation of reflected and refracted waves the absorption coefficient in the overlying and underlying media should be known.

Let us consider an example close to the conditions at the Mohorovičić discontinuity ( $p = \frac{1}{1,3}$ ,  $H = 25$  km). The frequencies of the motion will be taken equal to 10 c.p.s. (deep seismic sounding) and to 1 c.p.s. (seismology). The absorption coefficient in the overlying medium will be taken equal to  $5 \cdot 10^{-5}$  1/m for the frequency of

10 c.p.s. and  $0.5 \times 10^{-5}$  1/m for 1 c.p.s. The ratio  $\frac{\alpha_1}{\alpha_2}$  is unknown.

We shall seek for  $\frac{A_{refl.}}{A_{refr.}}$  at  $\frac{\alpha_1}{\alpha_2} = 2 \div 10$ . This range seems to cover all the possible ratios of  $\frac{\alpha_1}{\alpha_2}$  in real media.

At these conditions for  $f = 10$  c.p.s. the ratio  $\frac{A_{refl.}}{A_{refr.}}$  amounts to 10-13 in the vicinity of the beginning point and rather sharply decreases with distance. At  $x = 200 \div 240$  km  $\frac{A_{refl.}}{A_{refr.}} = 1$  and further  $A_{refl.} < A_{refr.}$ .

For  $f = 1$  c.p.s. the ratio  $\frac{A_{refl.}}{A_{refr.}}$  is close to 1 (it may be both somewhat greater and somewhat less than 1). The ratio  $\frac{A_{refl.}}{A_{refr.}}$  slowly decreases with distance. At  $\frac{A_{refl.}}{A_{refr.}}$  being equal or less than 1 we can hardly expect that in the subsequent part of the record a reflected wave will be distinguished since we must distinguish this wave against the background of other waves. A refracted wave can be distinguished in the region where it is recorded as the first arrival.

Thus according to the calculations for thick layers performed in the process of deep seismic sounding investigations (frequencies 10 c.p.s.) a reflected wave at  $x < 200$  km must be more intensive than a refracted one. For the conditions of seismology (1 c.p.s.) a reflected wave is rather unlikely to be distinguished in the subsequent part of seismograms.

*Experimental data.* It is established from the experimental data that the intensity relation of reflected and refracted waves beyond the initial point of the refracted waves may be different (table 1).

a) Reflected waves are intensive and are identified at great distances from the shot point corresponding to the angles of incidence of the wave on the reflecting boundary equal or greater than critical; refracted waves are less intensive and can be distinguished on records only beginning with the region of first arrivals.

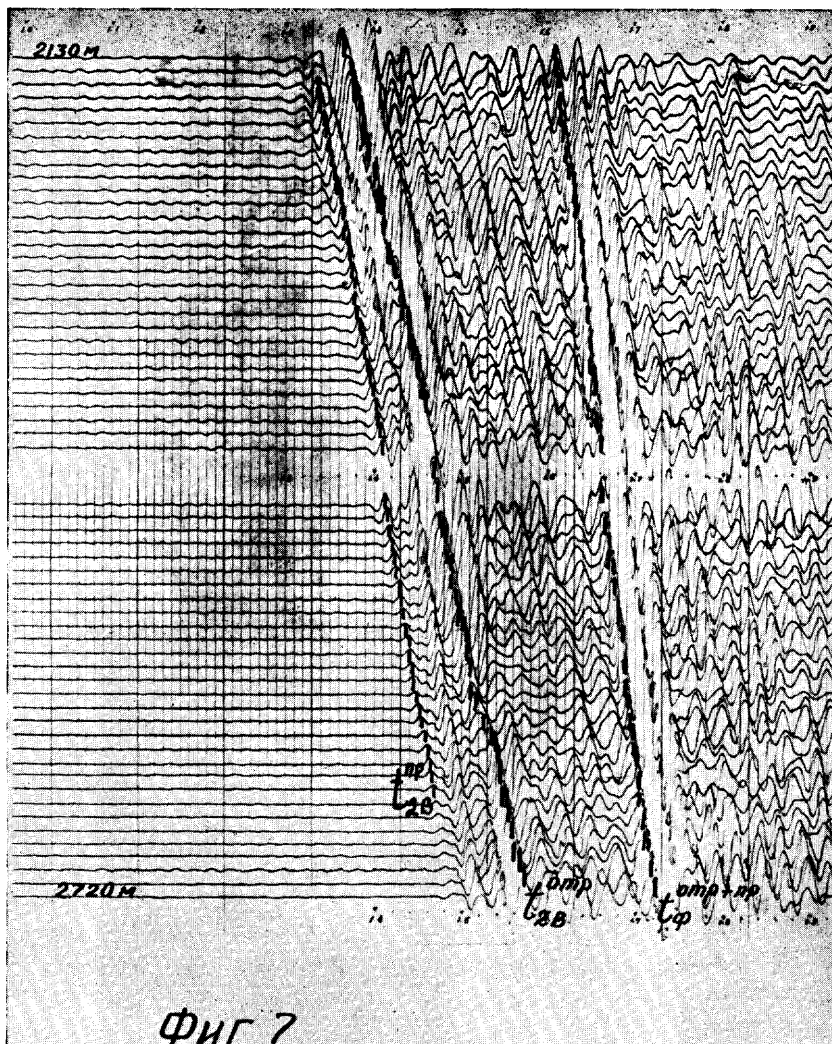


FIG. 7. — Seismograms. The intensity of the reflected wave  $t_{2B}^{\text{refl}}$  ( $H = 800 \text{ m}$ ,  $p = 0.7$ ) is 7 times greater than that of the refracted wave  $t_{2B}^{\text{refr.}}$  corresponding to the same boundary. The frequencies of the reflected waves are lower than those of the refracted. For the boundary at the depth  $H = 1650 \text{ m}$ ,  $p = 0.565$  beyond the beginning point the intensities of the reflected and refracted waves are close to each other, interference motion  $t^{\text{refl.} + \text{refr.}}$  is recorded. ( $t\varphi$ )

The record of fig. 7 can be given as an example, here reflected and refracted waves  $t_{2B}^{\text{refl}}$  and  $t_{2B}^{\text{refr.}}$  corresponding to one and the same boundary (sand-clay material — limestone,  $H = 800 \text{ m}$ ,  $p = 0.7$ ) are

recorded. The reflected wave is much more intensive than the refracted one. The ratio  $\frac{A_{\text{refl.}}}{A_{\text{refr.}}} = 4 \div 7$ . This value well agrees with the theoretical calculations.

b) Refracted waves are intensive, reflected waves are not distinguished (fig. 8).

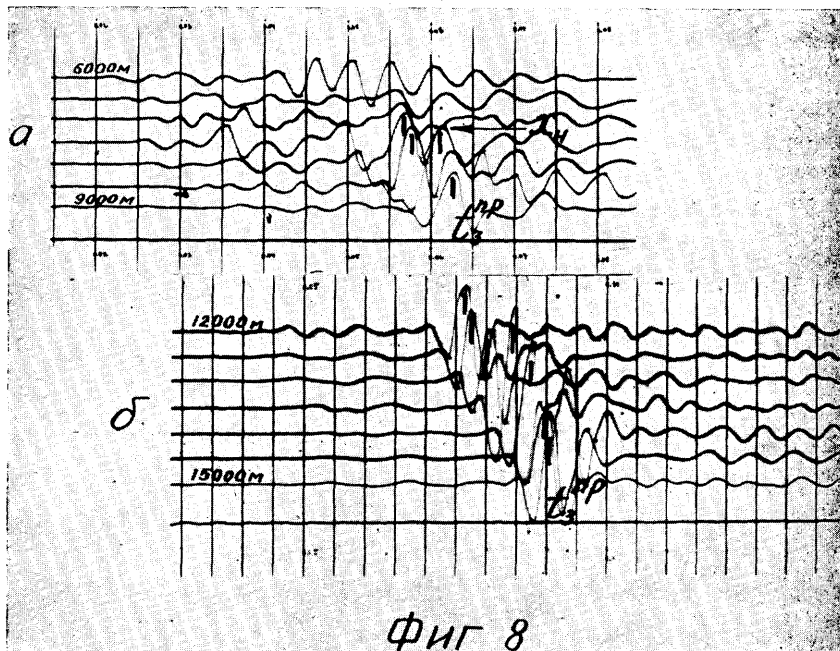


FIG. 8. — Seismograms. The refracted wave  $t_3^{\text{refr.}}$  ( $H = 30$ ;  $p = 0.8$ ) is very intensive. The reflected wave is not distinguished.

c) Reflected and refracted waves are approximately equally intensive (the amplitude ratio is 1 - 3). Interference motion is recorded (fig. 7, wave  $t^{\text{refl.}+ \text{refr.}}$ ).

For some regions the variability of the amplitude ratio of reflected and refracted waves is observed within the limits of small areas.

The dependence of  $\frac{A_{\text{refl.}}}{A_{\text{refr.}}}$  on some parameters of the medium, distance and wave length can be established on the basis of experimental data.

The relative intensity of reflected waves (as compared with the refracted ones) near the initial point is greater in the case of strong than weak interface boundaries. A similar dependence is established by means of theoretical calculations for absorbing media.

According to theory the ratio  $\frac{A_{refl.}}{A_{refr.}}$  increases with the increase of  $\frac{H}{\lambda}$ . The experimental data also suggest such dependence. The relative intensity of refracted waves increases with the decrease of frequency and the depth of the interface boundary.

A dependence of the relative intensity of a reflected wave on the absorbing properties of the overlying medium is established : at great absorption coefficients the reflected waves' intensity decreases as compared with the intensity of a refracted wave.

According to theory a decrease of the relative intensity of a reflected wave with the increase of the absorption coefficient is also noticed at great distances.

The experimental data obtained in the region of great distances suggest a decrease of the relative intensity of reflected waves with distance; and beginning with some distance a reflected wave is not identified on the record. A refracted wave is distinguished at great distances. The theoretical calculations for non-absorbing media imply that the intensity of a reflected wave is always greater than that of a refracted one and with the increase of distance the relative intensity of a reflected wave increases. In absorbing media the relative intensity of reflected waves decreases beginning with some distance which is the less the greater is the absorption coefficient of the overlying medium.

At great distances from the beginning points the intensity relation of reflected and refracted waves is mainly influenced by the absorption in media.

The absolute values of  $\frac{A_{refl.}}{A_{refr.}}$  determined by means of the experimental data are close to theoretical in some cases and in others are less than theoretical.

The data obtained as far are insufficient for the complete study of the problem of reflected and refracted waves' dynamics beyond the beginning point. They permit to formulate some laws mainly of the qualitative nature and pick out the problems the solution of which is particularly important.

The purpose of the further experimental investigations is to obtain reliable data about the absorption coefficients in overlying and underlying media since the comparison with the theoretical data is impossible without it. A more accurate allowance for the influence of absorption requires a further working out of the dynamic theory for absorbing media.

Especially important are the calculations for the region near the

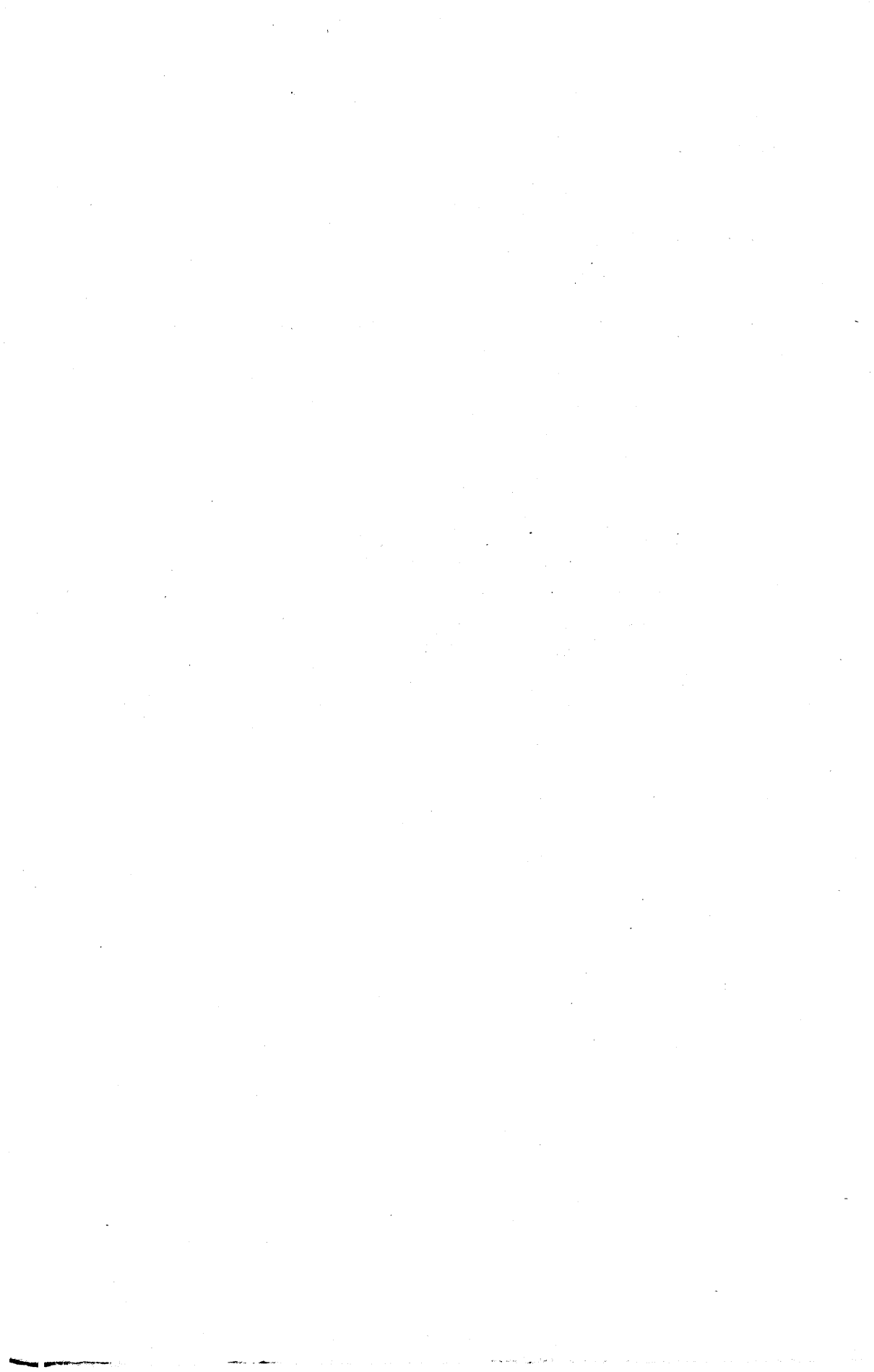
beginning points and the comparison of the experimental and theoretical data in this region.

*The main conclusions.*

1. Reflected waves with the angles of incidence greater than critical can have great intensity, a steady record shape and can be identified continuously at great distances.
2. The intensity relation of reflected and refracted waves beyond the beginning point of the refracted waves may be different. It is most greatly dependent on the values of the absorption coefficients and of ratio  $\frac{H}{\lambda}$ .

REFERENCES

- [1] YEPINATYEVA (A. M.), Study of Longitudinal Seismic Waves Propagating in Some Real Layered Media. Trudy Instituta Fiziki Zemli AN SSSR, N° 14 (181), 1960.
- [2] YEPINATYEVA (A. M.), On Reflected Waves with the Angle of Incidence Greater than Critical. Izvestiya AN SSSR, ser. geophys., N° 6, 1957.
- [3] MALINOVSKAYA (L. N.). On Dynamic Peculiarities of Longitudinal Reflected Waves beyond the Critical Angles. Izvestiya AN SSSR, ser. geophys., N° 5, 1957.
- [4] SMIRNOVA (N. S.), YERMILOVA (N. P.), On Construction of Theoretical Seismograms in the Vicinity of the Beginning Points. Collected Papers. Problems of the Dynamic Theory of Seismic Waves' Propagation. Izdatelstvo Leningradskogo Universiteta, 1959.



# ON SUPERCRITICAL REFLECTIONS FROM THE MOHOROVICIC DISCONTINUITY

By KOSMINSKAJA (I. P.), KRAKSHINA (R. M.)

## ABSTRACT :

Kinematic and dynamic characteristics of supercritical reflections from the Mohorovicic discontinuity recorded in the northern part of the Okhotsk sea having a continental crustal structure, are described. In regions with a crustal structure of the oceanic type no supercritical reflections were recorded.

Supercritical reflections are reflected waves recorded at distances from the shooting point exceeding those to the initial point of the time-distance curves for waves refracted from the same boundary.

Supercritical reflections are known from seismic prospecting. They were studied in detail by A. M. Yepinatyeva [1].

The possibility of recording supercritical reflections from the Mohorovicic discontinuity had been first suggested by Tuve and Tatle [2] in 1947, but this idea found no support with the seismologists.

In the USSR the question of recording supercritical reflections from the Mohorovicic discontinuity was raised by I. L. Nersesov [3] in 1956 who proposed to identify the  $P^*$  — waves not as connected with the intermediate boundary in the earth's crust, but as supercritical reflections from the Mohorovicic discontinuity. To substantiate this idea A. S. Aleksejev<sup>1</sup> carried out computations of the dynamic characteristics of supercritical reflections for different layered models of the earth's crust with constant and variable velocities in the layers.

The nature of the  $P^*$  — waves will not be discussed in the present communication, but we would like to notice that the question raised in [3] was of great importance for further investigations of the earth's crust. From 1957 on the soviet seismologists<sup>2</sup>

1. Leningrad affiliation of the Steklov Mathematical Institute of the Ac. Sci. USSR.

2. J. N. Godin, A. B. Egorkin, N. P. Ivanova, L. V. Molotova [4], I. S. Volkovski, B. S. Volvovski, I. V. Litvinenko, E. E. Fomenko and other carrying out DSS observations picked out supercritical reflections from the M discontinuity from seismograms obtained in different regions of the USSR : the Russian platform [5], the Fergan valley, Karelia, East Turkmenia, etc. The most extensive data on supercritical reflections were obtained in 1958 by I. V. Pomeranzeva and oth. in the Volga-Ural district (Investigations carried out by the All-Union Geophysical Research Institute of the Ministry for Geology and Conservation of Mineral Wealth).

when interpreting the extensive seismologic material and the data of deep seismic sounding (DSS) payed much attention to picking out waves which according to their kinematic and dynamic characteristics could be considered as supercritical reflections from the M discontinuity or from other boundaries in the crust.

In the present report are given the principal data on supercritical reflections from the M discontinuity recorded in the northern and central parts of the Okhotsk sea when carrying out investigations of the earth's crust by deep seismic sounding during the IGY [6, 7].

#### 1. The Principal Data on the Kinematic and Dynamic Characteristics of Supercritical Reflections from the M Discontinuity.

Let us state briefly the existing ideas about the kinematics and dynamics of the supercritical reflections from the M discontinuity.

For a two-layered model of the earth's crust the time-distance curve for the supercritical reflections approaches asymptotically the time-distance curve for the refracted  $P^*$  — waves (fig. 1, 2).

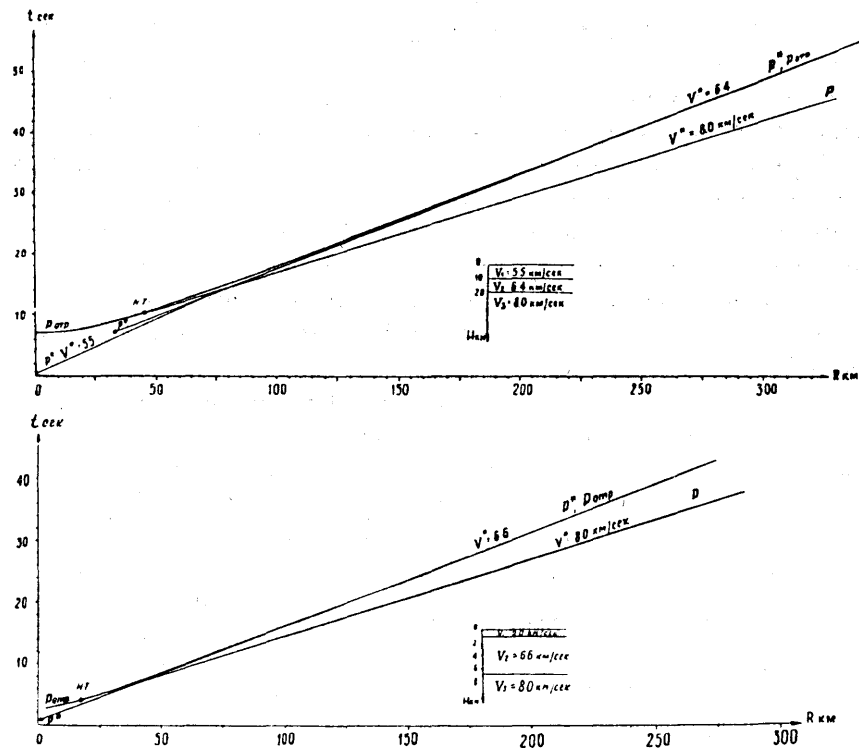


FIG. 1. — Time-distance curves for a two-layered crust of the continental type.  
FIG. 2. — Time-distance curves for a two-layered crust of an oceanic type.

In the region near the initial point of the time-distance curve for refracted P-waves the interference zone for reflected  $P_{refl}$ -waves and refracted P-waves is to be found. For a wave duration of about 0,5 seconds this zone has an extension of the order of 30-50 km. In this zone both waves have close apparent velocities and the first arrivals are represented by P-waves. When moving away from the initial point, the  $P_{refl}$ -waves pass into the subsequent part of the interference vibration.

Fig. 1, 2 show time-distance curves for direct, refracted and reflected waves corresponding to two sections of the earth's crust typical for the Okhotsk sea (fig. 1) and the ocean (fig. 2). For the first section the time-distance curve for the  $P_{refl}$ -waves becomes practically rectilinear beginning at a distance of 160 km from the shooting point and for the second section — at a distance of about 70 km. This corresponds in the first case to about  $8H$  and in the second — to about  $10H$ , where  $H$  is the depth of the M discontinuity. Computations were made of the apparent velocity of the  $P_{refl}$ -waves for different two-layered models of the earth's crust with different thickness ratios  $m$  and velocity ratios  $n$ . They have shown that with  $n$  varying from 0,7 to 0,9 and  $m = 1$  for distances  $r > 10H$  the apparent velocity  $V^*_{refl}$  varies but slightly and its deviation from the velocity in the overlying layer does not exceed 5 %. This should be taken into account when comparing the overlapping time-distance curves of the supercritical reflections.

The supercritical reflections for a layered model of the crust with variable velocities differs kinematically from the above considered case of a layered model with constant velocities in the layers : the time distance curve of the first contains a boundary point. At distances exceeding the abscissa of this point no supercritical reflections are kinematically possible. The distance to the boundary point is determined by the velocity gradient and the thickness of the crust. For gradients not exceeding 0,02 km/s/km which are typical for the earth's crust, these distances are about a tenfold thickness of the crust.

Computations of the dynamic characteristics of the waves for a perfectly elastic layered model of the crust with constant velocities in the layers [3] show that the intensity of the supercritical reflections  $P_{refl}$  should be by one order of magnitude greater than that of the P head waves at the Mohorovicic discontinuity (fig. 3). Such relation is maintained throughout the entire interval of coexistence of these waves. Beginning from a definite distance

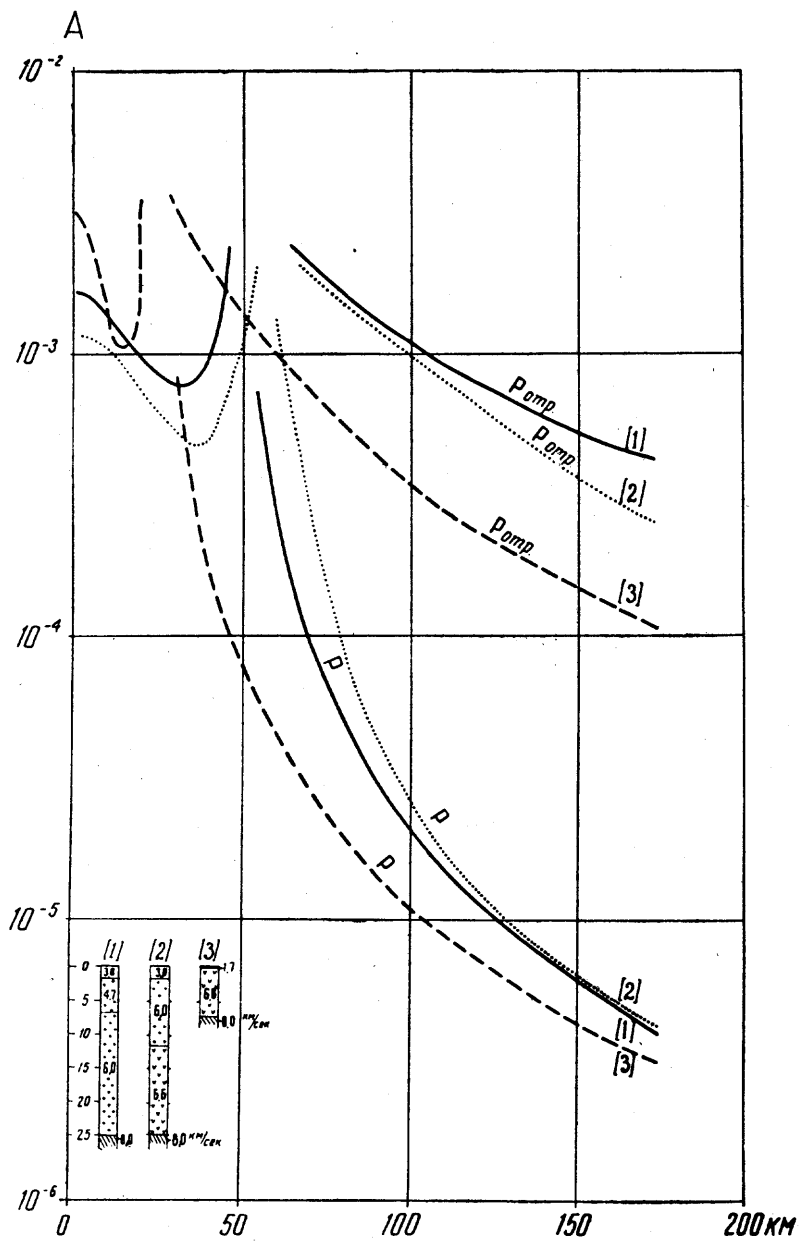


FIG. 3. — Amplitude curves for waves  $P_{retl.}$  and  $P$  calculated for different perfectly elastic layered models of the crust with constant velocities in the layers.

- 1, 2 — for continental crusts of different types characteristic of the northern part of the Okhotsk sea  
3 — for oceanic crusts.

to the initial point the difference between the amplitudes of the reflected and the head waves may decrease owing to the different absorption of these waves [1] and also to the existence of intermediate strongly reflecting boundaries. In case of a perfectly elastic layered model of the crust with variable velocities in the layers, with an abrupt change in velocity at the Mohorovicic discontinuity and a velocity gradient in the subcrustal layer, the intensity of the supercritical reflections will be of the same order as that of the refracted-slightly penetrating waves. Thus, in all above considered cases the "dynamic" probability of existence of supercritical reflections is according to theory higher than that of the head waves. This obliges one to be particularly careful when picking out such reflections from seismic records.

## 2. Characteristics of the Observed Waves.

Investigations of the earth's crust by deep seismic sounding in the zone of transition from the Asiatic continent to the Pacific ocean were carried out in the Okhotsk sea and in the parts of the Pacific ocean adjoining the Kurile islands. Mobile shooting points and one-point recording were used. Complete enough systems of reversed and overlapping time-distance curves were obtained.

An analysis of the obtained data [6, 7] has shown that the investigated region could be divided into three parts having different crustal structures : continental, oceanic and intermediate.

In these parts the following wave-groups were recorded  $P$  — waves having a velocity  $V^* < 5$  km/sec and connected with layers in the sediments;  $P^o$  — waves with a velocity  $V \approx 5 - 6,0$  km/sec connected with the "granitic" layer;  $P^*$  — waves having a velocity  $6,5-7,0$  km/sec and corresponding to the "basaltic" layer;  $P$  — waves with a velocity  $V \approx 8$  km/sec connected with the Mohorovicic discontinuity and  $P_{refl}$  — waves whose apparent velocity decreases with distance. They are considered as supercritical reflections.

The  $P_{refl}$  — waves are observed locally. They were picked out from seismograms recorded in the central and northern parts of the Okhotsk sea, in portions with a continental crustal structure [7] (*fig. 4, 5, 6*). These waves could not be picked out from seismogram recorded in portions having an oceanic or intermediate crustal structure (*fig. 7*).

The  $P_{refl}$  — waves are recorded at distances beginning from 40-50 km and up to 150-200 km.

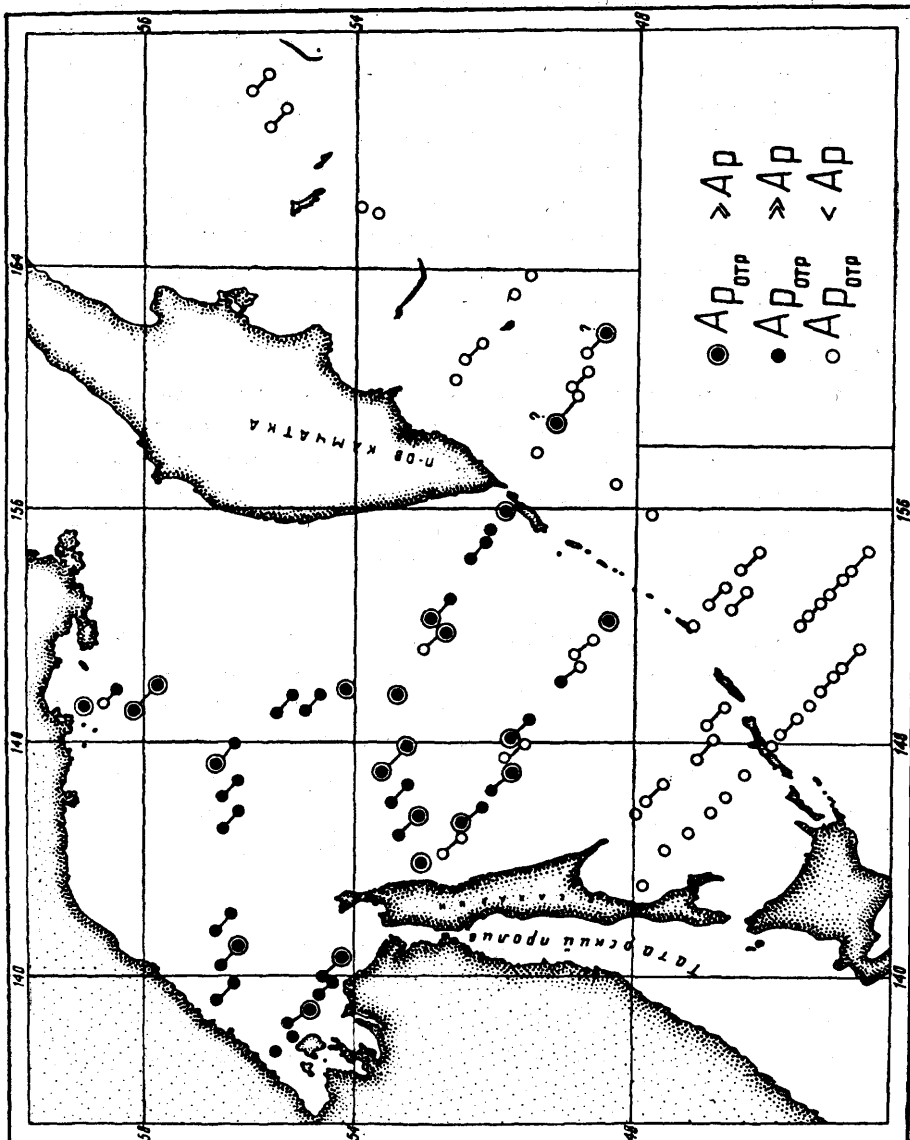


FIG. 4. — A map showing the regions in which head waves and reflected waves were recorded (for different intensity ratios).

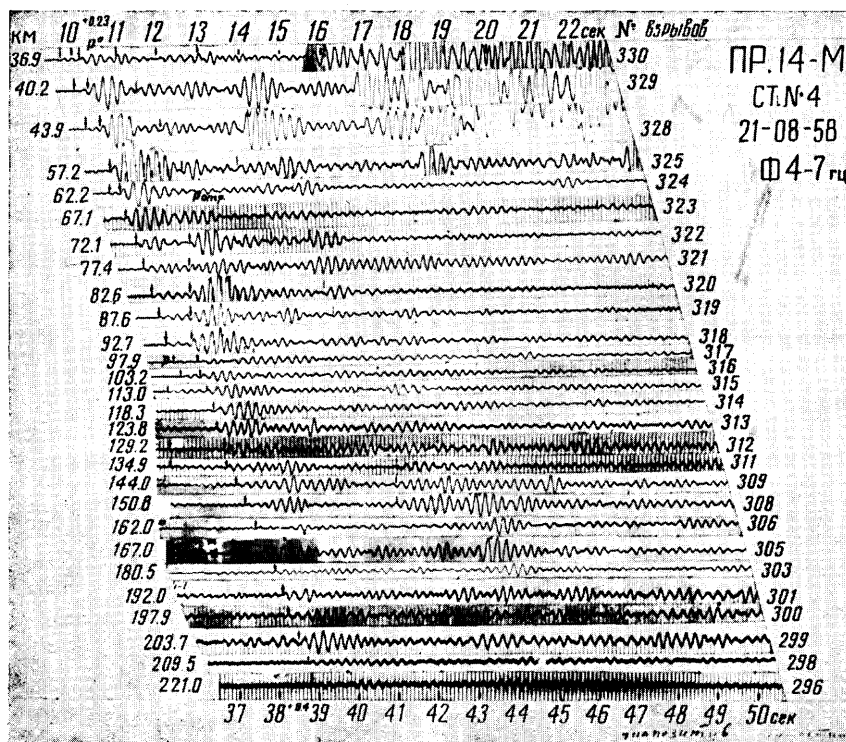


FIG. 5. — Seismograms obtained in the Okhotsk sea, north-west of the Skhalin island. The  $P_{refl.}$ -waves are of a complex nature and only slightly damped. The P-waves are difficult to pick out against the noise background.

It is characteristic of the  $P_{refl.}$ -waves, that they cannot be picked out at distances shorter than the critical ones although they should have existed there from geometric considerations. What regards the dynamic conditions, then according to theory, in the region preceding the initial point the intensity of the  $P_{refl.}$ -waves is by about half an order of magnitude less than the intensity of the supercritical reflections near the initial point (see fig. 3).

The supercritical reflections are very clearly identified by their form and intensity. In most cases their amplitudes prevail. The  $P_{refl.}$ -wave group is usually of a complex form (fig. 5) and of a duration no less than 1 second. In some portions this group is represented by a single wave of a simple form (fig. 6). The maximum intensity of the  $P_{refl.}$ -waves is observed in the region where following of these waves begins. The intensity of the  $P_{refl.}$ -waves falls off when moving away the shooting point

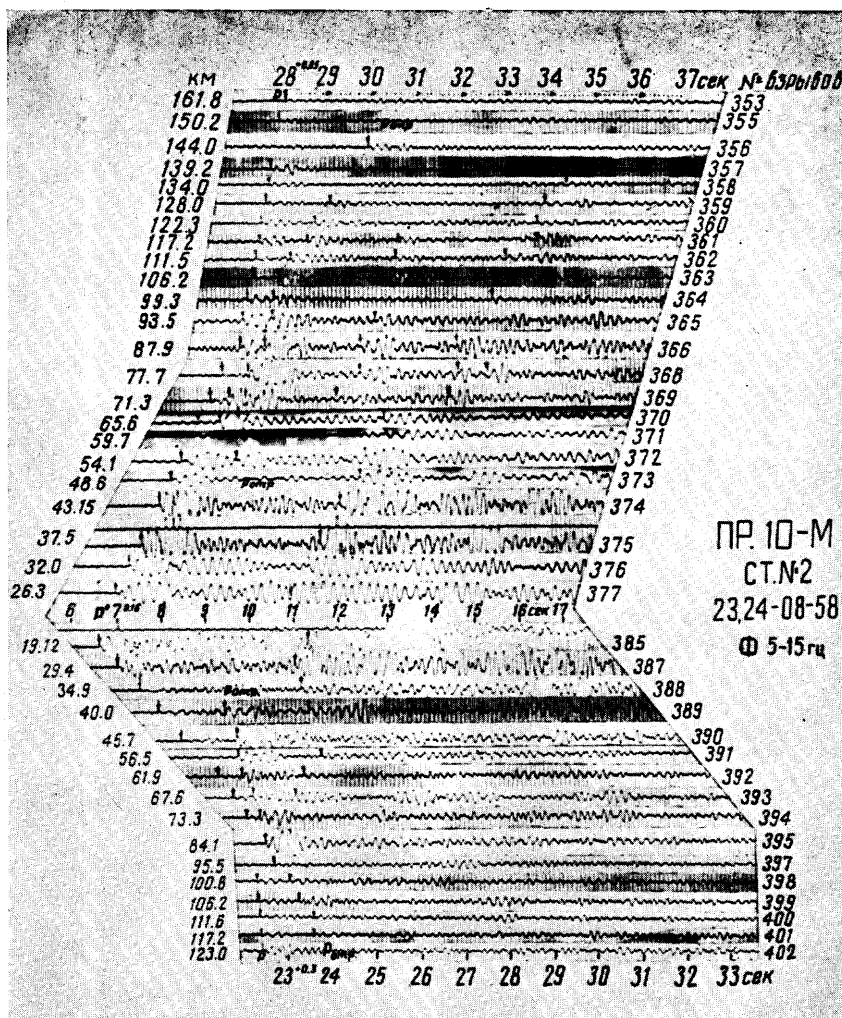


FIG. 6. — Seismograms obtained in the central part of the Okhotsk sea. The P-waves are comparable in amplitude with the  $P_{refl}$ -waves.

and at long distances becomes comparable with the intensity of the P-waves (fig. 8). On a number of profiles a sharp damping of the  $P_{refl}$ -waves is observed and there they become weaker than the P-waves or even are not picked out at all from the vibration background. Sometimes from the arrivals following the first waves a strong complex group of  $P + P_{refl}$ -waves is picked out and the velocity of the first waves of this group

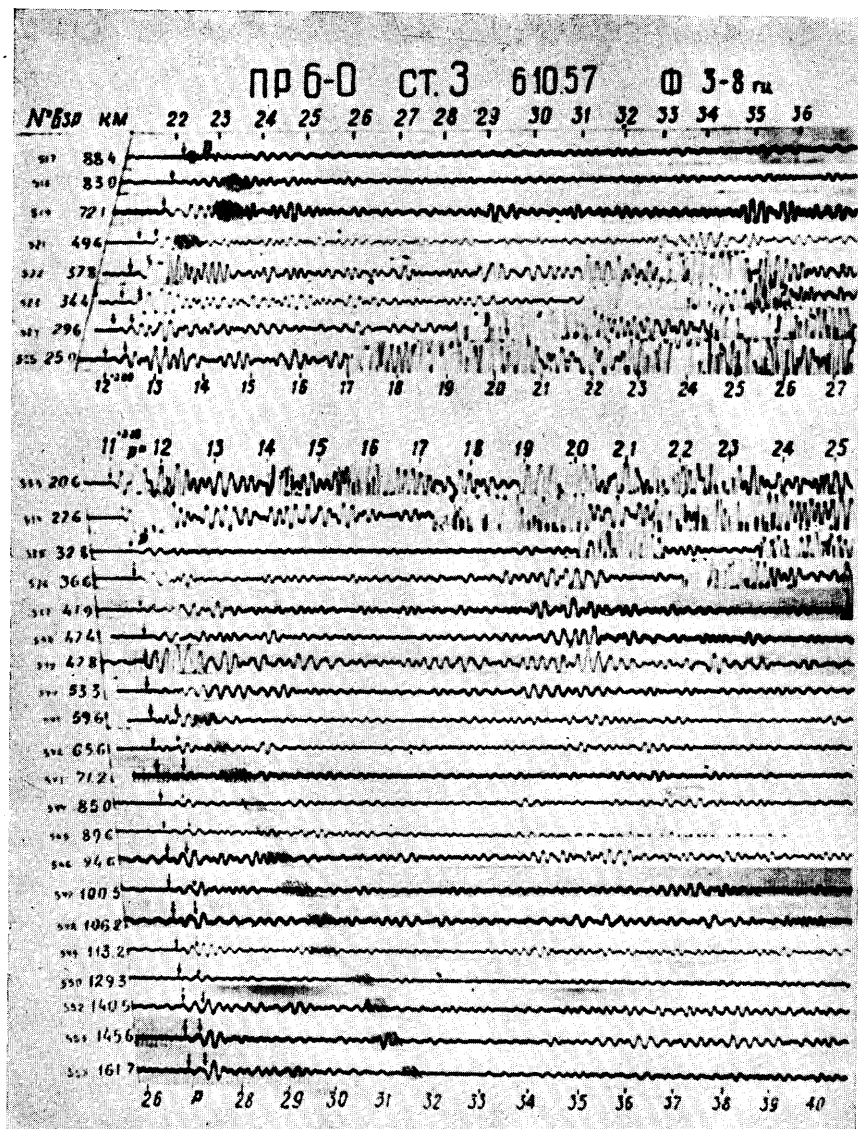


FIG. 7. — Seismograms obtained in the ocean, to the east of the axis of the Kurile-Kamchatka trough. Only P-waves are picked out. The regions in which the  $P_{refl}$ -waves should have been recorded are shaded.

is about 8 km/sec. In this case one gets the impression that the amplitudes of the P — waves prevail.



FIG. 8. — Dynamic time-distance curves obtained near the northern extremity of the Sakhalin island. The observed times of arrival are corrected for sea depth. Here the  $P_{retl}$ -waves prevail.

Let us enumerate the main criteria according to which the  $P_{refl.}$  — waves were identified as supercritical reflections from the M discontinuity<sup>3</sup>.

1. The time-distance curves for the  $P_{refl.}$  — waves are curvilinear, their apparent velocity decreases with distance from the shooting point. The overlapping time-distance curves are not parallel.

2. The time-distance curves for the  $P_{refl.}$  — waves fit into the nomogram of the calculated time-distance curves. The average velocity determined from the time-distance curves for the  $P_{refl.}$  — waves is close to the average velocity in the crust obtained from different data.

3. The relation between the experimental time-distance curves for  $P_{refl.}$  and P waves corresponds to the relation between the calculated time-distance curves.

4. The boundary velocities calculated from the coordinates of the assumed initial points are close to the boundary velocities obtained from the time-distance curves for the refracted P — waves.

5. The M discontinuity constructed from the time-distance curves for the  $P_{refl.}$  — waves practically coincides with that for the refracted P — waves.

Let us consider in more detail the amplitude curves of the  $P_{refl.}$  — waves.

There is a great variety of these curves. However they all have a common feature : the existence of an extremum in the region where the  $P_{refl.}$  — waves appear (*fig. 9*). On some of these curves the extrema are less clear and they alternate at definite intervals.

According to computations the first extremum is probably connected with the interference of  $P_{refl.}$  — waves and P — waves in the region containing the initial point. The successive extrema are apparently due to the complex nature of the vibrations in the  $P_{refl.}$  — group.

A comparison between the experimental and calculated amplitude curves of the  $P_{refl.}$  — waves for a perfectly elastic layered model of the crust with constant velocities in the layers shows that in most cases (curves 1-3 of *fig. 9*) the steepness of the experimental curves is equal to or less than that of the theoretical curves. The amplitude coefficient of absorption  $\alpha$  determined from the experimental curves is practically close to zero. Only

---

3. The kinematic criteria for identifying the supercritical reflections were formulated in [1].

from a small number of curves having a steeper slope (curve 4 in fig. 9) the following values of the amplitude coefficient  $\alpha$  and

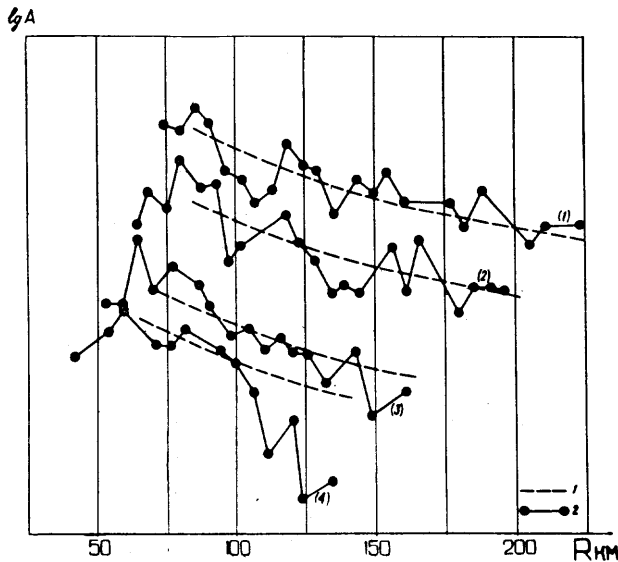


FIG. 9. — Amplitude curves for the  $P_{refl.}$ -waves.

1 — Experimental curves

2 — Curves calculated for waves reflected from the M discontinuity for a perfectly elastic layered model of the crust with constant velocities in the layers.

of the decrement of absorption  $\delta$  were obtained :  $\alpha = 0,05,1/\text{km}$  and  $\delta = 0,06$ . According to the data given by I. P. Pasechnik [8], the decrement of absorption for the  $P_n$ -waves characterising the subcrustal layer underlying the M discontinuity, is by about half an order of magnitude less than the above given. This may be considered as a qualitative agreement since it should have divergence of these waves when propagating in not perfectly elastic crust was stronger than below it.

The small damping of the  $P_{refl.}$ -waves might be due to the divergence of these waves when propagating in not perfectly elastic layered media with velocities and absorption in the layers varying according to complex laws. It is now difficult to say what kind of laws these are, but the conclusion that the damping of the  $P_{refl.}$ -waves was smaller than it should have been in case of a layered model of the crust with constant velocities in the layers even if perfect elasticity were assumed, should to our mind be of undoubted interest.

### 3. The Relation between the Amplitudes of the Reflected and Refracted Waves.

In the region under investigation the following relations between the amplitudes of reflected and refracted waves were observed in the zone of their supposed coexistence.

1.  $A_{P\text{ refl}} \geq A_P$
2.  $A_{P\text{ refl}} > A_P$
3.  $A_{P\text{ refl}} < A_P$

The first case corresponds to portions in which both the  $P_{\text{refl}}$  and  $P$ —waves were picked out from the seismograms. The  $P$ —waves were usually very weak and could be reliably followed only in the region of first arrivals at distances from the shooting point exceeding 100 km.

In regions where both types of waves were simultaneously recorded the ratios  $A_{P\text{ refl}}/A_P$  were determined in every point and the results are represented graphically in fig. 10.

74 ratios were determined and 72 % of them varied between 1 and 5. The remaining 28 % were distributed between values above 5 and below 1. In most cases no tendency towards a decrease with distance was observed. And only for some curves having a steep slope (A-curves of type (4) in fig. 9) such regularity was noticed.

The second case corresponds to regions in which only  $P_{\text{refl}}$ —waves were recorded, the intensity of the  $P$ —waves having been comparable to the ground noise level and so too low for being picked out. An analysis of the sensitivity of the apparatus used gives ground to consider in such cases the level of the  $P$ —waves as being no less than one fifth of the  $P_{\text{refl}}$  level.

The third case is characteristic of regions in which the  $P_{\text{refl}}$ —waves are not picked out from the part of the record following the first arrivals against the background of irregular seismic vibrations. Here the crustal structure is of the oceanic or intermediate type. A comparison of the background noise level in the part of the record following the first arrivals, with the amplitudes of  $P$ —waves leads to the following conclusion. The  $P_{\text{refl}}$ —waves could not be systematically followed only in such cases when even at small distances from the shooting point their intensity was about 2-3 times less than that of the first arrivals of  $P$ —waves. It should be noticed that in the ocean the intensity of the  $P$ —waves remains strong enough at distances from the shooting point up to 80 km.

In the first and second cases the observed amplitude ratios coincide qualitatively with those calculated for a perfectly elastic layered model of the earth's crust with constant velocities in the layers.

The calculated numerical ratios are greater than the experimental. It might be assumed that the observed decrease in the intensity of the reflected waves relative to the refracted ones was connected with a stronger absorption of the first, as was found in [1]. However this last assumption was correct only for amplitude curves  $A_{\text{refl.}}$  (curve R in fig. 9) having a steep slope which, as mentioned above, are very rarely observed.

For most of the slightly sloping amplitude curves for  $P_{\text{refl.}}$ —waves the level of the  $A_{\text{refl.}}/A_p$  ratio remains constant for long stretches of the profile. For them should be assumed that  $P_{\text{refl.}}$  and P waves are propagating in such real media in which the dampings of both types of waves obey close laws. According to Averjanov's computations<sup>4</sup> such crust might be represented by a model with a transition layer overlying the M discontinuity and a velocity gradient in the subcrustal layer.

The analysis of the third case might be of interest. Here conditions for producing  $P_{\text{refl.}}$  and P are foreseen which lead to

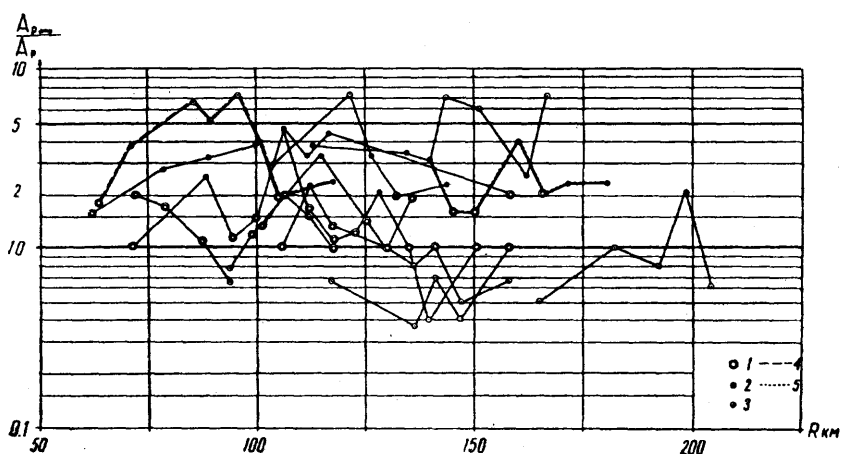


FIG. 10. — A graphical representation of the amplitude ratio  $A_{\text{prefl.}}/A_p$ .

- 1  $1 \leq A_{\text{prefl.}}/A_p \leq 2$  (41 % of all observations)
- 2  $2 < A_{\text{prefl.}}/A_p < 5$  (31 % of all observations)
- 3  $A_{\text{prefl.}}/A_p < 1$  and  $A_{\text{prefl.}}/A_p > 5$  (28 % of all the observations)
- 4 Variation of the  $A_{\text{prefl.}}/A_p$  ratio with distance corresponding to the  $A_{\text{prefl.}}/R$  curves of type /4/ in fig. 9
- 5 The same as /4/ corresponding to curves /1/ and /3/ in fig. 9.

4. Institute for Physics of the Earth of the Ac. Sci. URSS.

an increase in the intensity of the P — wave and a sharp decrease in that of the  $P_{refl.}$  — wave.

In the ocean the slope of the amplitude curves for the P — wave is smaller than or close to that calculated for the head wave. That is why the P — wave might be considered as a head wave or as a refracted-slightly penetrating wave whose path differs little from that of the wave gliding along the Mohorovicic discontinuity. Falling off and disappearance of the  $P_{refl.}$  — waves even at small distances might be formally explained by the existence of a sharp velocity gradient in the "basaltic" layer where absorption also occurs. For these reasons even at distances 60-80 km from the shooting point the  $P_{refl.}$  — waves become very weak when approaching the boundary point and so cannot be picked out from the seismogram (fig. 7).

However no data on velocity variation or absorption in the "basaltic" layer are at present available.

That such sharp damping of waves was possible in the region containing the boundary point was indicated by the calculated amplitude curves and also by experimental data on different multiple reflections in the water layer of the ocean [9] whose velocity gradient was about 10 m/sec/km.

Making use of the time-distance curves for the  $P_{refl.}$  — waves, we were able to determine the effective velocities in the earth's crust, construct the M discontinuity and also judge on the existence above the M discontinuity of an intermediate layer with a higher velocity and on its approximate depth.

#### CONCLUSION

In the seismograms obtained when carrying out deep seismic sounding of the earth's crust in the zone of transition from the Asiatic continent to the Pacific ocean following the first arrivals  $P_{refl.}$  — waves were recorded. According to their kinematic and dynamic characteristics these waves may be considered as supercritical reflections from the Mohorovicic discontinuity.

These waves are observed locally. They were picked out only from seismograms obtained in the northern and central parts of the Okhotsk sea having a continental crustal structure. In the ocean and in the deep-water parts of the Okhotsk sea where the crustal structure is of the oceanic or intermediate type, the  $P_{refl.}$  — waves could not be picked out.

The  $P_{refl.}$ —waves are mostly followed simultaneously with the weaker P—waves refracted from the M discontinuity.

A qualitative comparison of the experimental amplitude curves with the calculated ones shows that for both types of waves the damping is smaller than it should have been according to calculations for a layered medium with constant velocities in the layers even in case of perfect elasticity. This compels one to assume that the  $P_{refl.}$  and P waves are propagating in a layered media with variable velocities in the layers.

Association of the  $P_{refl.}$ —waves with portions characterised by a continental crustal structure, a slight velocity gradient and a feebly marked layering permits to consider these conditions as the most favourable for a reliable following of the supercritical reflections. In view of this the fact that in the ocean the  $P_{refl.}$ —waves could not be picked out might be explained by the existing there unfavourable conditions connected, for instance, with a sharper velocity gradient in the "basaltic" layer. It remains to prove these assumptions by further experiments and calculations.

#### REFERENCES

- [1] YEPINATYEVA (A. M.). Investigation of longitudinal seismic waves propagating in real layered media Transact. IPhE № 14, Publ. House of Ac. Sci. USSR.
- [2] The Earth's crust. A symposium ed. by Poldervart, Publ. House for For. Lit., 1959.
- [3] BUNE (V. I.), GZOVSKI (M. V.), ZAPOLSKI (K. K.), KEJLIS-BOROK (V. M.), KRESTNIKOV (V. N.), MALINOVSKAJA (L. N.), NERSESOV (I. L.), PAVLOVA (G. I.), RAUTIAN (G. G.), REISNER (G. I.), RIZNICHENKO (J. V.), KHALTURIN (V. I.). Methods for a detailed investigation of seismicity. Trans. IPhE, № 9/176, Publ. House. Ac. Sci. USSR, 1960.
- [4] MOLOTOVA (L. V.), Recording of deep reflected waves in seismic prospecting. Trans. IPhE, Ac. Sci. USSR, № 6/173, 1959.
- [5] GODIN (J. N.), Regional geophysical investigations. Jour. Geol. of Oil, № 6, 1957.
- [6] GALPERIN (E. I.), GORJACHEV (A. V.) m ZVIEREV (S. M.), Investigations of the earth's crust in the zone of transition from the Asiatic continent to the Pacific ocean. XIII section of program of IGY. № 3, Publ. House Ac. Sci. USSR, 1960.
- [7] VASILJEV (V. G.) and OTH., Investigations of the earth's crust in the zone of transition from the Asiatic continent to the Pacific ocean. Seismic investigations during the IGY, № 3, Publ. House Ac. Sci. USSR, 1960.
- [8] PASECHNIK (I. P.), Determination of the damping parameters for waves P<sub>n</sub> and S'. Proc. Ac. Sci. USSR, geoph. ser., № 8, 1960.
- [9] ZVIEREV (S. M.), Recording of water waves in the neighbourhood of the boundaries of shadow zone produced by the sea bottom. Proc. Ac. Sci. USSR, № 8, 1960.

## ABSORPTION OF SEISMIC WAVES IN ROCK

by B. F. HOWELL, JR.

In studying the attenuation of seismic waves, it is common practice to describe the changes in the first or the largest single amplitude of the pulse examined (e.g. Duvall and Petkof 1959; Jolly 1953; Ricker and Sorge 1951). Howell (1959) has discussed some of the limitations of this procedure. Because the energy of a seismic wave spreads in time as well as in space and because of interference patterns, variation in the amplitude of a particular phase is not necessarily a good measure of the change in its total energy. This paper is a brief report of two experimental measurements of the variation of total kinetic energy in a pulse. To avoid the problem of changing pulse shapes, the rates of attenuation of Fourier frequency components were measured.

The first experiment consisted of the measurement of three orthogonal velocity components of ground motion at 5-foot intervals out to 100 feet and at 110 and 120 feet from a mechanical vibrator running, at each distance, at a series of nine frequencies from 40 to 80 cps. The measurements were made on the floor of a strip-mine near Philipsburg, Pennsylvania. The surface rock was a sandy shale about forty feet thick overlying a sequence of shales, sandstones and coal seams. Figure 1 shows four plots

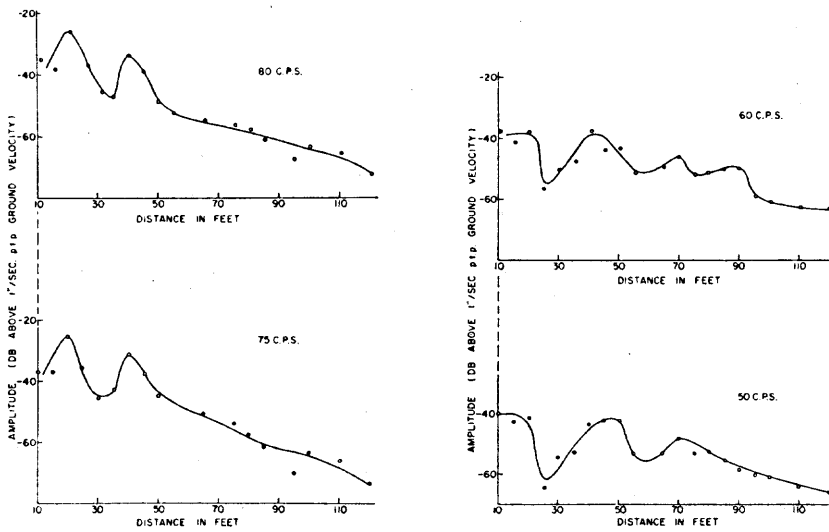


FIG. 1. — Amplitude variation at four frequencies, continuous-wave case.

of amplitude of ground motion as a function of distance. Fluctuations in amplitude of the type shown were observed at all frequencies. They persisted to larger distances at low than at high frequencies. They are believed to be an interference phenomenon, either between body and surface waves or among the various components of the surface waves.

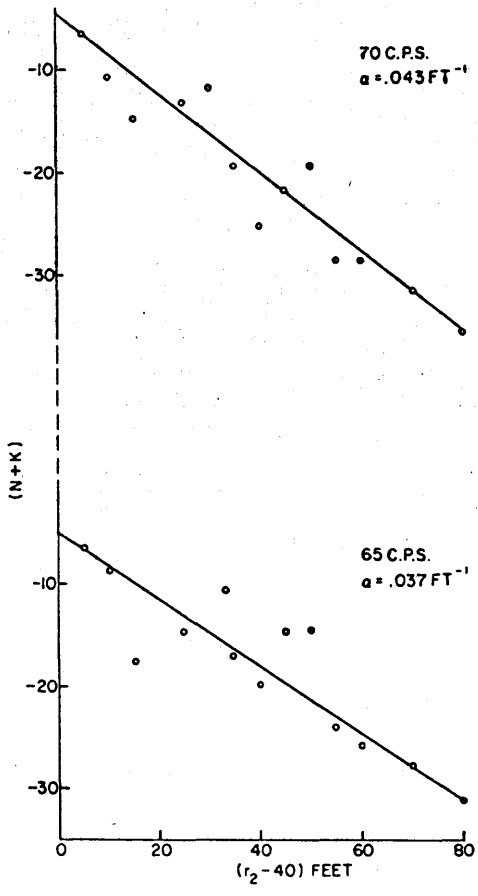


FIG. 2. — Amplitude  $\times$  (distance) $^{1/2}$  in decibels vs. distance, continuous-wave case.

The ground motion was predominantly retrograde elliptical except at 20 feet, where the motion was direct elliptical at some frequencies, retrograde at others. Phase velocities for these waves fell in the range 1280 to 1760 feet per second. The compressional-wave velocity in the ground was 8000 feet per second. It is concluded that the recorded motion belongs predominantly to the Rayleigh-wave family, except possibly within 40 feet of the source.

The absorption coefficient  $\alpha$  was calculated on the assumption that attenuation along the surface is describable by the formula :

$$A = A_0 r^{-n} e^{-\alpha r}$$

where  $r$  is distance and the value of  $n$  is fixed by the nature of the geometrical spreading. If all data are compared to the observations at 40 ft, assuming spreading in two dimensions as a Rayleigh wave ( $n = 1/2$ ), this becomes

$$\frac{A_r}{A_{40}} = \left( \frac{r_s}{40} \right)^{-\frac{1}{2}} e^{-\alpha(r_s - 40)} \quad (2)$$

Solving for  $\alpha$  and expressing the numerator in decibels

$$\begin{aligned} \alpha &= - \frac{\log A_r - \log A_{40} + \frac{1}{2}(\log r_s - \log 40)}{(r_s - 40) \log e} \\ &= - \frac{N + K}{8.69(r_s - 40)} \end{aligned} \quad (3)$$

Figure 2 shows two typical plots of  $N + K$  against  $(r_s - 40)$ . Amplitude data for distances less than 40 feet have not been used, since the interference phenomena observed close to the source make it uncertain how these data should be interpreted. Values of  $\alpha$  have been found from the slopes of these lines and are plotted against frequency on log-log paper in Figure 3. The least-squares

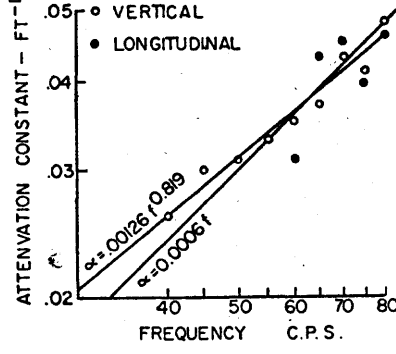


FIG. 3. — Attenuation factor assuming  $n = \frac{1}{2}$ , continuous-wave case.

straight line thru these data is  $\alpha = 0.00126 f^{0.819}$ , where  $f$  is frequency. The line  $\alpha = 0.0006f$  is also shown for comparison. The data are not good enough to prove that the exponent of  $f$  departs significantly from the value one.

In the second experiment a transient pulse was generated by a falling weight. Three orthogonal velocity components of the

ground motion resulting from a series of impacts were again measured, this time at 2.5 foot intervals over the distance range 2.5 to 180 feet. The site of the experiments was again a strip mine. It was not possible to carry out both experiments in the same mine because mining operations were resumed in the first mine between the times of the two experiments. The two mines were about one mile apart. The surface rock in the impact experiment was a claystone about ten feet thick overlying a series of sands, clays and coal seams.

Figure 4 shows tracings of typical records obtained. The group velocity of the maximum of this pulse is 2325 ft/sec. An air-coupled pulse traveling at 1057 ft/sec is recognizable as a train of constant-frequency waves in the coda of many of the records. The principal part of the energy of these pulses is retrograde elliptical. In order to study in detail the nature of the attenuations, the motions were broken into their Fourier integral spectrums using the method described by Howell, Andrews and Huber (1959; see also Howell 1959, fig. 10).

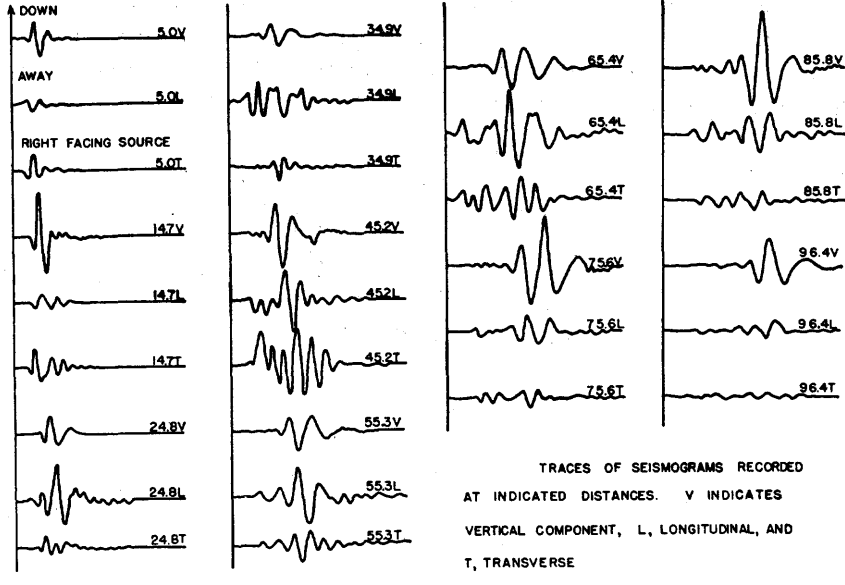


FIG. 4.

In the continuous-wave experiment, assuming Rayleigh waves, a value of  $1/2$  was expectable for  $n$  in formula (1). For a transient pulse, the situation is not so simple. By analogy with simple-layering systems (see e.g. Ewing, Jardetzky and Press 1957, espe-

cially sect. 4-4 pp. 156-189), the amplitudes of the various components can be expected to fall off at different rates. There are body-wave pulses whose maximum amplitude should attenuate at a rate inversely proportional to the square of the distance; and there are Rayleigh-type modes having geometrical attenuations proportional to  $r^{-1}$  or, in the case of the Airy phase,  $r^{-5/6}$ . The more rapid attenuation of instantaneous amplitudes compared to the continuous-wave case results from the pulse's spreading in time as well as in space.

In the method of analysis used here, the total pulse is treated. It might, therefore, be expected that a rate of attenuation would be observed which is a combination of the three different rates. At different distances, different phases might predominate. Because the total pulse is treated by this method, rather than instantaneous amplitudes, it might be expected that the effects of dispersion on amplitude attenuation would be largely eliminated.

As a first step in choosing which rate to use, the attenuation factor  $\alpha$  of equation (1) was assumed zero giving :

$$A = A_0 r^{-n} \quad (4)$$

Figure 5 shows typical plots of  $A$  in decibels against  $r$  in feet on semilog paper. The coefficient  $n$  is determined from the slope of this line. The values of  $n$  obtained range from 0.77 for 50 cps to 1.65 for 160 cps, as shown in Table I. Unfortunately, the data at the lower frequencies are badly scattered, so that it is impossible to say with assurance that the geometric attenuation is at a rate less than  $r^{-1}$ . It can be concluded, however, that  $n$  is not 2. The

TABLE 1

Divergence factor, pulse experiment									
Freq. c.p.s.)	30	40	50	60	80	100	120	140	160
$n$	1.03	0.85	0.77	0.79	1.04	1.33	1.57	1.59	1.65

values of  $n$  at frequencies above 60 cps increase rapidly because in the  $e^{-\alpha r}$  term of the absorption  $\alpha$  increases with frequency.

As a second step, amplitude times the square root of distance in decibels was plotted against distance in feet (fig. 6). The slope of the least-squares line thru these points determines the value of  $\alpha$  in formulas 2 and 3, which are based on the assumption  $n = 1/2$ .

Next, amplitude times distance was plotted against distance as shown in Figure 7. The slope of this line determines the value of

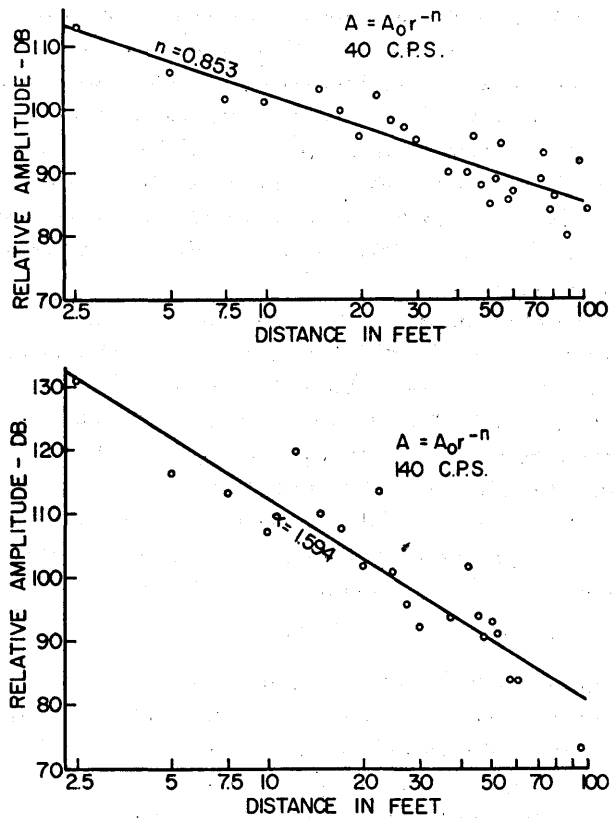


FIG. 5. — Ground-amplitude variation at two frequencies, pulse case.

$\alpha$  in the following formula, in which it is assumed that  $n = 1$  :

$$\begin{aligned}\alpha' &= - \frac{\log A_{r_1} - \log A_{r_2} + (\log r_1 - \log r_2)}{(r_1 - r_2) \log e} \\ &= - \frac{N + 2K}{8.69(r_2 - r_1)}\end{aligned}\quad (5)$$

Figure 8 shows the variation of attenuation constant with frequency in the two cases. For assumed divergence as the first power of distance (right-hand curve) the estimated values of  $\alpha'$  at 40 and 50 cps are not plottable : — 0.0038 and 0.0000. It is obvious that, since the values of  $n$  obtained from least-squares plots of the data for 40, 50 and 60 cps (Table 1) are less than unity assuming  $\alpha = 0$ , negative values are expectable for  $\alpha'$ . The lines  $\alpha = 2.35 \times 10^{-6} f^2$  (for  $n = 1/2$ ) at the left and  $\alpha' = 5.5 \times 10^{-3} f^{1.24}$  (for  $n = 1$ ) are least-squares lines thru the data. The line

$\alpha' = 1.6 \times 10^{-3}f$  (for  $n = 1$ ) has been added for comparison. No value was calculated for the case  $n = \frac{5}{6}$ . The scatter of the data is so great that it is impossible to select with assurance the correct value of  $n$ :  $\frac{1}{2}$ ,  $\frac{5}{6}$  or 1.

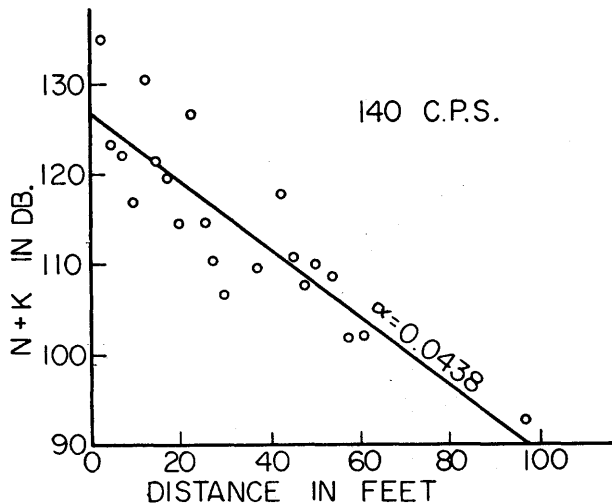
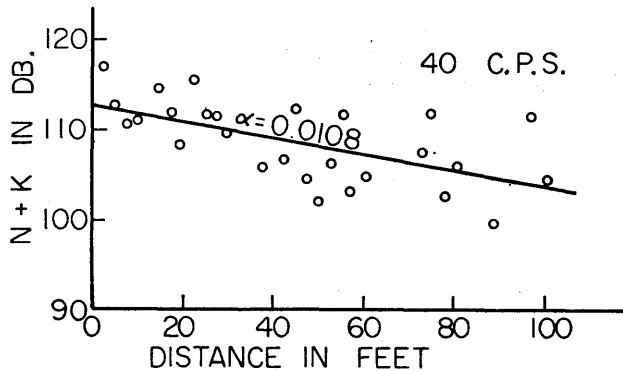


FIG. 6. — Amplitude  $\times$  (distance) $^{1/2}$  in decibels vs. distance, pulse case.

Comparing the continuous-wave and impact data, it appears that the attenuation was greater in the continuous-wave experiment than in the impact case. At 80 cps the continuous-wave-experiment value of attenuation constant (0.046/ft) was 3.4 times as large as the impact value (0.0135/ft).

Other investigators have observed absorption varying with both the first and second powers of frequency. Collins and Lee (1956), Birch and Bancroft (1938), Bruckshaw and Mahanta (1954), Ewing and Press (1954 A.B.) and McDonal et al. (1958) have presented

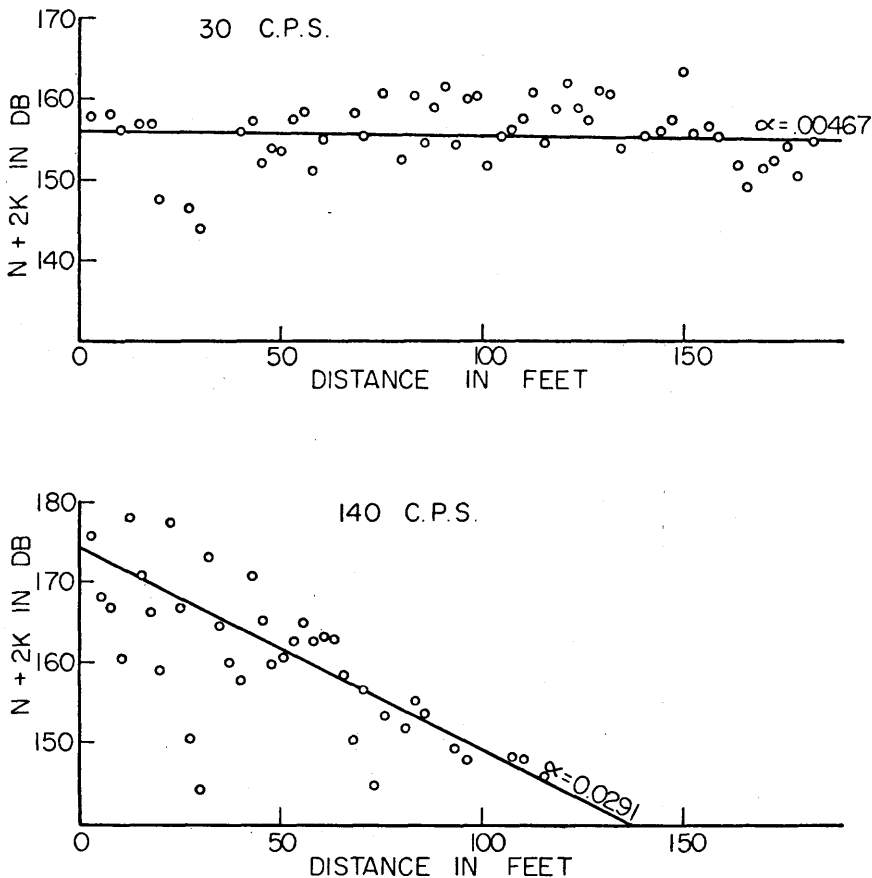


FIG. 7. — Amplitude  $\times$  distance in decibels vs. distance, pulse case.

evidence favoring an increase with the first power. Ricker's (1953) work is consistent with an increase proportional to the second power. Born (1941) found a first-power relation in dry rocks and a second-power dependence in moist rocks. The data reported here are all consistent, within the limits of accuracy of the measurements, with an absorption coefficient proportional to the first power of frequency. However, this conclusion is based on the assumption that the geometric spreading of the impact-generated waves introduces an attenuation with the inverse first power of distance. This

is a more rapid attenuation than is predicted by the best fit to the observed data. Hence it seems more reasonable to suppose that the spreading factor,  $n$ , has a smaller value. In this case, attenuation increases for the pulse data more rapidly than with the first power.

There is no reason to suppose that only one type of attenuation acts in the earth. It may be that at the low end of the spectrum solid friction is the principal source of absorption and  $\alpha$  is roughly proportional to frequency, but that above 60 cps viscous friction becomes predominant and  $\alpha$  becomes more nearly proportional to  $f^2$ . To decide this question, data should be gathered at surface distances or at depths beneath the surface where the different wave-types will arrive separately and hence can be more clearly identified. As a matter of practical experience, it is clear that experiments such as these should be conducted only in relatively uniform formations where pulse shapes are complicated as little as possible by internal reflections and refractions.

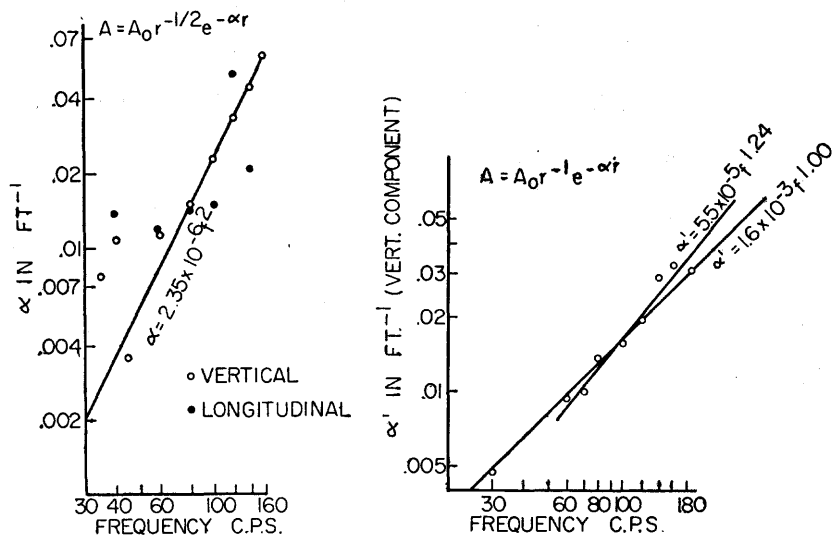


FIG. 8. — Attenuation factor assuming  $n = \frac{1}{2}$  and  $n = 1$ , pulse case.

The data on which this paper is based were gathered as parts of the Ph. D. theses of two students : A. B. Andrews (1957) and R. J. Watson (1958). Many of the computations including most of the least-squares fits were made by Y. Nakamura. Their important contributions were gratefully acknowledged. Apparatus and funds for the research were furnished by the National Science Foundation and the Office of Naval Research of the United States of America. Their essential support is greatly appreciated.

REFERENCES

- ANDREWS (A. B.), 1957. Frequency dependence of seismic wave attenuation : Unpublished Ph. D. thesis, Pennsylvania State Univ.
- BIRCH (F.), PANCROFT (D.), 1938. Elasticity and internal friction in a long column of granite : Bull. Seis. Soc. Am. 28 : 243-254.
- BORN (W. T.), 1941. Attenuation constant of earth materials : Geophysics 6 : 132-148.
- BRUCKSHAW (J. McG.), MAHANTA (P. G.), 1954. The variation of elastic constants of rocks with frequency : Petroleum 17 : 14-18.
- COLLINS (F.), LEE (C. C.), 1956. Seismic wave attenuation characteristics and pulse experiments : Geophysics 21 : 16-40.
- DUVALL (W. I.), PETKOFF (B.), 1959. Spherical propagation of explosion-generated strain pulses in rock : U. S. Bur. Mines Rpt. Invest. 5483.
- EWING (M.), PRESS (F.), 1954 A. An investigation of mantle Rayleigh waves : Bull. Seis. Soc. Am. 44 : 127-147.
- 1954 B. Mantle Rayleigh waves from the Kamchatka earthquake of Nov. 4, 1952 : Bull. Seis. Soc. Am. 44 : 471-479.
- EWING (W. M.), JARDETZKY (W. S.), PRESS (F.), 1957. Elastic waves in layered media; McGraw Hill.
- HOWELL (B. F.), Jr., 1959. Energy represented by seismic waves from small explosions : Assoc. Seis. Phys. Inter. Terre, Trav. Sci. A 20 : 55-66.
- HOWELL (B. F.) Jr., ANDREWS (A. B.), HUBER (R. E.), 1959. Photomechanical method of frequency analysis of seismic pulses : Geophysics 24 : 692-705.
- JOLLY (R. N.), 1953. Deep-hole geophone study in Garvin County, Oklahoma : Geophysics 18 : 662-670.
- MCDONAL (F. J.), ANGONA (F. A.), MILLS (R. L.), SENGBUSH (R. L.), VAN NOSTRAND (R. G.), WHITE (J. E.), 1958. Attenuation of shear and compressional waves in Pierre Shale : Geophysics 23 : 421-439.
- RICKER (N.), 1953. The form and laws of propagation of seismic wavelets : Geophysics 18 : 10-40.
- SORGE (W. A.), 1951. The primary seismic disturbance in shale : Bull. Seis. Soc. Am. 41 : 191-204.
- WATSON (R. J.), 1958. Ground vibrations from a periodic source : Unpublished Ph. D. Thesis, Pennsylvania State Univ.

Contribution N° 60-24 :  
Department of Geophysics and Geochemistry  
College of Mineral Industries  
The Pennsylvania State University  
University Park, Pennsylvania, U.S.A.

## METHODS AND SOME RESULTS OF INTERPRETATION OF DATA OF SEISMIC WAVES' SPECTRUM ANALYSIS

by I. S. BERZON

Recently spectra of seismic waves of different classes from shots and earthquakes have been studied on a large scale in seismology and seismic prospecting. Special instruments are designed for the determination of wave spectra (for instance [1]) and methods of obtaining the spectra by means of calculations are suggested [2]. The data of the spectrum analysis of seismic waves can be used : 1) to improve the wave recording methods — to choose the optimal frequency characteristics of seismic instruments, 2) to obtain new information about the investigated medium — to determine the absorption coefficients of different types of waves in different layers and the coefficients of reflection of waves from thin layers as functions of frequency. At present spectrum analysis data are chiefly used for the first of the indicated tasks. Relatively few works are available which deal with the quantitative interpretation of the results of spectrum analysis and these mainly refer to the interpretation of the spectra of direct waves recorded in boreholes and generated by shots [3, 4]. In the present paper some points of the quantitative interpretation of the reflected waves' spectra are discussed.

*Initial Data* The amplitude spectrum of a reflected wave corresponding to the boundary that is overlaid by a homogeneous medium is

$$A(f) = \frac{Q(f)}{l} e^{-\alpha(f) l}, \quad (1)$$

where  $Q(f)$  is the motion spectrum generated at the boundary of the elastic strain zone or briefly the spectrum of the source<sup>(1)</sup>;  $l$  is the length of the wave path;  $K$  — is the reflexion coefficient which does not depend on frequency in case of thick layers and is the function of frequency in case of thin layers, and  $\alpha(f)$  is the amplitude absorption coefficient which is a function of frequency.

For a multilayered medium the expression for the amplitude spectrum of the reflected wave is

$$A(f) = \frac{Q(f)}{\delta} K_{i+1} e^{-\sum \alpha_i(f) l_i} \prod_{i=1}^i (1 - K_i), \quad (2)$$

---

1. Further we shall speak about the spectrum of the shot.

where  $\delta$  is the divergency function depending on the thickness of each layer and on the velocity  $V_i$  of wave propagation in layers,  $K_i$  is the reflexion coefficient at the boundary of each layer;  $l_i$  and  $\alpha_i(f)$  are respectively the length of the wave path and absorption coefficients in each layer.

Formulas (1) and (2) show that the amplitude spectra of waves depend on the spectrum of the shot whose properties are almost not studied yet. The spectrum of the shot must be excluded from the observed spectra to determine the absorption coefficients of waves and coefficients of reflexion from thin layers as functions of frequency using the observed spectra of reflected waves. This can be done by obtaining the ratio of the spectra of two reflected waves recorded by one and the same recording channel from one shot. When obtaining this ratio besides the spectrum of the shot the influence of the filter properties of the receiver on the spectra of both waves are excluded; this refers also to the influence of the frequency response of the installation seismograph-ground which may be of a resonance form in the operation range of frequencies.

*Determination of the absorption coefficients in media between reflecting boundaries.*

If the spectra of two reflected waves corresponding to the boundaries of thick layers are known the absorption coefficients of waves as functions of frequency at that additional section of the path which is covered by one wave in relation to the other one can be determined. And we can use two single waves (fig. 1 a) as well

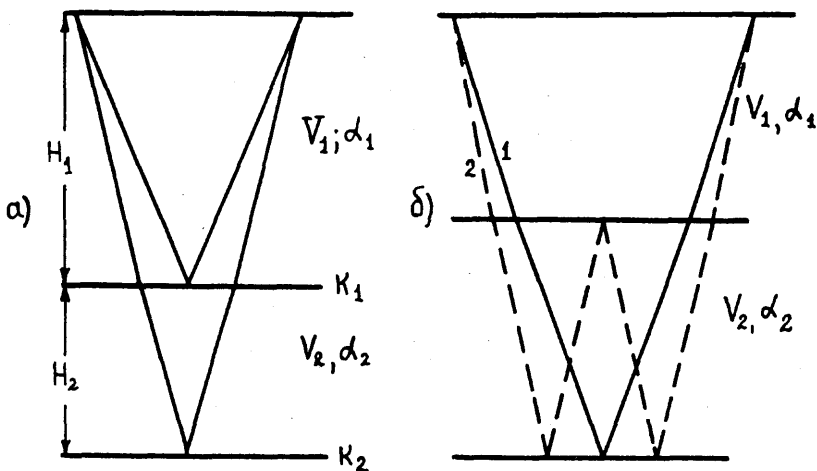


FIG. 1. — a) Paths of the rays of two single reflected waves; b) Paths of the rays of a single /1/ and a double /2/ wave.

as one single wave and one multiple wave (*fig. 1 b*). Now we shall discuss the joint interpretation of the spectra of two single waves; examples of the records of single waves obtained by wide-band instruments [1] and their amplitude spectra used in further determinations are given in *fig. 2*. For simplicity we shall consider the

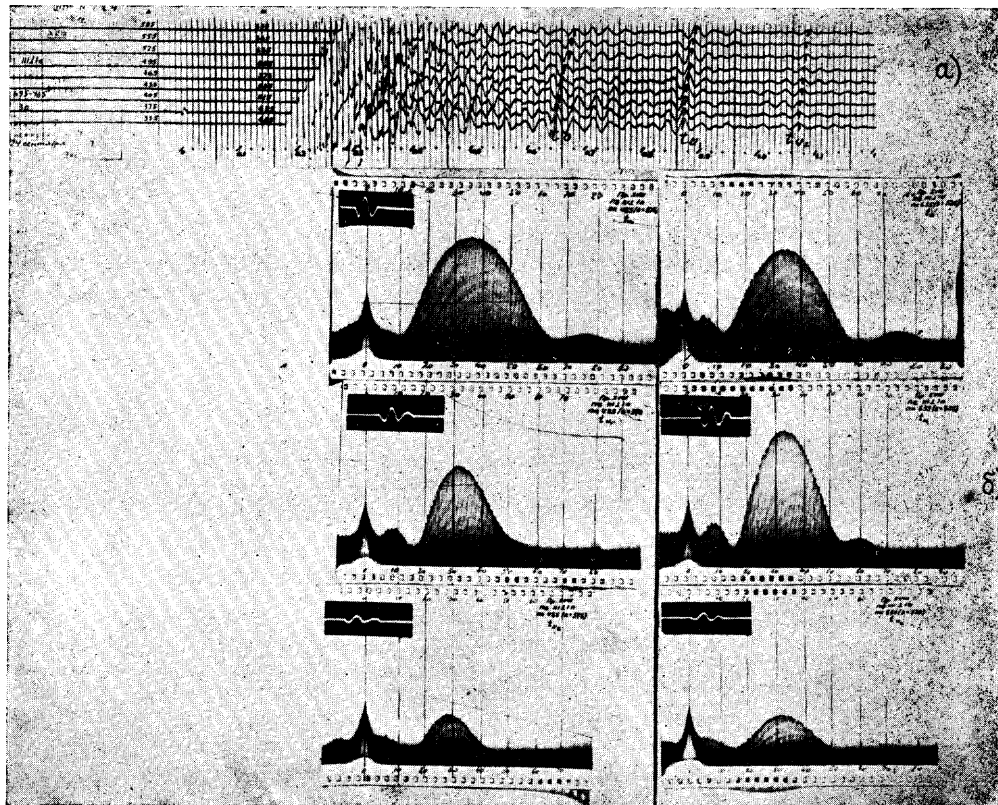


FIG. 2. — Records (a) and spectra (b) of the wave  $t_n$  corresponding to a thin layer and of the waves  $t_{u_1}$  and  $t_{u_2}$  corresponding to the boundaries of two thick layers.

case of a normal incidence of the wave onto the boundaries of layers; the derived formulas can also be easily generalized for the case of the arbitrary incidence angles of the wave.

The ratio of the spectra of two reflected waves is

$$\frac{A_1(f)}{A_2(f)} = \left(1 + \frac{H_2}{H_1} \frac{V_2}{V_1}\right) \frac{K_1}{K_2(1-K_1^2)} e^{j\alpha_2(f) H_2}, \quad (3)$$

where  $H_i$  and  $V_i$  ( $i = 1, 2$ ) are respectively the thicknesses of layers and the propagation velocities of waves in these layers.

For the case in question when obtaining the ratio of spectra the absorption in the medium overlying the upper boundary is excluded along with the spectrum of the shot.

If the reflecting layers are thick the values  $K_1$  and  $K_2$  do not depend on frequency. Thus only the absorption coefficient  $\alpha_2$  in the layer between both reflecting boundaries as a function of frequency must be determined.

Expression (3) can be written for convenience as :

$$\ln \frac{A_1(f)}{A_2(f)} = C + 2 \alpha_2(f) H_s \quad (4)$$

where the constant  $C$  does not depend on frequency. Having plotted  $\ln \frac{A_1(f)}{A_2(f)}$  as a function of frequency we can determine the dependence of  $\alpha_2$  on frequency  $f$ . An example of the plots

$\frac{A_1(f)}{A_2(f)} = \varphi(f)$  is shown in fig. 3. If the plots can be approxi-

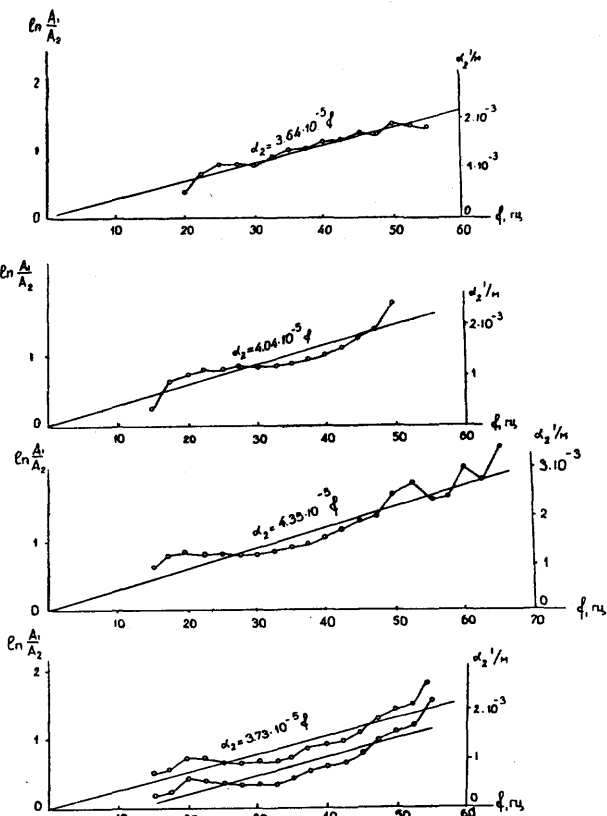


FIG. 3. — Plots of the ratio of the spectra of single reflected waves which were used for the determination of the function  $\alpha_2$  of frequency in a layer of marls at the depth from 1500 to 1900 m.

mated by straight lines the dependence of  $\alpha_2$  on frequency is linear in the frequency range under consideration. In this case we need not know the values  $K_1$ ,  $K_2$ ,  $H_1$  beforehand; only the value  $H_2$  must be known.

An approximating straight line is drawn through the experimental points and then taking into consideration that at  $f = 0$  the absorption coefficient is  $\alpha_2 = 0$  the straight line is transferred parallel to itself so that its extension might pass through the beginning of the coordinates (fig. 3, the lower plot). Absorption coefficient  $\alpha_2$  as a function of frequency is determined from the angular coefficient of the straight line. In the examples under consideration  $\alpha_2 = \alpha_2(f)$  was determined for the layer of marls at the depth between 1500 and 1900 m. As the plots show the value  $\alpha_2$  for the frequency  $f = 50$  c.p.s. is of the order of 1 to  $2 \cdot 10^{-3}$  1/m.

The methods of the extrapolation of the plots  $\ln \frac{A_i}{A_s} = \varphi(f)$  to the values of the frequency  $f \rightarrow 0$  analogous to the method that was considered can be applied for other sufficiently simple functions  $\alpha_2$  of frequency for instance at  $\alpha_2 = mf^n$  where  $m$  and  $n$  are constants. In the general case if the function  $\ln \frac{A_i}{A_s} = \varphi(f)$  is more complex the values of the reflection coefficients  $K_1$  and  $K_2$  and the depth  $H_1$  must be known to determine  $\alpha_2$ , if these values are not known the absolute values of  $\alpha_2$  can not be determined and only the differences of the absorption coefficients for different frequencies can be determined by means of the formula

$$\Delta \alpha_2 = \frac{1}{2H_2} \Delta \ln \frac{A_i}{A_s}, \quad (5)$$

where  $\Delta \ln \frac{A_i}{A_s}$  is the difference of the values  $\ln \frac{A_i}{A_s}$  for the two frequencies under consideration.

Using the suggested method we can successively determine the absorption coefficients or their differences as functions of frequency in different thick layers.

This method can also be applied for the determination of the absorption coefficients from the spectra of single and multiple waves, the absorption coefficients being determined in the layer when the multiple wave travelled twice.

By means of this method the absorption coefficient in sand and clay layers with the total thickness of 1300 m as a function of frequency was determined from the spectra of single and double

waves and  $\alpha$  as a function of frequency close to linear was also obtained [5].

It must be noted that the values  $\alpha_2$  determined from the spectra of reflected waves should be considered as effective. The decrease of amplitudes of different spectral wave components inside thick layers may be caused not only by the non-ideal elasticity of the medium but by the reflection and refraction phenomena at the velocity interface boundaries which are usually observed even in relatively homogeneous layers and are often unknown and therefore can not be taken into account in the process of interpretation.

*Determination of the coefficients of reflection from thin layers.*

In real media thin layers with low and high velocities are usually present with which the appearance of intensive reflected and in the case of layers with high velocity also of head waves is connected. Probably in deep part of the Earth's crust the layers with high and low velocities whose thickness  $d$  is much less than the wave length  $\lambda_2$  are present ( $d/\lambda_2 = 0.15 - 0.25$ ). The determination of the coefficients of reflection from thin layers using the experimental data is of interest for the choice of the optimal conditions of wave recording as well as for the study of the nature of reflection boundaries. In a number of cases even a qualitative solution of the problem whether the reflecting layer is thin or thick for a certain frequency range is also of interest.

At some simplifying assumptions of the medium structure the determination of the reflection coefficients as functions of frequency is possible [6]. Earlier a ratio of two single reflected waves was discussed. If to assume that the upper reflecting layer is thin the right part of the expression (4) would include two frequency functions : the reflection coefficient  $K_1$  as a function of frequency and the absorption coefficient  $\alpha_2$  as a function of frequency in the medium between two reflecting layers. If we know the function  $\alpha_2 = \alpha_2(f)$  from some data or specify it we can calculate the function  $K_1 = K_1(f)$ . The analysis of the errors in the determination of the function  $K_1 = K_1(f)$  due to the errors in the determination of  $\alpha_2 = \alpha_2(f)$  shows that with functions  $\alpha_2 = \alpha_2(f)$  possible in real media the allowance for the absorption essentially changes the values of the reflection coefficients while the form of the spectral curve  $K_1 = K_1(f)$  changes little. This permits to determine the main peculiarities of the spectrum  $K_1 = K_1(f)$  even if the exact data of the absorption in the lower medium are not available.

Fig. 4 and 5 show the results of the determination of the function

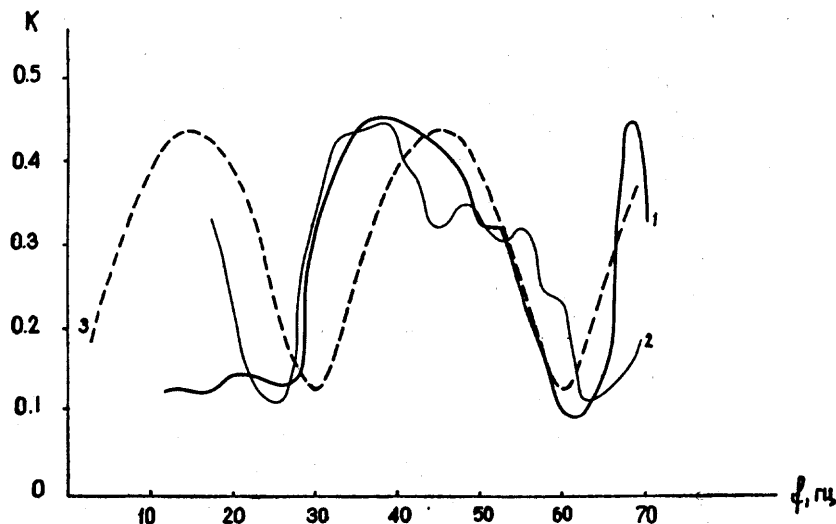


FIG. 4. — Plots  $K_r = K_r(f)$  for a thin layer with a low velocity determined from the experimental data /1,2/ and calculated according to the Rayleigh formula /3/. For these calculations we assumed that  $d = 45$  m,  $V_1 = 5500$  m/sec,  $V_s = 3050$  m/sec,  $V_3 = 4300$  m/sec.

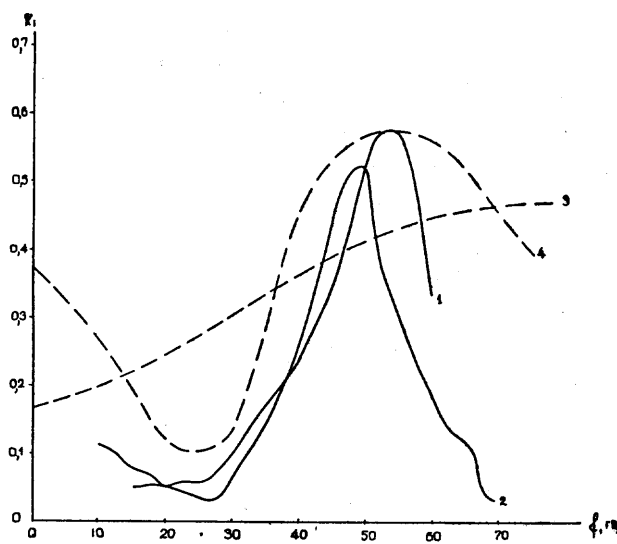


FIG. 5. — Plots  $K_r = K_r(f)$  for a thin layer with high velocity determined from the experimental data and calculated theoretically 3,4.

Curve 3 :  $d = 15$  m,  $V_1 = 2500$  m/sec,  $V_s = 5000$  m/sec,  $V_3 = 3600$  m/sec.  
Curve 4 :  $d_1 = 15$  m,  $d_s = 22$  m,  $V_1 = 2500$  m/sec,  $V_s = 5000$  m/sec,  
 $V_3 = 3600$  m/sec,  $V_4 = 5500$  m/sec.

$K_1 = K_1(f)$  from experimental data and their comparison with the results of theoretical calculations performed by means of the Rayleigh formulas [7, 8] for the stationary synusoidal waves.

In fig. 4 plots  $K_1 = K_1(f)$  are represented for the layer with the thickness  $d = 45$  m with low velocity lying at the depth of about 2 km. For the calculations of  $K_1 = K_1(f)$  spectra of the waves reflected from this layer and from the surface of the crystal basement were used. In this example the experimental plots  $K_1 = K_1(f)$  agree in the main with those calculated theoretically for the case of a thin layer between two semi-spaces with different parameters. Fig. 5 represents spectra for the case of a layer with the thickness  $d = 15$  m with high velocity lying at the depth  $H = 1100$  m. The curves  $K = K(f)$  determined from the experimental data are characterized by a considerably less width than those calculated for the case of one thin layer between two semi-space (curve 3). Besides that the frequency of the maximum of the experimental plots is shifted to the range of lower frequencies. The indicated differences of the experimentally determined plots  $K_1 = K_1(f)$  from the theoretical ones seem to be due to the fact that the real medium is more complicated than the simple models accepted for the calculations. In particular the presence of thin layers with other velocities which immediately underlie the thin layer in question may be of rather great importance. The performed calculations show that if the reflecting layer is not homogeneous and consists of two layers of different thicknesses the shape of the curve  $K_1 = K_1(f)$  may essentially change and approach the observed one (fig. 5, curve 4).

The experimental data concerning the sharply resonant shape of the plots of the reflection coefficients agree well with the results of the recording of waves, the frequency curves of the instruments used being different. The observations showed that the frequency of the maximum of the apparatus characteristic being changed the predominant frequencies of the reflection wave corresponding to a thin layer remained unchanged while the frequencies of other waves and the microseismic background considerably changed. At the same time the ratio of the reflected wave amplitude to the background amplitude sharply decreased in cases when the maximum of the apparatus frequency characteristic did not coincide with the maximum of the curve  $K_1 = K_1(f)$ . These data confirm the conclusion about the small width of the curve of the reflection coefficient against frequency that was drawn on the basis of the interpretation of the reflected waves' amplitude spectra.

*On the joint determination of the coefficients  
of reflection from thin layers and the absorption coefficients.*

Earlier the methods of the separate determination of the absorption coefficients and the reflection coefficients as functions of frequency from the ratio of the spectra of two waves were considered. In some cases a joint determination of the functions  $\alpha = \alpha(f)$  and  $K = K(f)$  in the investigated medium is possible if the spectra of three reflected waves corresponding to two interface boundaries are known. Let us dwell on one of the possible versions of the determination of  $\alpha = \alpha(f)$  and  $K = K(f)$ .

In the case discussed above when a thin layer and an underlying thick layer are present in the medium if besides the spectra of single reflected waves corresponding to each of the layers the spectrum of a double wave reflected from a thin layer is known the absorption coefficient in the medium and the coefficient of reflection from a thin layer as functions of frequency can be jointly determined.

It should be noted that in the case of a thin layer the determination of the absorption coefficient  $\alpha$  as a function of frequency using only the spectra of single and double waves becomes impossible since the function  $K = K(f)$  should be known for the determination of  $\alpha = \alpha(f)$ . The joint use of three spectra, i.e. the two spectrum ratios as functions of frequency permits to determine two frequency functions  $\alpha = \alpha(f)$  and  $K = K(f)$ . If there being grounds to consider that the absorption in media overlying and underlying the thin layer may be essentially different a functional dependence between absorption coefficients in both media should be specified. Now not dwelling on the consideration of calculations formulas we shall show some results of the determination of  $K = K(f)$  and  $\alpha = \alpha(f)$  from the spectra of three waves. In fig. 6 an example of the plots  $K = K(f)$  and  $\alpha = \alpha(f)$  calculated by means of the discussed method is represented. These calculations were made on the assumption that the absorption coefficients  $\alpha_1$  and  $\alpha_2$  in sand-clay layers overlying and underlying the thin layer are the same, i.e. the average values of the absorption coefficient in the medium were determined.

The plots shows that in this case the function  $\alpha$  of frequency is complex, which seems to be connected with the mentioned above physical sense of the coefficient  $\alpha$ , being an effective value. The investigation of the variation of the plots  $K_1 = K_1(f)$  and  $\alpha = \alpha(f)$  on different assumptions as to the dependence between the absorption coefficients  $\alpha_1 = \alpha_1(f)$  and  $\alpha_2 = \alpha_2(f)$  showed that the shape of

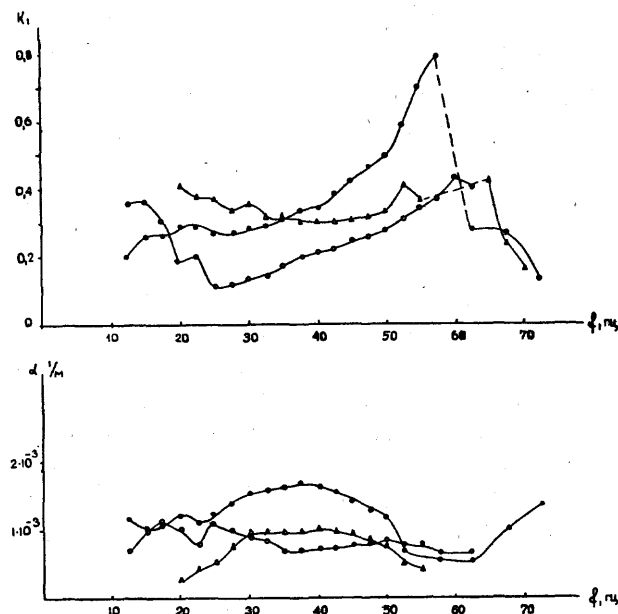


FIG. 6. — Plots  $K_1 = K_1(f)$  and  $\alpha = \alpha(f)$  calculated from the spectra of a single and a double wave reflected from a thin layer and a single wave reflected from an underlying thick layer. The depth of the thin layer is 400 m, of the thick one — 1200 m. The plots  $K_1 = K_1(f)$  and  $\alpha = \alpha(f)$  corresponding to each other are designated by the same symbols.

the plots  $K_1 = K_1(f)$  and  $\alpha_1 = \alpha_1(f)$  varies little with the change of this dependence meanwhile the values  $K = K(f)$  and  $\alpha_1 = \alpha_1(f)$  change not more than by 1.5 to 2 times within the physically possible limits of the ratios  $\frac{\alpha_1}{\alpha}$ . The indicated range of the values being determined for the reflection coefficients is great while for the absorption coefficients it is within the accuracy of the determination of this parameter in real media by other methods. Therefore we can assume that this method permits to determine the values of the absorption coefficients in the investigated medium and the shape of the curves  $K_1 = K_1(f)$  of the coefficients of reflection from a thin layer within the limits of error.

*On the determination of the differences of the absorption coefficients of longitudinal and shear waves.*

The problem of the differences of the absorption coefficients  $\alpha_p$  and  $\alpha_s$  of longitudinal and shear waves in the same media is of rather great interest both for seismology where the waves of these two types are long ago used for the study of the inner structure of the Earth and for seismic prospecting where the use of non-longitu-

dinal — shear and transformed waves began only recently [9 to 11 and others].

The experimental data of the study of the ratio  $\frac{\alpha_s}{\alpha_p}$  in different media are scarce yet. The seismic prospecting data show that in terrigene sediment media the absorption coefficient  $\alpha_p$  of longitudinal waves is much less than the absorption coefficient  $\alpha_s$  of shear waves [4, 5], while in crystal rocks either  $\alpha_p$  is somewhat less than  $\alpha_s$ , or these values are practically equal. The equality of the values  $\alpha_p$  and  $\alpha_s$  for the same frequencies was noted also for the upper mantle of the Earth [12].

Now we shall discuss one of the possible methods of the determination of the absorption coefficients' differences of shear and longitudinal waves from the ratio of the spectra of a longitudinal (PP) wave and a reflected transformed wave (PS) corresponding to the boundary of a thick layer. Since both waves in question emerge from the source as longitudinal the spectrum of the source is excluded from consideration when finding the ratios of their spectra. The ratios of the spectra of both waves can be written as

$$\ln \frac{A_{pp}(f)}{A_{ps}(f)} \approx C + \frac{\alpha_s - \alpha_p}{\cos \gamma} H, \quad (6)$$

where  $C$  is a constant depending on the reflection coefficients and the conversion coefficients,  $\gamma$  is the reflection angle of a shear wave,  $H$  is the depth of the reflecting boundary.

Fig. 7 represents an example of the record of waves PP and PS reflected from the bottom of the ice of a high-mountain glacier and the plots of spectrum ratios of both waves. With the frequency  $f < 75$  c.p.s. the ratio  $\frac{A_{pp}}{A_p}$  remains unchanged and the curves are approximated by horizontal straight lines; with the frequency  $f > 75$  c.p.s. the ratio  $\frac{A_{pp}}{A_p}$  becomes greater. Using the methods similar to those discussed above we find  $\Delta\alpha = \alpha_s - \alpha_p$  as a function of frequency. The plot shows that with  $f < 75$  c.p.s.  $\Delta\alpha = 0$  and in the range of frequencies  $f = 75$  to 130 c.p.s.  $\Delta\alpha$  increases with frequency according to the law close to linear. Thus at higher frequencies shear waves attenuate greater than longitudinal and at lower frequencies the attenuation of both waves is practically the same. These results explain the systematically observed records of higher frequencies of longitudinal waves PP as compared with the transformed waves PS [13]. Analogous dependencies may be observed not only in the ice but in various solid media as well but for rocks the frequency  $f_2$  is lower beginning

with which shear waves attenuate stronger than longitudinal ones. This assumption is based on the fact that in crystal rocks and in

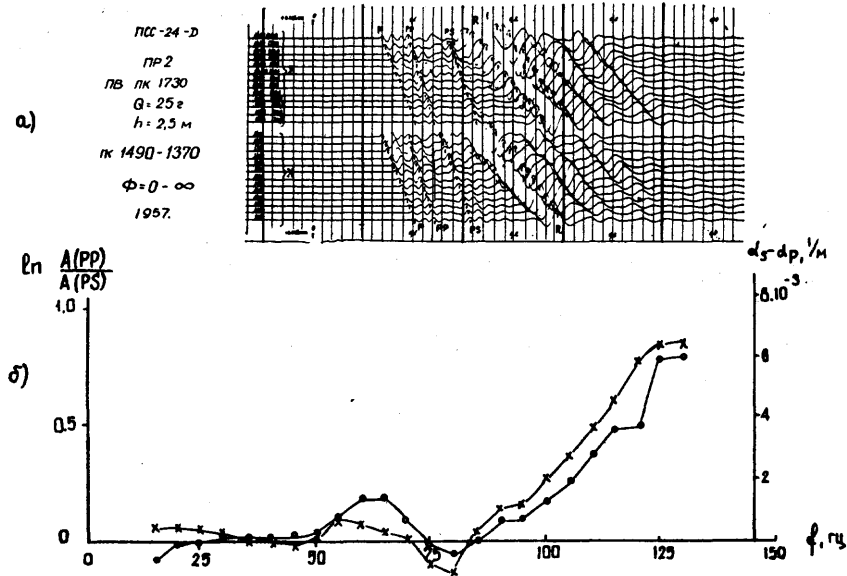


FIG. 7. — a) Records of the waves PP and PS reflected from the bottom of the glacier (depth 115 m) for which the spectra were determined.

b) Plots of the ratios of the the PP and PS waves' spectra by which the difference  $\Delta\alpha = \alpha_s - \alpha_n$  of the absorption coefficients of longitudinal and shear waves as a function of frequency is determined.

limestones the head waves PSP that are very intensive on records obtained by instruments with mean frequency ( $f_{max} = 25$  to 75 c.p.s.) and low frequency ( $f_{max} = 10$  to 25 c.p.s.) characteristics can not be identified on records obtained by intruments with a high frequency characteristic ( $f_{max} = 70$  to 200 c.p.s.) while the high frequency components of PPP waves corresponding to the same interface boundary can be recorded.

In conclusion it should be noted that the discussed methods of the determination of absorption coefficients and coefficients of reflection from thin layers can be applied not only for the waves recorded in the process of seismic prospecting investigations but also for the waves recorded for the purpose of seismological study and deep seismic sounding of the earth's crust. In particular the joint interpretation of the spectra of longitudinal waves generated by one and the same shot and reflected from two boundaries in the Earth's crust will enable the determination of the absorption coeffi-

cients of waves in a layer of the crust between these boundaries as an average function of frequency. The joint interpretation of the spectra of transformed waves and longitudinal transmitted waves generated from earthquakes with the sources in deep parts of the earth's crust or in the mantle will permit to determine the differences of the absorption coefficients of longitudinal and shear waves and their variation with frequency in different layers.

#### REFERENCES

- [1] KHUDZINSKY (L. L.), MELAMUD (A. Ya.), Station of Frequency Analysis of Seismic Motion. Izvestiya AN SSSR, ser. geophys., N° 9, 1957.
- [2] GOLTZMAN (F. M.), Graphycal-Analytical Method of Frequnce Analysis of Seismic Waves within Great Frequency Range. Vestnik Leningradskogo Universiteta, N° 22, 1957.
- [3] McDONALD (F. J.), ANGONA (F. A.), MILLS (R. L.), SENGBUSH (R. L.), VAN NOSTRAND (R. G.), WHITE (J. E.), Attenuation of Shear and Compressional Waves in Pierre Shale. Geophysics XXIII, N° 3, 1958.
- [4] JHADIN (V. V.), Investigation of Attenuation and Dispersion of Seismic Waves by means of Observations in Boreholes Collected Papers II, Problems of Dynamic Theory of Seismic Waves' Propagation. Izdadelstvo L.G.U., 1959.
- [5] YEPINATYEVA (A. M.), Study of Longitudinal Seismic Waves Propagating in Real Layered Media. Trudy Instituta Fiziki Zemli AN SSSR, N° 14 (181), 1960.
- [6] BERZON (I. S.), Determination of Spectrum of Coeffcient of Reflection of Longitudinal Waves from Thin Layer. Trudy Instituta Fiziki Zemli AN SSSR, N° 6 (173), 1959.
- [7] RAYLEIGH (D. V.), Theory of Sound, v. 2 GITTL, 1955.
- [8] BERZON (I. S.), On Some Spectral Peculiarities of Waves Reflected from Thin Layers. Izvestiya AN SSSR, ser. geophys., N° 5, 1959.
- [9] VASILYEV (Yu. I.), Study of Transformed Refracted Waves in Seismic Prospecting. Izvestiya AN SSSR, ser. geophys., N° 3, 1957.
- [10] VOLIN (A. P.), Experience of Reflected Shear Waves' Recording. Collected Papers II Problems of Seismic Waves' Propagation Dynamic Theory Izdatelstvo Leningradskogo Gosudarstvennogo Universiteta, 1959.
- [11] BERZON (I. S.), Some Problems of Interpretation of Transformed Reflected Waves' Plots. Trudy Instituta Fiziki Zemli AN SSSR, N° 6 (173), 1959.
- [12] GUTENBERG (B.), Attenuation of Seismic Waves in the Earth's Mantle.
- [13] BERZON (I. S.), BOKANENKO (L. I.), ISAEV (V. S.), Seismic Investigations on the Tuyuk Su Glacier. Izdatelstvo AN SSSR NM, 1959.



# THE SEISMIC HEAD PULSE

by C. H. DIX.

## ABSTRACT :

Using approximations to a theory originally due to Cagniard, the shape of the seismic head pulse is compared with the shape of the reflected pulse for small angles of incidence from the same source. The source used is the step in the radial displacement potential which is approximately the same as a negative step pressure in a small spherical cavity. The reflection pulse is the sum of a delta function and a step function. In contrast, the head pulse is a step function with no delta function. Spectra for the two pulses are compared and implications regarding detecting instruments are discussed. A numerical example is worked out.

## I. Introduction

In this paper the seismic head pulse is discussed in approximate fashion. We suppose the simplest case in which there is a source in one medium. The second medium is supposed to be elastic, isotropic, homogeneous, semi-infinite, and joined everywhere on an infinite plane. The source is supposed to be spherically symmetrical and longitudinal. The source consists of a step in the potential for the radial displacement. Except for the algebraic sign this source corresponds approximately to the source one would get if one suddenly applied a step pressure in the spherical cavity.

The theory of this case has been completely worked out by Cagniard (Cagniard, 1939). The present treatment is only an approximation designed to make the exact, but very complicated treatment, more useful.

We follow the same procedures that have been followed in previous papers (Dix, 1960).

## II. Theory

In order to make this paper somewhat self-contained, we rewrite the basic result as equation (1) below. This will be recognized as a relation similar to several that occur in (Cagniard, 1939). The path of integration in equation (1) goes from point P to P'' to P''' (*fig. 1*).

$$G_j(r, z, t) = \frac{1}{\pi} (t - t_{Pi})^{\frac{1}{2}} \operatorname{Im} \int_C \frac{c_j(u) u du}{a(u^* r^* + (t - ah - g_j z)^*)^{1/2}} \quad (1)$$

where  $(r, z)$  and  $(o, h)$  are cylindrical coordinates of the receiver and source respectively,  $t$  is time,  $t_{fi}$  is the time of first arrival

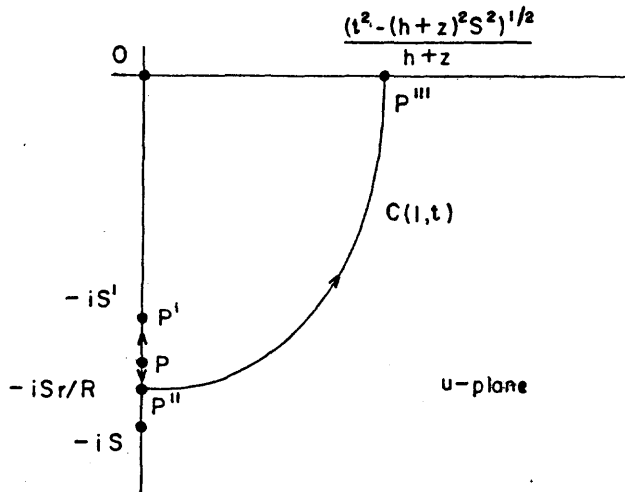


FIGURE I

of the  $j$  contribution,  $u$  is a separation variable,  $\text{Im}$  is "imaginary part of",  $c_1 = af_1$ ,  $c_2 = u^2 \varphi$ ,  $c_3 = f_1$ ,  $c_4 = b\varphi_1$ ,  $a = (u^2 + S^2)^{1/2}$ ,  $b = (u^2 + s^2)^{1/2}$ ,  $a' = (u^2 + S'^2)^{1/2}$ ,  $b' = (u^2 + s'^2)^{1/2}$ ,  $f_1 = (D_2 - D_1)/(D_2 + D_1)$ ,  $\mu = \rho/s^2$ ,  $\mu' = \rho'/s'^2$ ,  $C = \mu/[2(\mu - \mu')]$ ,  $C' = -\mu/[2(\mu - \mu')]$ ,  $D_1 = u^2(u^2 + Cs^2 + C's'^2)^2 - a'b'(u^2 + Cs^2)^2 + Cs^2 C's'^2 a'b'$ ,  $D_2 = u^2 ab a'b' - ab(u^2 + C's'^2)^2 + Cs^2 C's'^2 ab'$ ,  $g_1 = g_3 = a$ ,  $g_2 = g_4 = b$ ,  $\varphi_1 = 2a[(u^2 + Cs^2 + C's'^2)(u^2 + C's'^2) - a'b'(u^2 + Cs^2)]/(D_2 + D_1)$ ,

$S$  and  $S'$  are longitudinal wave slownesses,  $s$  and  $s'$  are transverse wave slownesses,  $\rho$  and  $\rho'$  are densities in the unprimed medium (containing the source) and the primed medium. The indicial displacement components (response to unit step source) are

$$L_z = L_{z0} + L_{zL} + L_{zT}, L_r = L_{r0} + L_{rL} + L_{rT}, L_{zL} = -(\partial/\partial t) C_1, \\ L_{zT} = -(\partial/\partial t) C_2, L_{rL} = (\partial/\partial r) C_3, L_{rT} = (\partial/\partial r) C_4.$$

Here  $L_{z0}$  and  $L_{r0}$  are incident contributions. The subscripts L and T refer to longitudinal and transverse contributions. The

path  $C(j, t)$  is the map in the  $u$ -plane of  $0 \leq \omega \leq \pi/2$  by  $t = iur \cos \omega + ah + g, z$  for fixed  $t$ .

We concern ourselves only with the case  $j = 1$  so that we are looking only at the vertical longitudinal part.

Using arguments employed many times (e.g. (Dix, 1960)), the path  $C(1, t)$  may be replaced by the path  $PP'$  along the negative imaginary axis.

We use dimensionless variables  $v = u/S$ ,  $w = v^2$ ,  $\tau = t/Sh$ ,  $\eta = r/h$ ,  $\xi = z/h$ ,  $R_0 = R/h$   $(R^2 = r^2 + (z+h)^2)$

$\alpha = a/S$ ,  $\alpha' = a'/S$ ,

$\beta = b/S$ ,  $\beta' = b'/S$ ,  $\gamma_i = g_i/S$ ,

$J = S'/S$ ,  $j = s/S$ ,  $j' = s'/S$ ,  $d_1 = D_1/S^6$ ,

$d_2 = D_2/S^6$  and  $\gamma = \rho'/\rho$ .

Then  $C's'^2 = -\gamma Cs^2$  or  $C'j'^2 = -\gamma Cj^2 = -\gamma B$ .

We transfer from the  $u$ -plane to the  $v$ -plane. Then we pass over to the  $\alpha$ -plane. When we do this the path  $PP'$  in Figure 1 goes over into the path  $QQ'$  as shown in Figure 2.

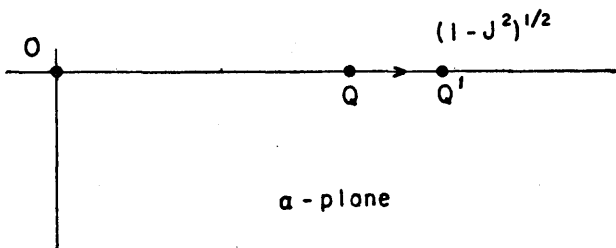


FIGURE 2

Making these changes (1) becomes (for  $j = 1$ )

$$C_i(r, z, t) = 1(t - t_{F_i}) \frac{2S}{\pi h} \operatorname{Im} \int_Q^{Q'} \frac{(G_b + a' G_a) a da}{R_0(a^2 - 2a_i a + a_i^2 + a_s^2)^{1/2}} \quad (2)$$

where  $(d_2 - d_1)/(d_2 + d_1) = G_5 + \alpha' G_6$ ,

$$G_5 = (G_1 G_3 - G_2 G_4 \alpha'^2) / (G_3^2 - G_4^2 \alpha'^2),$$

$$G_6 = (G_2 G_3 - G_1 G_4) / (G_3^2 - G_4^2 \alpha'^2),$$

$$G_1 = -(w - \gamma B^2) \alpha \beta - \gamma B^2 \alpha \beta' - w(w + B(1 - \gamma))^2,$$

$$G_2 = w \alpha \beta \beta' + (w + B)^2 \beta' + \gamma B^2 \beta, G_3 = G_1 + 2w(w + B(1 - \gamma))^2,$$

$$G_4 = -G_2 + 2w \alpha \beta \beta',$$

$$\alpha_1 = (1 + \xi)/R_0^2 \text{ and } \alpha_2 = \pi(\tau^2 - R_0^2)^{1/2}/R_0^2.$$

The  $G_5$  contribution is zero because it is purely real.  $G_6$  is real on  $QQ'$  as is also the rest of the integrand except for  $\alpha'$  which is negative imaginary. So (2) may be written

$$C_1(r, z, t) = -1(t - t_{F1}) \frac{2S}{\pi R} \int_Q^{Q'} \left[ \frac{\alpha((1-J^*)^{1/2} + \alpha)^{1/2} G_6}{(\alpha - \alpha_i - i\alpha_s)^{1/2}} \right] \left\{ \frac{((1-J^*)^{1/2} - \alpha)^{1/2}}{(\alpha - \alpha_i + i\alpha_s)^{1/2}} \right\} d\alpha \quad (3)$$

where the square bracket term is slowly varying in the interval  $Q \leq \alpha \leq Q'$  and the curly bracket expression is singular at each end being infinite at  $Q$  and zero at  $Q'$ . (3) is exact.

It seems hopeless to try to integrate (3) exactly. However, the square bracket expression may be computed numerically for various cases and it is seen that its variation is small (if we avoid times close to the reflection time,  $SR!$ ). We can use the mean value theorem and

$$\int_Q^{Q'} \frac{((1-J^*)^{1/2} - \alpha)^{1/2}}{(\alpha - i\alpha_i + i\alpha_s)^{1/2}} d\alpha = \frac{\pi}{2}(Q - Q') \quad (4)$$

to get

$$C_1(r, z, t) = -1(t - t_{F1}) \frac{S(Q' - Q)}{R} \text{mean} \left[ \frac{\alpha((1-J^*)^{1/2} + \alpha)^{1/2} G_6}{(\alpha - \alpha_i - i\alpha_s)^{1/2}} \right] \quad (5)$$

Notice that at  $t = t_{F1}$ ,  $Q' = Q$  so  $C_1(R, z, t_{F1}) = 0$  as a limit as  $t \rightarrow t_{F1}$ , from values of  $t$  such that  $t > t_{F1}$ . Thus the graph of  $C_1$  will look like Figure 3 as  $G_6$  is negative.

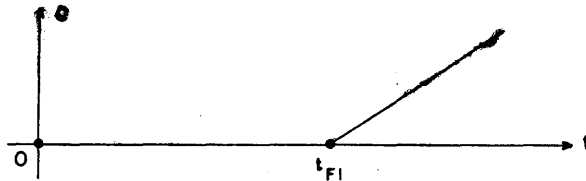


FIGURE 3

Consequently  $L_{zL}$  looks like Figure 4.

### III. Comparison with reflections.

Referring to (Dix, 1960) and to Figure 4 above, we see that the principle difference between the reflected seismic pulse and the head pulse is that the head pulse contains only the step function whereas the reflected pulse contains the step function and also the

delta function. The delta function has a flat spectrum whereas the step function has a spectrum which is inversely proportional to the

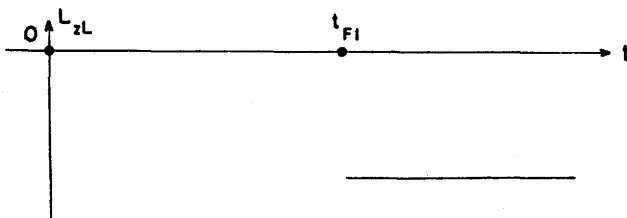


FIGURE 4

frequency. Thus, recording equipment which is to be used for recording reflections is generally peaked at as high a frequency as possible so as to take advantage of the delta function contribution and minimize the step function contribution. On the other hand, recording equipment designed to record head waves should cut high frequencies relatively to low frequencies so that the delta function contributions will not be emphasized.

Naturally it is to be understood that in practice a pure head wave may only rarely exist largely because of the fact that the velocity of propagation tends to increase with increasing depth. This being the case, what we refer to as a head wave is likely to be a mixture of a true head wave and an ordinary refracted wave. Irregularities in the interface will also lead to such a mixture.

It seems clear that if we wish our instruments to separate head waves from other waves, it is generally desirable to cut the high frequency response and increase the low frequency response.

The above remarks are to be taken in an approximate sense as the source is not the idealized step in the radial displacement potential.

#### IV. Numerical example.

The following example represents a very rough approximation to the situation encountered in the crust of the earth. The velocity corresponding to the crustal velocity is taken to be 7.3 kilometers per second and the subcrustal velocity is taken to be 8.1 kilometers per second. We suppose Poisson's ratio is  $1/4$  in each medium and that the density ratio ( $\rho'/\rho$ ) is  $4/3$ . The source is taken to be 40 kilometers from the interface and the receiver positions are also 40 kilometers from the interface on the same side as the source.

The critical horizontal distance for this case is 165 kilometers beyond which the head wave begins to appear. In order to avoid confusion with the rather singular reflected wave, we consider a horizontal distance of 240 kilometers. We apply the result of formula (5) to this case making the calculations partly with the help of a digital computer for  $G_6$ , and with the help of a slide rule for all of the other computations. The values of the square bracket expression in formula (5) are shown in Figure 5 for four times after

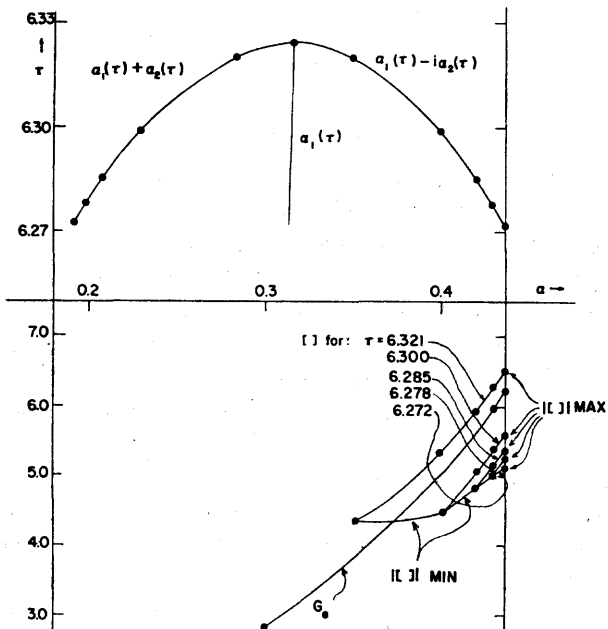


FIGURE 5

the time of the beginning of the head pulse. It is seen from the figure that the variation of the square bracket expression is small. We can, in fact, use the maximum value and the minimum value to get outside limits of the range of variation of  $G_6$ . This we have done in Figure 6 which shows that Figures 3 and 4, though not entirely accurate, are nevertheless good enough for practical purposes in the present example. We can, in fact, compare the vertical component of the displacement due to the head wave at a distance of 240 kilometers with the reflection using the same source but recording at a distance of 40 kilometers. The numerical values are shown as the relation

$$L_{zL}(40, 40, 12.3) \approx -1.92 \times 10^{-4} \delta(t - 12.3) - 3.81 \times 10^{-5} 1(t - 12.3)$$

(ref. 1) (6)

$$L_{zL}(240, 40, 34.4) \approx -5.5 \times 10^{-4} 1(t - 34.4) \text{ (head).}$$

The reflection part comes from the work in the earlier paper (Dix, 1960).

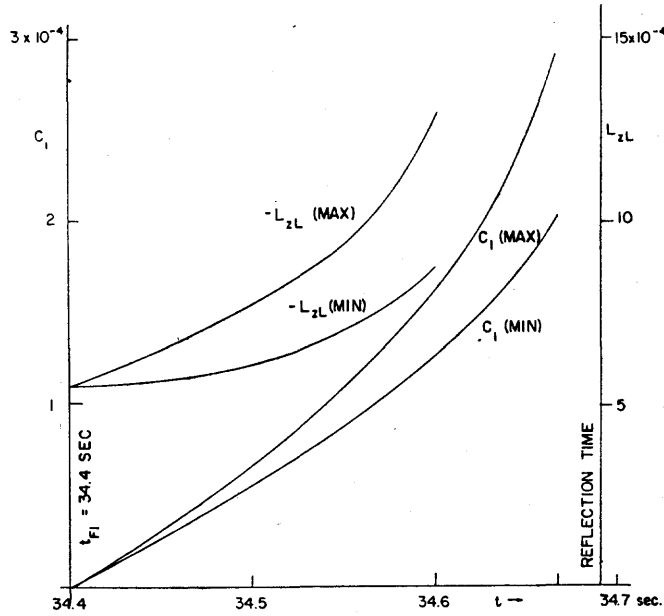


FIGURE 6

The only part of this calculation that is particularly difficult is the calculations of  $G_6$  and this is tabulated for several values of the elastic parameters in the Table. Using the Table a fairly large class of numerical examples may be computed using a slide rule.

TABLE

$\sigma$	$\sigma'$	$Y$	$G_6$ for $J = 0.9$	$G_6$ (for $J = 0.7$ )
0.25	0.25	4/3	— 6.29	— 4.59
0.25	0.25	1	— 5.77	— 4.42
0.25	0.25	3/4	— 4.75	— 4.48
0.25	0.35	4/3	— 3.72	— 3.44
0.25	0.35	1	— 3.89	— 3.64
0.25	0.35	3/4	— 3.90	— 3.70
0.35	0.25	4/3	— 8.05	— 6.22
0.35	0.25	1	— 7.21	— 5.91
0.35	0.25	3/4	— 6.14	— 5.36
0.35	0.35	4/3	— 5.18	— 7.06
0.35	0.35	1	— 5.69	— 4.37
0.35	0.35	3/4	— 5.32	— 4.46

REFERENCES

CAGNIARD (L.), Réflexion et Réfraction des Ondes Séismiques Progressives, Paris (1939).

DIX (C. H.), The Reflected Seismic Pulse, Journal of Geophysical Research, Vol. 66, 1961, p. 227-233.

# DOUBLE REFRACTION IN AEOLOTROPIC LAYERS AND SOME PECULIARITIES OF LOW VELOCITY LAYER IN EARTH'S MANTLE

by BALAKINA (L. M.), SHIROKOVA (H. I.), VVEDENSKAYA (A. V.).

I. The presented paper contains the results of the investigation of the structure of the Earth's mantle based on the use of the observed amplitudes of the first displacements in longitudinal and transverse waves from earthquakes. Since the values of these amplitudes depend both on the conditions of the generation of waves in an earthquake source and on the conditions of their propagation the problem of the investigation of the Earth's mantle structure is inseparably connected with the study of the peculiarities of earthquakes' sources, being directed sources of disturbances. For this purpose we consider theoretical fields of displacements with a directed source of disturbances in isotropic and homogeneous elastic space. Such a source of disturbances is a fault area (accepted in the form of a circle with the radius  $\rho$ ) whose opposite faces move one relative to the other in the fault plane by the value «  $b$  ». The area is located in the plane  $xz$  of the system  $xyz$  and includes the origin of the coordinates. The axis  $y$  is the normal to the area.

To determine the position of the area corresponding to the position of the fault surface in the source in relation to the observatories a system of coordinates  $\bar{x}$ ,  $\bar{y}$ ,  $\bar{z}$  is introduced whose origin coincides with the origin of the system  $x$ ,  $y$ ,  $z$ , and the axes are directed to North, East, Zenith respectively. The coordinates  $\bar{x}$ ,  $\bar{y}$ ,  $\bar{z}$  of the observatories in this system can be obtained by means of the following formulas

$$\bar{x} = R \cos e \cos Az, \quad \bar{y} = R \cos e \sin Az, \quad \bar{z} = R \sin e$$

where  $Az$  is the azimuth from the epicentre to the station,  $e$  is the angle made by a ray or a tangent to the ray emerging from the source with a horizontal plane,  $R$  is the distance along the ray from the source to the station.

The displacements in waves P, SV and SH for a selected source of disturbances can be determined by the formulas [1].

$$U_p = -\frac{c^*}{\pi a^*} \frac{yz}{R^* \sqrt{R^* - y^*}} \varphi b \quad (1)$$

$$U_{SH} = \frac{\rho b}{2\pi R^* \sqrt{R^* - y^*} \cos e} \left[ y (\bar{x}n_x - \bar{y}m_x) + z (\bar{x}n_y - \bar{y}m_y) \right] \quad (2)$$

$$U_{SV} = \frac{\rho b}{2\pi R^* \sqrt{R^* - y^*} \sin e \cos e} \left[ 2yz \sin^2 e + \bar{z} (zl_y + yl_z) \right] \quad (3)$$

where  $a$  and  $c$  are the propagation velocities of longitudinal and transverse waves;  $m_i$ ,  $n_i$ ,  $l_i$  are the cosines of the angles made by the direction  $x$ , ( $x_i = y, z$ ) with the axes  $\bar{x}$ ,  $\bar{y}$ ,  $\bar{z}$  respectively.

The position of the fault plane in a source or the position of the axes  $x$ ,  $y$ ,  $z$  in the system  $\bar{x}$ ,  $\bar{y}$ ,  $\bar{z}$  is established on the basis of the observed signs of displacements in longitudinal and transverse waves (We believe that the heterogeneity of the structure of the Earth's mantle does not change these characteristics of the displacement field). The position of the axes  $x$ ,  $y$ ,  $z$  is determined as a result of the construction on the Wulff stereographic projection whose axes coincide with the axes of the system  $\bar{x}$ ,  $\bar{y}$ ,  $\bar{z}$ . Using the observed signs of displacements in P, SV, SH we do not solve the problem about the position of the axes  $y$  and  $z$  unambiguously. As formulas (1), (2), (3) imply the change of the places of the axes  $y$  and  $z$  does not change the sign of the values  $U_p$ ,  $U_{sv}$ ,  $U_{sh}$ . Taking into account the direction of radiation we use such values that do not depend on this ambiguity.

II. For the study of the upper layers of the Earth's mantle [2] the observations of only longitudinal waves were used since at near epicentral distances the use of the S-waves' records is rather difficult. The values  $U_p$  from the formula (1) can be found with the accuracy to the factor  $\rho b$  which is an unknown value for each separate earthquake. To exclude this value we used the ratio of displacements in points of the location of seismic stations to the displacement in one of these points.

$$\frac{U_{P_k}}{U_{P_i}} = \frac{y_k z_k R_i^* \sqrt{R_i^* - y_i^*}}{y_i z_i R_k^* \sqrt{R_k^* - y_k^*}} = K_{(p)} \quad (4)$$

If for some points of the space to calculate the relative displacements  $K_{(p)}$  in the wave P on the basis of formula (4) and to compare them with the observed values for the same points then all the differences (if not to take into account the errors due to the incomplete coincidence of the observed source with the theoretical one) of the observed data from theoretical will be caused by the differences

of the properties of the Earth's mantle from the properties of the homogeneous and elastic medium.

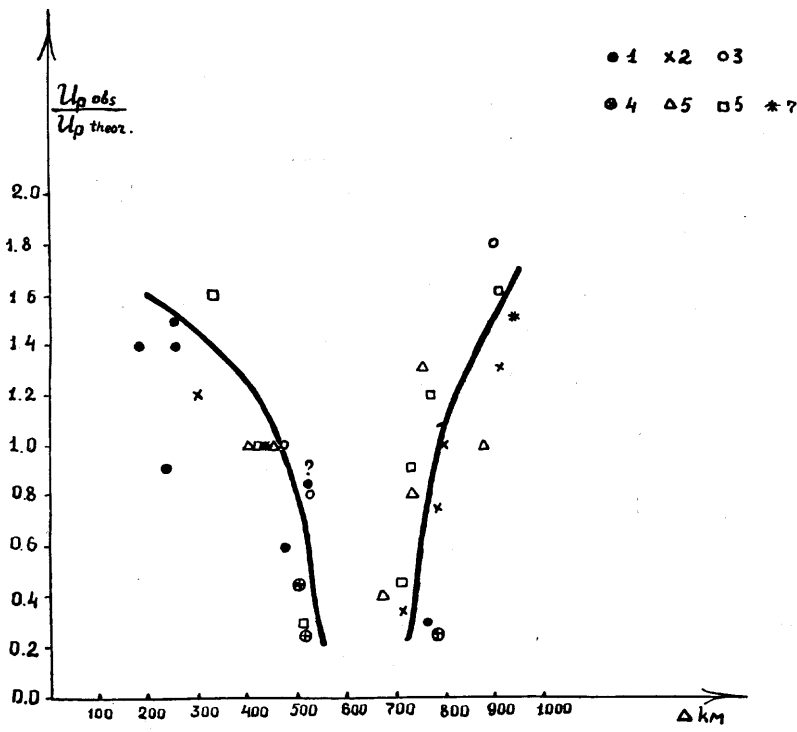
To compare the observed data with theoretical we must take into account the effect of the earth's surface and the interface boundary within the earth's crust on the amplitudes of displacements in incident waves. This was accomplished with the help of the data presented in paper (3). When calculating the observed displacement values the characteristics of the instruments for a sinusoidal impulse was taken into consideration [4].

Records of deep Hindu-Kush earthquakes obtained at seismic stations of the Soviet Union are used for the present investigations.

7 earthquakes with the focal depth about 200 km and coordinates  $\varphi \approx 36^{\circ}5$  N;  $\lambda \approx 70^{\circ}5$  E were interpreted.

Fig. 1 represents the plot of the value of the ratio of the observed one to theoretical calculated from formula (4) against epicentral distance.

Fig. 1 imply that at epicentral distances from 500 to 700 km the minimum of the displacement amplitudes is observed. The pre-



1-9.IX.1954; 2-4.X.1951; 3-2.VIII.1954; 4-16.III.1955; 5-5.VI.1952; 6-12.VI.1951; 7-27.XI.1952.

sence of such a minimum can be explained by the existence of a low velocity layer in the upper layers of the Earth's mantle.

The fact that up till now the shadow zone for the earthquakes with the focal depth of about 200 km is not observed seems to be explained by two factors :

a) the shadow zone at such depths has an insignificant width and could be overlooked in the process of determinations performed without taking into account the direction of radiation; b) in various regions of the globe the character of the velocity variation with depth in the upper layers of the mantle may be different.

The presence of the amplitude minimum at such epicentral distances permits to conclude that the character of the velocity variation with depth in the upper layers of the Earth's mantle (up to 200 km) considerably differs from the existing conception. The law of the velocity variation must be such that the following conditions might be satisfied : 1) the calculated arrival times must be equal to the observed ones, 2) the shadow zone must begin at the distance of about 500 km, 3) the width of the shadow zone must be of the order of  $2^{\circ}$ . The following velocity cross-section satisfies these conditions (fig. 2).

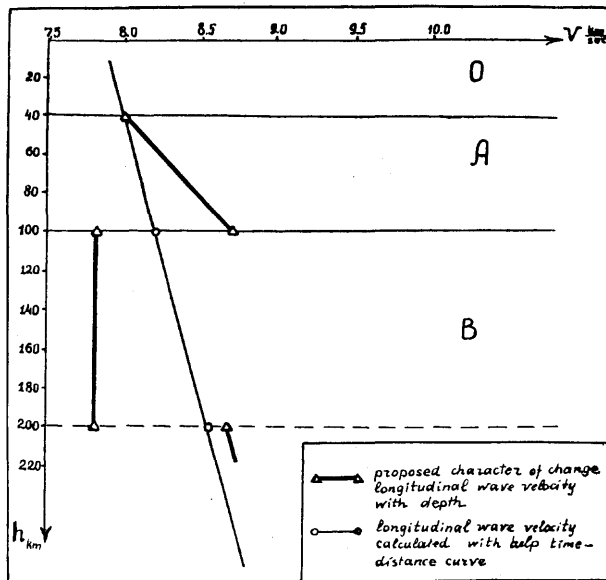


FIG. 2.

Beginning with the bottom of the earth's crust and to the depth of 100 km the velocity changes according to the law [5].

$$v = v_1 \left( \frac{r}{r_1} \right)^{-b} \quad (5)$$

where  $v_1$  is the velocity under the bottom of the Earth's crust equal to 8.00 km/sec,  $r_1$  is the distance from the centre of the Earth to the bottom of the earth's crust,  $b = \text{const}$ . We found that  $b = 9$ . At the depth of 100 km the velocity amounts to the value  $v_2 = 8.71$  km/sec according to formula (5). After that it jumps down to the value 7.8 km/sec and preserves the value to the depth of 200 km (fig. 2). At this depth the velocity jumps up to the value 8.65 km/sec and varies according to the law (5) at  $b = 4$ .

Using the method of Båth [5] we calculate the distance at which the shadow zone must begin and the time necessary for the propagation of the wave from the source to the beginning of the shadow zone on the accepted assumptions concerning the character of the velocity variation with depth. The horizontal projection of the ray S propagating in the interval A (fig. 2) will be the following

$$S = \frac{l_2 - l_1}{1 + b} \quad (6)$$

The travel time for this section will be

$$t = \frac{r_1^{-b}}{v_1} \int_{r_1}^{r_2} \frac{r^{1+b} dr}{(r^{1+b} - r_1^{1+b} \sin i_i)^{1/2}} = \frac{r_1}{v_1(1+b)} \left\{ \cos i_i - \left[ \left( \frac{r_2}{r_1} \right)^{1+b} - \sin i_i \right]^{1/2} \right\} \quad (7)$$

For the beginning of the shadow zone  $i_2 = 90^\circ$ , hence

$$t = \frac{r_1}{v_1(1+b)} \cos i_i \quad (8)$$

The travel time of the P wave to the point corresponding to the beginning of the shadow zone and the distances from the epicentre to the shadow zone according to fig. 2 are equal respectively :

$$t = t_0 + t_A + t_B \quad ; \quad S = S_0 + S_A + S_B.$$

If to accept the following thicknesses of layers  $d$  and the velocity values  $v$  for the earth's crust : for granite  $d_{01} = 25$  km,  $v_{01} = 5.5$ ; for basalt  $d_{02} = 15$  km,  $v_{02} = 6.00$  km/sec then  $t = 72$  sec and  $S = 506$  km. The width of the shadow zone can be calculated approximately using formula (6). It will be equal to  $2^\circ$ .

In fig. 3 the travel time curves of Rozova, Jeffreys-Bullen and the travel time curve calculated for a given velocity model are repre-

sented. The figure shows that the calculated curve lies between the Rozova curve and the Jeffreys-Bullen curve. It should be borne

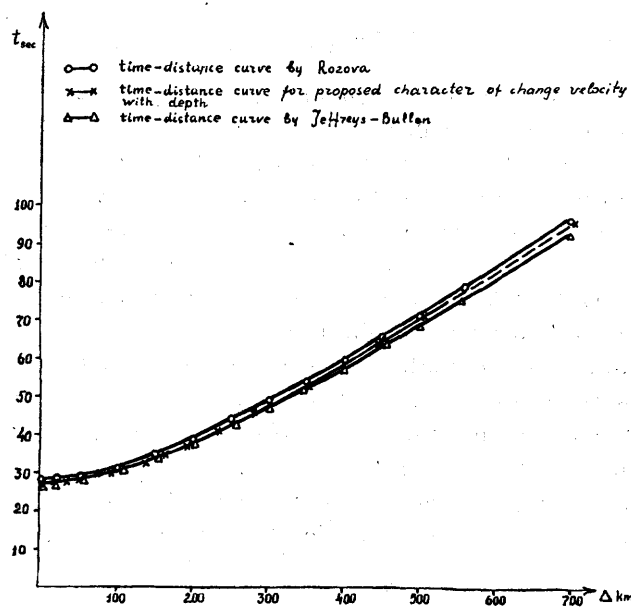


FIG. 3.

in mind that the discussed model is not the single one. The indefiniteness in choosing the thickness of the layer and its depth does not permit to establish the exact value of the velocity and its gradient.

The obtained results permit only to say that :

1) The velocity variation from the bottom of the earth's crust to the upper boundary of the low velocity layer has a considerably greater gradient than according to the velocity curve constructed using the data of the travel time curve.

2) The boundaries of the low velocity layer are sharp (the variation of the velocities  $\sim 10^\circ$ ).

III. As is known [6] the observations of the displacement field of longitudinal P and transverse (SV and SH) waves propagating in deeper layers of the earth's mantle show an increase of amplitudes of waves P and SV in relation to waves SH when seismic rays penetrate to the depths : 250 to 500; 900 to 1 000; 1 200 to 1 300, 1 800 and about 2 200 km. The plot of this function is given in fig. 4. Where the abscissa axis represents the epicentral distances of observatories and the corresponding depths of the penetration of seismic rays for each curve. The ordinate axis represents the

values  $\frac{U_p}{U_{SH}}$  and  $\frac{U_{SV}}{U_{SH}}$  obtained from observations being related to the function  $\mathcal{F}_1$  and  $\mathcal{F}_2$  that are determined on the basis of formulas (1), (2) and (3)

$$\mathcal{F}_1 = \frac{-2yz \cos e}{y(\bar{x}n_z - \bar{y}m_z) + z(\bar{x}n_y - \bar{y}m_y)} \quad (9)$$

$$\mathcal{F}_2 = \frac{-2yz \sin^2 e + \bar{z}(z l_y + y l_z)}{[y(\bar{x}n_z - \bar{y}m_z) + z(\bar{x}n_y - \bar{y}m_y)] \sin e} \quad (10)$$

It can be shown that these peculiarities of the displacement field may be connected with the phenomenon of the polarization of transverse waves with a double refraction in aeolotropic layers of the Earth's mantle corresponding to the above-mentioned depths. And the properties of the aeolotropic medium must be such that the velocity gradient of the SH wave is different from that of the SV wave while the velocity ratio of the P and SV waves remains constant and equal to the velocity ratio of longitudinal and transverse waves in the isotropic part of the mantle.

Such relations between the velocities of waves P, SV and SH can occur in the transversely isotropic medium whose axis of symmetry is the vertical direction. If the axis Z coincides with the axis of symmetry of the material the following relations are fulfilled between the elastic constants not equal to zero of the aeolotropic medium [7].

$$C_{11} = C_{22} = A$$

$$C_{33} = C$$

$$C_{13} = C_{23} = F$$

$$C_{44} = C_{55} = L$$

$$C_{66} = \frac{1}{2}(C_{11} - C_{13}) = N$$

In the general case of the transversely isotropic medium disturbances are not divided into longitudinal and transverse waves [8]. The propagation of longitudinal and transverse waves becomes possible when the following relation between the elastic constants is fulfilled [8].

$$A = C = F + 2L$$

Three values of the propagation velocities of disturbances are determined on the basis of the motion equations in the transversely isotropic elastic medium with the density  $\rho$ .

1. The velocity of longitudinal waves :  $a = \sqrt{\frac{A}{\rho}}$

2. The velocity of transverse waves whose plane of motion passes through the Z axis and the direction of propagation is

$$C_V = \sqrt{\frac{\mathcal{L}}{\rho}}$$

3. The velocity of transverse waves whose plane of motion is perpendicular to this plane :  $C_H = \sqrt{\frac{\mathcal{N} \sin^2 i + \mathcal{L} \cos^2 i}{\rho}}$  where  $i$  is the angle between the direction of propagation and the axis Z.

If the axis Z is directed to the zenith, i.e. it coincides with the  $\bar{z}$  axis the last two values of the velocities correspond to waves SV and SH. The greatest difference between the velocities of waves SV and SH is when the motion is horizontal where the velocity of

SH waves is equal to  $\sqrt{\frac{\mathcal{N}}{\rho}}$

Thus in relation of the SV and SH waves the medium is a single axis crystal, the ray of the SV wave being an analog to a common and the ray SH an analog to an uncommon ray in optics.

If the medium possesses some absorption the waves P and SV will be absorbed equally in all directions, but the absorption of the SH waves will depend on the angle between the direction of propagation and the axis  $\bar{z}$ .

Now let the waves P, SV and SH propagating in the Earth's mantle penetrate into layers whose mechanical properties answer the properties of a transverse isotropic body for which  $\lambda = C = J + 2L$ . In this layer the rays SH will deviate from the rays SV. Since in the isotropic and transversely isotropic media the wave-surfaces of

P and SV are concentric spheres at the condition  $\frac{\lambda + 2u}{\mu} = \frac{J + 2L}{\mathcal{L}}$

the fronts of these waves remain parallel and the rays coincide when transmitting from one medium into another. Therefore the change of the mechanical properties of the medium at the interface boundary will have no effect on the amplitude ratios of displacements in P and SV waves. It will cause a change of amplitudes of displacements in P and SV waves in relation to SH waves. If the medium possesses some absorption the aeolotropy of the attenuation can also cause an increase of amplitudes of waves P and SV in relation to waves SH. Both effects are the most strong in the cases when the angle of incidence at the aeolotropic layer is close to right, i.e. when the tops of the rays are within the layer. They disappear when the incidence of rays is more steep and the rays' tops are within an isotropic medium.

Let the Earth's mantle satisfy the properties of an elastic body in general as it concerns seismic waves but its separate layers are aeolotropic.

Having this condition in mind we shall make attempts to find the dependence between the elastic constants at the depths where the phenomenon of double refraction is observed being the cause of the maxima of the curves in fig. 4. Let one of such maxima corres-

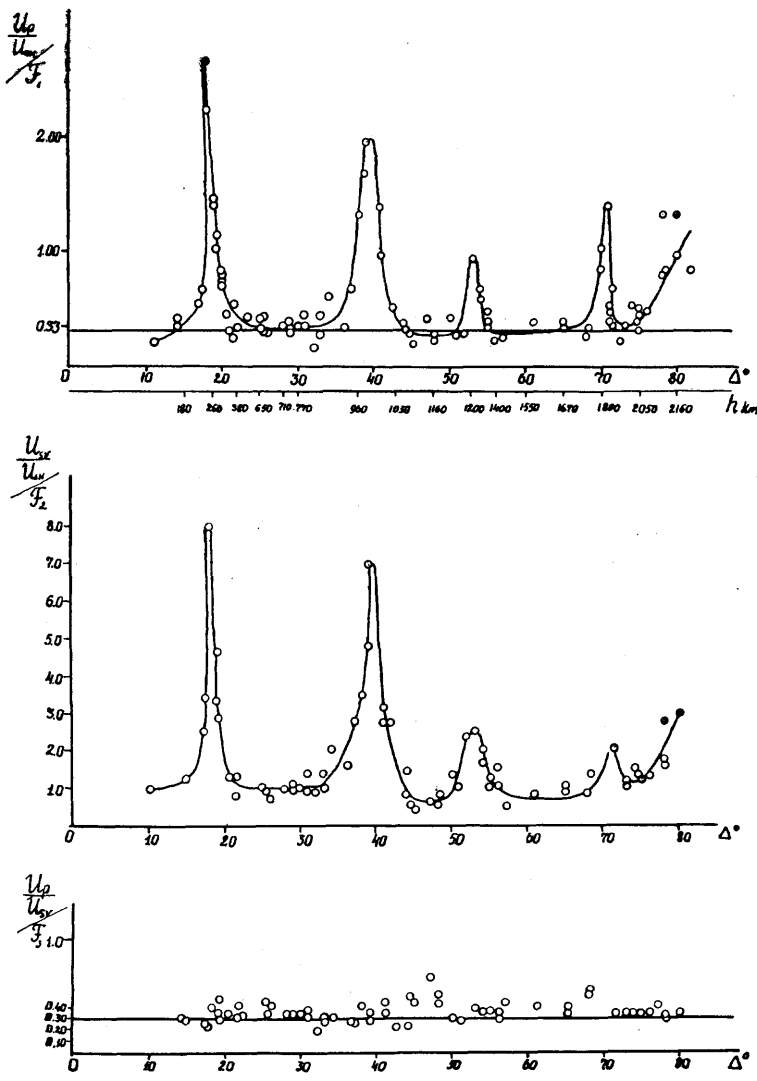


FIG. 4.

pond to the epicentral distance  $\theta'$ . We assume that the functions  $\mathcal{F}_1$  and  $\mathcal{F}_2$  determining the direction of the radiation from the source remain constant within the limit of the ray pencil under consideration.

The displacement amplitudes at the distance  $\theta$  are determined by the following expression [9]

$$U = \frac{1}{R} \sqrt{\frac{\mathcal{K}}{\sin \theta} \frac{ctg e}{d\theta}} \quad (14)$$

where  $R$  is the radius of the Earth,  $\mathcal{K}$  is the energy radiated by the source within a single solid angle in the direction  $e$ . Using formula (14) we assume that the change of the angle of emergence with the epicentral distance is such that the function  $e = f(\theta)$  is continuous and  $\frac{de}{d\theta} > 0$ . This assumption excludes from our consideration the maximum on the curve at  $20^\circ$  (if the loop of the curve does exist there).

Proceeding from formula (14) we can write the following expression for the displacement ratios in waves P, SV and SH.

$$\frac{U_P}{U_{SH}} = \sqrt{\frac{\mathcal{K}_P}{\mathcal{K}_{SH}} \frac{ctg e_P \left( \frac{de}{d\theta} \right)_P}{ctg e_{SH} \left( \frac{de}{d\theta} \right)_{SH}}}; \quad \frac{U_{SV}}{U_{SH}} = \sqrt{\frac{\mathcal{K}_{SV}}{\mathcal{K}_{SH}} \frac{ctg e_{SV} \left( \frac{de}{d\theta} \right)_{SV}}{ctg e_{SH} \left( \frac{de}{d\theta} \right)_{SH}}}$$

The last expression implies that the ratios of the values  $\mathcal{K}_P$ ,  $\mathcal{K}_{SV}$ , and  $\mathcal{K}_{SH}$ , are equal to those of the displacement amplitudes squared in waves P, SV and SH in isotropic homogeneous medium with a constant velocity ratio of waves P and S. Therefore according to expressions (1) and (2) we obtain

$$\frac{\mathcal{K}_P}{\mathcal{K}_{SH}} = \frac{c^4}{a^4} \mathcal{F}_1(m, n, l, \lambda z, e); \quad \frac{\mathcal{K}_{SV}}{\mathcal{K}_{SH}} = \mathcal{F}_2(m, n, l, \lambda z, e)$$

Hence :

$$\sqrt{\frac{ctg e_P \left( \frac{de}{d\theta} \right)_P}{ctg e_{SH} \left( \frac{de}{d\theta} \right)_{SH}}} = \frac{c^4}{a^4} \frac{U_P}{U_{SH}} / \mathcal{F}_1; \quad \sqrt{\frac{ctg e_{SV} \left( \frac{de}{d\theta} \right)_{SV}}{ctg e_{SH} \left( \frac{de}{d\theta} \right)_{SH}}} = \frac{U_{SV}}{U_{SH}} / \mathcal{F}_2$$

$$\frac{a^4}{c^4} \frac{U_P}{U_{SH}} / \mathcal{F}_1 = K_1(\theta); \quad \frac{U_{SV}}{U_{SH}} / \mathcal{F}_2 = K_2(\theta)$$

Then we obtain

$$\operatorname{ctg} e_P \left( \frac{de}{d\theta} \right)_P = K^*(\theta) \operatorname{ctg} e_{SH} \left( \frac{de}{d\theta} \right)_{SH}$$

$$\operatorname{ctg} e_{SV} \left( \frac{de}{d\theta} \right)_{SV} = K^*(\theta) \operatorname{ctg} e_{SH} \left( \frac{de}{d\theta} \right)_{SH}$$

Let us integrate these equations in the interval of  $\theta_1$  to  $\theta'$  where  $\theta_1$  is the epicentral distance at which the ray emerges propagating still in the isotropic part of the mantle. The critical values of the angles of emergence in the interval  $\theta_1 — \theta'$  will be designated :  $e_1$  and  $e_P', e_V', e_H'$ . Using the theorem of the average we obtain the following relation between the angles of emergence of waves P, SV and SH as a result of the integration of the latter equations

$$\ln \sin e_P' — \ln \sin e_1 = K^2 (\ln \sin e_H' — \ln \sin e_1) \quad (15)$$

$$\ln \sin e_V' — \ln \sin e_1 = K^2 (\ln \sin e_H' — \ln \sin e_1)$$

Now we shall pass on to the values of velocities and depths of ray penetration from the angles of emergence in these formulas. For this purpose the dependence determined by the formula will be used :

$$\cos e = \frac{v_0}{R} \cdot \frac{r}{v}$$

where R is the radius of the Earth, r is the radius of the ray top, v is the velocity in the top of the ray,  $v_0$  is the velocity at the surface of the Earth. Let the limiting values of the velocity values and the depths of ray penetration in the interval  $\theta_1 — \theta'$  be :  $a, c, r$  and  $a', c_V', c_H', r_P', r_V', r_H'$ .

Applying the method of series and limiting ourselves to the first terms of the expansion we shall write the expression (15) as follows

$$\frac{r_P'^2}{a'^2} a^2 = \frac{r_V'^2}{c_V'^2} c^2 ; \frac{r_H'^2}{c_H'^2} = \frac{\frac{r_V'^2}{c_V'^2} + (K^2 - 1) \frac{r^2}{c^2}}{K^2}$$

If the values of the velocities  $a', c_V', c_H'$  in the ray tops penetrating into the aeolotropic layer are determined on the basis of expressions (11), (12) and (13) at  $\cos i = 0$  we can write

$$A = \frac{\lambda + 2\mu}{\mu} L ; \quad \frac{r_H'^2}{q_b} = \frac{\frac{r_V'^2}{L} + (K^2 - 1) \frac{r^2}{\mu}}{K^2}$$

Such relations can be true for the elastic constants A, L and q<sub>b</sub> at the depths 900 to 1 000, 1 200 to 1 300; 1 800 and about 2 200 km.

Within the accuracy of our determinations the values K in these expressions can be accepted equal to half of the values of the corresponding maxima in fig. 4. If the layers possess absorption the values K should be respectively corrected.

The changes of the mechanical properties of the Earth's mantle connected with the aeolotropic properties of the medium at the depths of 250 to 500, 900 to 1 000, 1 200 to 1 300, 1 800 and about 2 200 km may be due either to the heterogeneity of the mantle structure or the influence of the mechanical deformations caused by additional loadings at these depths (artificial aeolotropy).

#### REFERENCES

- [1] VVEDENSKAYA (A. V.), On Displacement Field for Rupture on the Continuity of the Elastic Medium. Izvestiya AN SSSR, ser. geophys., N° 4, 1959.
- [2] SHIROKOVA (H. I.), Some Data on Velocity Variation Character in Upper Layers of Earth's Mantle. Izvestiya AN SSSR, ser. geophys., N° 8, 1959.
- [3] KOGAN (S. D.), Dynamic Parameters of Sources of Deep Earthquakes. Transactions of the Geophysical Institute, N° 30, 1955.
- [4] KIRNOS (D. P.), KONDORSKAYA (N. V.), On calculation of Real Values of Ground Motion First Amplitude of Seismic Waves' Onsets. Izvestiya AN SSSR, ser. geophys., N° 12, 1959.
- [5] BATH (M.), Shadow Zones, Travel Times and Energies of Longitudinal Seismic Waves in the Presence of an Astenosphere Low Velocity Layer. Trans. Am. Geophys. Un., 38, N° 4, 1957.
- [6] VVEDENSKAYA (A. V.), BALAKINA (L. M.). On Some Peculiarities of the Displacement Fields of the Longitudinal and Transverse Waves Propagating in the Earth's Mantle. Publ. du Bureau Centr. Séism. Intern., sér. A, Travaux Sci., fasc. 20, 1959.
- [7] LOVE (A.), A Treatise on the Mathematical Theory of Elasticity. Cambridge at the University Press, 1927.
- [8] STONELEY (R.), The Seismological Implications of Aeolotropy in Continental Structure. Monthly Notices of the Royal Astronomical Society. Geophys. Suppl. 5, N° 8, 1949.
- [9] SAVAREN SKY (E. F.), KIRNOS (D. P.), Elements of Seismology and Seismometry, M. Gostechizdat, 1955.

**RECHERCHES EXPÉRIMENTALES  
SUR MODÈLES SISMIQUES :  
PROBLÈMES DE DIFFRACTION ET DE RÉFRACTION**

par Michel LAVERGNE  
(Institut Français du Pétrole)

*Introduction.*

Nous avons étudié quelques propriétés de la propagation des ondes sismiques dans des cas particuliers où les solutions mathématiques sont difficiles à établir, en utilisant les lois de la propagation des impulsions élastiques ultra-soniques dans les modèles.

Dans la première partie, nous décrivons les modèles à ultra-sons et l'appareillage électronique que nous avons construits pour réaliser cette étude.

Nous abordons en deuxième partie le problème des diffractions causées dans un solide homogène par un écran semi-infini parfaitement réfléchissant et en troisième partie le problème des couches minces en sismique-réfraction.

**NOMENCLATURE.**

$C_0$	: capacité propre de la pastille piézo-électrique;	$V_s$	: vitesse de propagation de l'onde transversale;
$D$	: constante piézo-électrique ( $5,2 \times 10^4$ uescgs pour le $\text{TiO}_3$ utilisé);	$V_o$	: vitesse de propagation dans les céramiques;
$F$	: force;	$Z_o$	: impédance acoustique des céramiques ( $Z_o = \rho_o V_o S$ );
$H$	: épaisseur de la couche constituant le marqueur de sismique-réfraction;	$Z$	: impédance acoustique;
$I$	: intercept;	$S$	: surface;
$i$	: courant électrique;	$\Phi$	: rapport du transformateur utilisé dans le schéma équivalent de la pastille piézo - électrique ( $\Phi = DC_o$ );
$j$	: $\sqrt{-1}$ ;	$\Lambda$	: longueur d'onde;
$e$	: épaisseur des pastilles piézo-électriques;	$\omega$	: pulsation;
$Q$	: charge électrique;	$\omega_R$	: pulsation de résonance de la pastille piézo-électrique libre;
$U$	: tension électrique;	$\rho_o$	: densité des céramiques;
$u_r$	: déplacement radial des particules;	$\rho$	: densité;
$u_t$	: déplacement tangentiel des particules;	$\sigma$	: coefficient de Poisson (milieu tridimensionnel);
$v$	: vitesse des particules.	$\sigma'$	: pseudo-coefficient de Poisson (plaques);
$V$	: vitesse de propagation;	$\theta$	: angle de réfraction limite.
$V_p$	: vitesse de propagation de l'onde longitudinale;		
$V_{p^l}$	: vitesse de propagation de l'onde longitudinale de plaque;		

### I. TECHNIQUE DES MODÈLES SISMIQUES A ULTRA-SONS.

Nous utilisons des modèles bidimensionnels, constitués de plaques de matériaux usuels accolées sur la tranche. Pour éviter que les plaques ne soient le siège de propagation d'ondes dispersives, on les a choisies d'épaisseur faible devant les longueurs d'onde des impulsions qu'on y fait s'y propager : l'épaisseur ne dépasse pas 5 mm, ce qui permet d'obtenir pour les longueurs d'onde supérieures à 5 cm des vitesses de propagation pratiquement constantes et voisines de la vitesse limite de plaque (OLIVER, PRESS et EWING, 1954).

Les matériaux employés dans cette étude seront essentiellement les suivants :

TABLEAU I. — *Caractéristiques des matériaux utilisés.*

	DENSITÉ	VITESSE LONG. DE PLAQUE $V_p^{\text{pl}}$ (m/s)	VITESSE TRANSVERS. DU MILIEU $V_s$ (m/s)	PSEUDO- COEFF. DE POISSON $\sigma'$ (PLAQUE)
Plexiglass. . . . .	1,2	2 330	1 410	0,21
Duralumin AU 4 G.	2,8	5 350	3 110	0,24

Une force est appliquée sur la tranche des plaques (fig. 1) par une pastille piézo-électrique excitée par un générateur d'impulsions

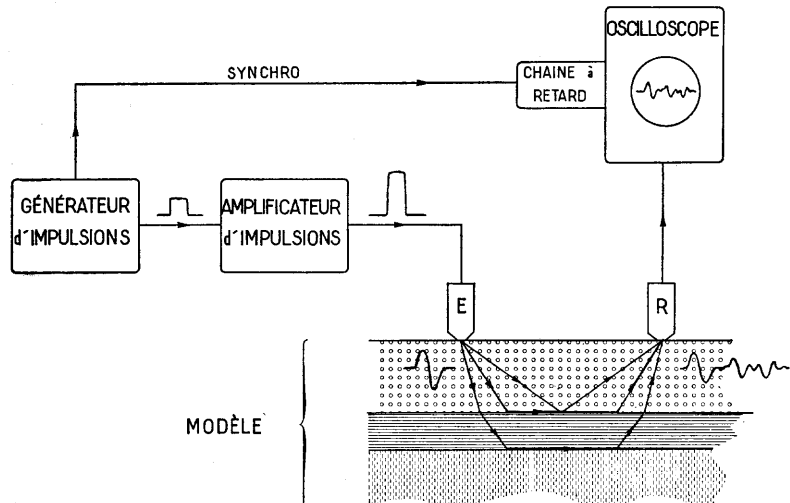


FIG. 1. — Principe des modèles à ultra-sons.

et vibrant longitudinalement, son axe mécanique et son axe électrique étant confondus et perpendiculaires à la tranche. La répartition directionnelle de l'énergie d'un tel système est connue.

Après propagation, les diverses arrivées sont captées par une pastille piézo-électrique analogue à la pastille émettrice, amplifiées, filtrées et observées sur l'écran d'un oscilloscope.

Remarquons que les pseudo-coefficients de Poisson :

$$\sigma' = \frac{1/2 - (V_s/V_p^{II})^2}{1 - (V_s/V_p^{II})^2}$$

des matériaux ci-dessus utilisés sous forme de plaques sont voisins de 1/4, donc voisins des coefficients de Poisson souvent rencontrés dans les roches, alors que les coefficients de ces mêmes matériaux, utilisés sous forme de blocs, sont voisins de 1/3. Pour conserver les coefficients de Poisson des roches, tout en utilisant les matériaux commodes au laboratoire, il est donc préférable d'utiliser des modèles en plaques plutôt que des modèles en bloc.

Par contre, il est évident que les lois d'atténuation géométrique de l'amplitude dans les milieux à deux dimensions sont différentes des lois d'atténuation dans les milieux à trois dimensions.

### 1. *Émetteurs et récepteurs (fig. 2).*

Les pastilles de céramiques piézo-électriques de 4 mm de diamètre sont constituées essentiellement de titanate de baryum polarisé. Pour les raisons que nous allons voir ci-dessous, nous avons accolé sur la face de la pastille qui n'est pas au contact du modèle un long cylindre de même diamètre et d'impédance acoustique appropriée.

Etudions les fonctions de transfert de l'émetteur et du récepteur ainsi constitués.

#### a. *Fonction de transfert de l'émetteur.*

Pour une pastille vibrant suivant l'épaisseur de façon que la plus courte longueur d'onde du signal soit supérieure à dix fois le rayon de la pastille, le système d'équation reliant la tension  $U$  et le courant  $i$  d'attaque, la force totale  $F_1$  sur la surface et la vitesse  $v_1$  des particules sur la face supérieure, la force totale  $F_2$  sur la surface et la vitesse  $v_2$  des particules sur la face inférieure s'écrit (MASON, 1948<sup>(1)</sup>; MASON, 1956<sup>(2)</sup>) :

(1) P. 399-403.

(2) P. 61-68.

On voit que la fonction de transfert de l'émetteur dépend des impédances acoustiques qui chargent les deux faces de la pastille.

L'étude des variations de  $T(\omega)$  en module et en phase, en fonction de  $\frac{\omega}{\omega_R}$ , pour différentes valeurs de l'impédance acoustique  $Z_1$  du cylindre qui surmonte la pastille, montre que, pour  $\frac{\omega}{\omega_R}$  inférieur à 0,2 environ, la force transmise au modèle croît avec  $Z_1$ .

Pour  $Z_1$  voisin de  $Z_0$  la fonction de transfert est sensiblement linéaire (LAVERGNE et CHAUVEAU, 1961).

Pour avoir une fonction de transfert particulièrement simple dans la bande de fréquences utilisées (pente 1 de 0 à 50 kc/s) et un bon rendement, nous avons utilisé des pastilles émettrices suffisamment minces (2 mm) pour que leur fréquence de résonance en faces libres ( $\omega_R = 2\pi \cdot 1250$  kc/s) soit nettement supérieure à la plus haute fréquence de la bande que nous utilisons, et nous avons chargé la face supérieure de la pastille par un cylindre métallique de même diamètre et d'impédance appropriée ( $Z_1 \approx Z_0$ ).

La longueur de ce cylindre a été choisie suffisamment grande pour que la réflexion se produisant à son extrémité ne vienne pas perturber les arrivées intéressantes, soit que les ondes parasites ainsi créées aient été complètement amorties avant leur retour, soit que leur instant d'arrivée soit postérieur à celui des phénomènes qui nous intéressent.

#### b. Fonction de transfert du récepteur.

Le schéma équivalent, décrit plus haut (fig. 3), peut également représenter le récepteur. La fonction de transfert du récepteur, rapport de la tension électrique recueillie à la force exercée par le modèle sur la face inférieure de la pastille, s'écrit :

$$T'(\omega) = \frac{\Phi U'}{F'_s}$$

La résolution du système des équations du réseau de la figure 3 donne l'expression de  $T'(\omega)$ . Supposons, pour simplifier, que la tension  $U'$  est mesurée à l'aide d'un électromètre à très forte impédance d'entrée; on obtient :

$$T'(\omega) = - \frac{\Phi^*}{j\omega C_s Z_s} \frac{1}{1 - \frac{jZ_0}{\sin \frac{\omega e}{V_0} (jZ_0 t + Z_s)}}$$

avec  $t = \operatorname{tg} \frac{\omega e}{2V_0}$ .

$$\left\{ \begin{array}{l} v_2 = v_1 \cos \frac{\omega e}{V_*} + j \frac{F_1 + DQ}{Z_*} \sin \frac{\omega e}{V_*} \\ F_2 + DQ = (F_1 + DQ) \cos \frac{\omega e}{V_*} - j v_1 Z_* \sin \frac{\omega e}{V_*} \\ j \omega C_* U = i + DC_* (v_2 - v_1) \end{array} \right.$$

Pour pouvoir introduire commodément les impédances acoustiques des matériaux au contact de la pastille piézo-électrique, nous allons représenter le schéma équivalent à celle-ci dans l'analogie électrique-mécanique suivante (tableau II) :

TABLEAU II. — Analogie électrique-mécanique.

MÉCANIQUE		ÉLECTRIQUE	
self charge	$\frac{Q}{\mathcal{L}}$	masse déplacement	$\frac{M}{L}$
courant $i$ tension $U$	$\frac{QT^{-1}}{\mathcal{L}QT^{-2}}$	vitesse $v$ force $F$	$\frac{LT^{-1}}{MLT^{-2}}$

Si nous supposons que la pastille d'impédance acoustique  $Z_*$  est chargée d'un côté par une impédance acoustique  $Z_1$  et de l'autre par une impédance acoustique  $Z_2$ , le schéma équivalent s'écrit comme l'indique la figure 3.

L'impédance acoustique  $Z_1$  du long cylindre accolé à la face supérieure de la pastille est pratiquement une résistance acoustique pure (ROCARD, 1949<sup>(3)</sup>).

La fonction de transfert de l'émetteur, rapport de la force transmise au modèle à la tension électrique fournie, s'écrit :

$$T(\omega) = \frac{F_2}{\Phi U}$$

où  $\Phi$  est le rapport du transformateur du schéma équivalent.

On a la relation (MASON, 1948) :

$$\Phi = DC_*$$

La résolution des équations du réseau de la figure 3 donne l'expression de  $T(\omega)$  :

$$T(\omega) = \frac{Z_2 (Z_1 + j Z_* t)}{Z_* \left( \frac{-\Phi^2}{j \omega C_* Z_*} - \frac{j}{\sin \frac{\omega e}{V_*}} \right) (Z_1 + Z_2 + 2j Z_* t) + (Z_1 + j Z_* t) (Z_2 + j Z_* t)}$$

$$\text{avec } t = \operatorname{tg} \frac{\omega e}{2 V_*}.$$

(3) P. 84.

et vibrant longitudinalement, son axe mécanique et son axe électrique étant confondus et perpendiculaires à la tranche. La répartition directionnelle de l'énergie d'un tel système est connue.

Après propagation, les diverses arrivées sont captées par une pastille piézo-électrique analogue à la pastille émettrice, amplifiées, filtrées et observées sur l'écran d'un oscilloscope.

Remarquons que les pseudo-coefficients de Poisson :

$$\sigma' = \frac{1/2 - (V_s/V_p^{II})^2}{1 - (V_s/V_p^{II})^2}$$

des matériaux ci-dessus utilisés sous forme de plaques sont voisins de 1/4, donc voisins des coefficients de Poisson souvent rencontrés dans les roches, alors que les coefficients de ces mêmes matériaux, utilisés sous forme de blocs, sont voisins de 1/3. Pour conserver les coefficients de Poisson des roches, tout en utilisant les matériaux commodes au laboratoire, il est donc préférable d'utiliser des modèles en plaques plutôt que des modèles en bloc.

Par contre, il est évident que les lois d'atténuation géométrique de l'amplitude dans les milieux à deux dimensions sont différentes des lois d'atténuation dans les milieux à trois dimensions.

### 1. *Émetteurs et récepteurs (fig. 2).*

Les pastilles de céramiques piézo-électriques de 4 mm de diamètre sont constituées essentiellement de titanate de baryum polarisé. Pour les raisons que nous allons voir ci-dessous, nous avons accolé sur la face de la pastille qui n'est pas au contact du modèle un long cylindre de même diamètre et d'impédance acoustique appropriée.

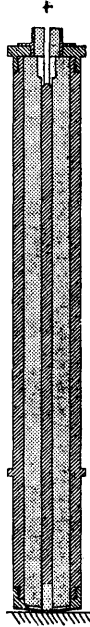
Etudions les fonctions de transfert de l'émetteur et du récepteur ainsi constitués.

#### a. *Fonction de transfert de l'émetteur.*

Pour une pastille vibrant suivant l'épaisseur de façon que la plus courte longueur d'onde du signal soit supérieure à dix fois le rayon de la pastille, le système d'équation reliant la tension  $U$  et le courant  $i$  d'attaque, la force totale  $F_1$  sur la surface et la vitesse  $v_1$  des particules sur la face supérieure, la force totale  $F_2$  sur la surface et la vitesse  $v_2$  des particules sur la face inférieure s'écrit (MASON, 1948<sup>(1)</sup>; MASON, 1956<sup>(2)</sup>) :

(1) P. 399-403.

(2) P. 61-68.



- isolant
- laiton
- céramique piézo-électrique

FIG. 2. — Récep-  
teur piézo-élec-  
trique.

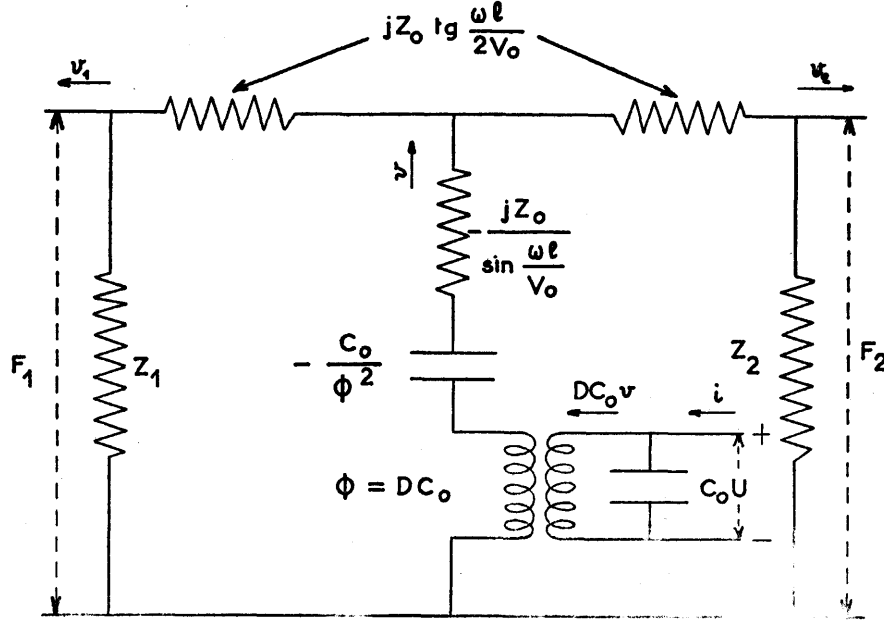


FIG. 3. — Schéma électrique équivalent de la pastille piézo-électrique

On voit que la fonction de transfert de l'émetteur dépend des impédances acoustiques qui chargent les deux faces de la pastille.

L'étude des variations de  $T(\omega)$  en module et en phase, en fonction de  $\frac{\omega}{\omega_R}$ , pour différentes valeurs de l'impédance acoustique  $Z_1$  du cylindre qui surmonte la pastille, montre que, pour  $\frac{\omega}{\omega_R}$  inférieur à 0,2 environ, la force transmise au modèle croît avec  $Z_1$ .

Pour  $Z_1$  voisin de  $Z_0$  la fonction de transfert est sensiblement linéaire (LAVERGNE et CHAUVEAU, 1961).

Pour avoir une fonction de transfert particulièrement simple dans la bande de fréquences utilisées (pente 1 de 0 à 50 kc/s) et un bon rendement, nous avons utilisé des pastilles émettrices suffisamment minces (2 mm) pour que leur fréquence de résonance en faces libres ( $\omega_R = 2\pi \cdot 1250$  kc/s) soit nettement supérieure à la plus haute fréquence de la bande que nous utilisons, et nous avons chargé la face supérieure de la pastille par un cylindre métallique de même diamètre et d'impédance appropriée ( $Z_1 \approx Z_0$ ).

La longueur de ce cylindre a été choisie suffisamment grande pour que la réflexion se produisant à son extrémité ne vienne pas perturber les arrivées intéressantes, soit que les ondes parasites ainsi créées aient été complètement amorties avant leur retour, soit que leur instant d'arrivée soit postérieur à celui des phénomènes qui nous intéressent.

*b. Fonction de transfert du récepteur.*

Le schéma équivalent, décrit plus haut (fig. 3), peut également représenter le récepteur. La fonction de transfert du récepteur, rapport de la tension électrique recueillie à la force exercée par le modèle sur la face inférieure de la pastille, s'écrit :

$$T'(\omega) = \frac{\Phi U'}{F'},$$

La résolution du système des équations du réseau de la figure 3 donne l'expression de  $T'(\omega)$ . Supposons, pour simplifier, que la tension  $U'$  est mesurée à l'aide d'un électromètre à très forte impédance d'entrée; on obtient :

$$T'(\omega) = - \frac{\Phi^*}{j\omega C_* Z_*} \frac{1}{1 - \frac{\sin \frac{\omega e}{V_*} (jZ_0 t + Z_1)}{\sin \frac{\omega e}{V_*} (jZ_0 t + Z_1)}}$$

avec  $t = \operatorname{tg} \frac{\omega e}{2V_*}$ .

On voit que la fonction du transfert du récepteur dépend des impédances acoustiques qui chargent les deux faces de la pastille et qu'elle est inversement proportionnelle à  $C_0$  donc que  $U'$  croît avec l'épaisseur de la pastille.

L'étude des variations de  $T'(\omega)$  en fonction de  $\frac{\omega}{\omega_R}$ , pour différentes valeurs du paramètre  $Z_1$  montre que pour  $\frac{\omega}{\omega_R} < \frac{1}{3}$ , la tension électrique délivrée par le récepteur croît avec  $Z_1$ . Pour  $Z_1$  voisin de  $Z_0$ , la fonction de transfert admet une pente sensiblement nulle tant que  $\frac{\omega}{\omega_R}$  reste inférieur à  $\frac{1}{4}$ . (Lavergne et Chauveau, 1961.)

Pour obtenir une réponse simple (pente nulle dans la bande des fréquences utilisées), nous avons chargé la face supérieure de la pastille réceptrice par un cylindre métallique de même diamètre et d'impédance  $Z_1$  voisine de  $Z_0$ . Sa longueur a été choisie suffisamment grande pour les mêmes raisons que celles énoncées à propos de l'émetteur.

Pour obtenir une bonne amplitude, nous avons pris une épaisseur aussi grande que possible pour la pastille réceptrice ( $e = 10$  mm), mais cependant suffisamment faible pour que la fréquence de résonance de la pastille libre (250 kc/s pour  $e = 10$  mm) soit nettement supérieure à la plus haute fréquence de la bande utilisée (50 kc/s).

## 2. Appareillage électronique.

### a. Emission.

On dispose de deux types de générateurs d'impulsions électriques (tableau III). Pour obtenir des impulsions à front raide, on utilise un appareil qui amplifie les impulsions fournies par les générateurs usuels. On obtient ainsi un signal électrique en forme de crête de durée variable. Pour obtenir des impulsions arrondies, on utilise un amplificateur constitué d'un transformateur de base de temps de téléviseur, qui fournit un signal électrique ayant la forme indiquée sur la figure 4 a.

TABLEAU III. — Générateurs d'impulsions électriques utilisés.

	IMPULSION A FRONT RAIDE	IMPULSIONS ARRONDIÉES
Temps de montée	< 0,5 $\mu$ s sur 1 000 picofarads	environ 10 $\mu$ s
Durée . . . . .	1 à 10 $\mu$ s	20 à 30 $\mu$ s
Amplitude . . . . .	1 500 V	1 500 à 3 000 V

*b. Réception.*

Un amplificateur et un filtre passe-bande  $5 \text{ kc/s} = 100 \text{ kc/s}$  permettent d'éliminer à la réception les bruits à basse fréquence du laboratoire et les éventuelles oscillations parasites à haute fréquence.

Le balayage de l'oscilloscope est synchronisé avec l'impulsion d'attaque de l'émetteur, et le phénomène est répété quelques dizaines de fois par seconde, fournissant ainsi une trace stable sur l'écran. La trace est photographiée à chaque position du récepteur au moyen d'une caméra appropriée.

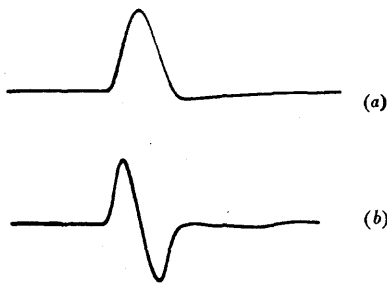


FIG. 4. — Impulsion d'attaque de l'émetteur et réponse du récepteur.

*3. Forme de l'impulsion.*

Du fait de la forme de la fonction de transfert de l'émetteur et de la fonction de transfert du récepteur entraînées par le choix de  $Z_i$  ( $Z_i \simeq Z_0$ ), le signal électrique reçu au récepteur, après propagation dans un milieu homogène n'introduisant aucune déformation, sera sensiblement la dérivée du signal électrique d'attaque de l'émetteur.

A titre d'exemple, on a représenté sur la figure 4 b la réponse de l'ensemble constitué par l'émetteur et le récepteur accolés bout à bout à un signal électrique d'attaque (fig. 4 a) ayant la forme indiquée. C'est ce signal particulièrement simple qui sera utilisé dans les parties II et III.

*4. Mesure des amplitudes.*

Lorsqu'on mesure les amplitudes des arrivées dans des études particulièrement simples, par exemple dans le cas de la transmission à travers une plaque de largeur constante (fig. 9), on constate que les résultats obtenus, compte tenu de l'atténuation géométrique dans la plaque, sont inférieurs aux résultats théoriques déduits des fonctions de transfert et des diagrammes polaires de

l'émetteur et du récepteur, dans un rapport  $K$  dû aux imperfections des contacts et à l'absorption dans la plaque. Si on prend la précaution d'utiliser un lubrifiant approprié (oppanol) pour améliorer les contacts entre les pastilles et le matériau, les fluctuations de cette constante ne dépassent pas 5 à 10 % lorsqu'on déplace le récepteur. Des mesures comparatives d'amplitude sont alors possibles.

## II. ÉTUDE DE LA DIFFRACTION CRÉÉE DANS UN SOLIDE PAR UN ÉCRAN EN FORME DE DEMI-PLAN PARFAITEMENT RÉFLÉCHISSANT.

Parmi les premières études théoriques sur la diffraction, la théorie de la diffraction de la lumière de SOMMERFELD (1895) a joué un rôle capital : elle a été appliquée par MAGNUS (1941) à la diffraction des ondes électromagnétiques planes, puis par FRIEDLANDER (1946) et Fox (1948, 1949) à la diffraction du son par un écran en forme de demi-plan. CAGNIARD (1935) traite directement par la méthode de CARSON le problème de la diffraction d'une onde progressive par un écran en forme de demi-plan parfaitement réfléchissant.

La plupart de ces études théoriques ont été faites en supposant qu'il existe une seule vitesse de propagation dans le milieu considéré (milieu fluide).

Dans le cas des solides, qui peuvent être le siège de deux vitesses de propagation, il faut tenir compte de la conversion, sur l'écran diffracteur, de l'onde de dilatation incidente en onde de distorsion réfléchie et diffractée et de l'onde de distorsion incidente en onde de dilatation réfléchie et diffractée.

Récemment, KNOPOFF (1959) a établi les diagrammes polaires d'une source de diffraction sphérique lorsqu'elle est excitée par une onde de dilatation et par une onde de distorsion. Dans les deux cas, il y a production simultanée d'ondes de dilatation et d'ondes de distorsion diffractées.

Le but de notre étude est d'établir expérimentalement quelques propriétés des ondes diffractées qui prennent naissance dans un solide lorsqu'une onde de dilatation incidente rencontre un écran en forme de demi-plan parfaitement réfléchissant.

Nous étudierons la répartition directionnelle des deux types d'ondes diffractées, ondes de dilatation et ondes de distorsion, issues de l'extrémité I de l'écran diffracteur. Différents cas seront considérés, qui correspondent à différents angles de chute de l'onde incidente sur l'écran diffracteur.

Les modèles utilisés sont des plaques de plexiglass de 5 mm d'épaisseur, dans lesquelles a été taillée une fente qui constituera le demi-plan diffracteur. Nous avons fait successivement les expé-

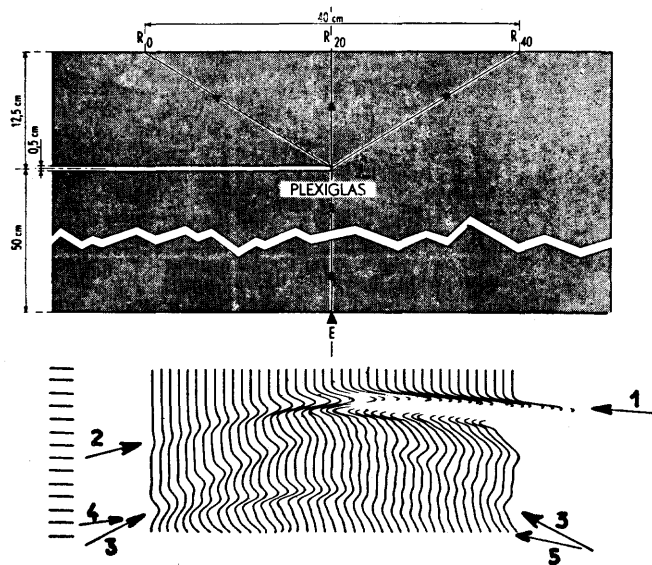


FIG. 5. — Diffractions créées par l'arrivée au point I d'une onde longitudinale sous une incidence de  $-9^\circ$ .

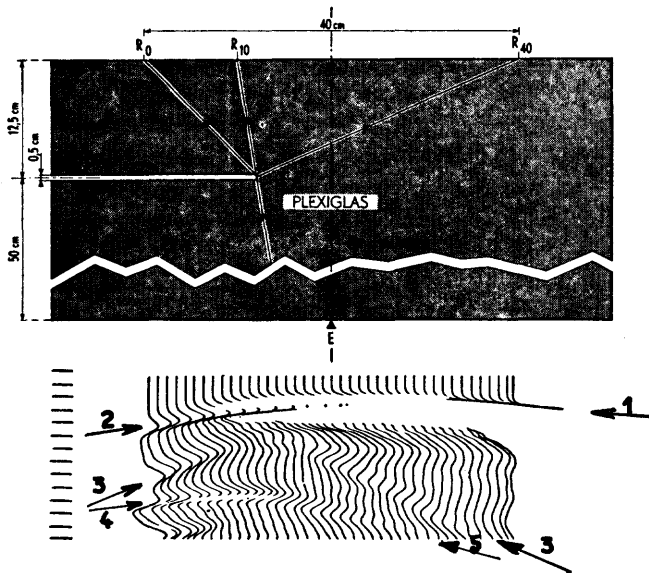


FIG. 6. — Diffractions créées par l'arrivée au point I d'une onde longitudinale sous une incidence normale.

riences avec des fentes de 0,5, 1, 2, 5 et 10 cm dont les extrémités ont été taillées en demi-cercle.

La longueur d'onde moyenne des impulsions émises est de 8 cm.

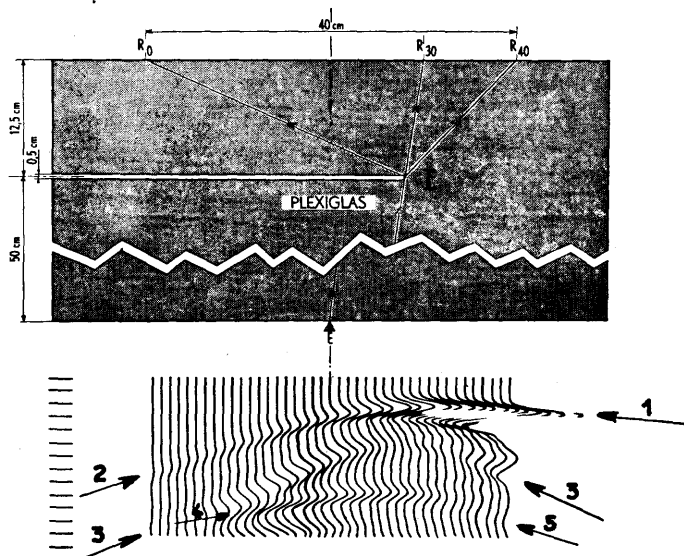


FIG. 7. — Diffractions créées par l'arrivée au point I d'une onde longitudinale sous une incidence de + 9°.

L'émetteur a été disposé successivement en des positions qui correspondent à des angles d'incidence de -9°, 0°, +9° sur le demi-plan diffracteur au voisinage de son extrémité I (fig. 5, 6, 7).

On a disposé le récepteur en une succession de positions derrière l'écran diffracteur, de R<sub>0</sub> à R<sub>40</sub> afin d'observer la zone des arrivées directes et la zone d'ombre.

Les figures 5, 6, 7 représentent, à l'aplomb de chaque position du récepteur, le signal reçu. L'échelle des distances, en abscisse, est de 10 mm entre traces. L'échelle des temps, en ordonnée, est graduée toutes les 10  $\mu$ s.

Nous allons borner notre étude aux arrivées 1, 2 et 3, qui sont visibles à la fois dans la zone d'ombre et la zone de lumière. L'arrivée 1, visible dans la zone de lumière, correspond à l'arrivée directe de dilatation issue de E. L'arrivée directe de distorsion arriverait au-delà de la limite du film. L'étude des temps d'arrivée de 2 et 3 indique que les ondes correspondantes sont toutes deux issues du point I, extrémité du demi-plan diffracteur, qu'elles ont pris naissance au moment où l'onde incidente de dilatation issue de E atteignait le point I et qu'elles se sont propagées dans le plexi-

glass respectivement à la vitesse des ondes longitudinales de plaque et à celles des ondes transversales du milieu.

Ces résultats indiquent que le point I peut être assimilé à une source et émet, à l'instant où il est atteint par l'onde incidente de dilatation issue de E, un ébranlement ayant une composante de dilatation et une composante de distorsion.

Nous avons cherché à mesurer la distribution angulaire de la composante radiale et de la composante tangentielle du déplacement dans une direction donnée derrière l'écran diffracteur, autrement dit à déterminer les diagrammes polaires des ondes P diffractées et S diffractées issues de I<sup>(1)</sup>.

Les diagrammes polaires de divers types de sources ont été étudiés théoriquement par MILLER et PURSEY (1954) pour divers coefficients de Poisson. Ces auteurs étudient notamment le cas d'une source étroite et infiniment longue qui vibre, perpendiculairement à elle-même, sur la surface d'un solide à trois dimensions. Nous allons supposer que ce cas peut être étendu à celui d'une source ponctuelle vibrant perpendiculairement à la tranche d'une plaque solide, c'est-à-dire au cas de nos modèles. Cette hypothèse n'est pas déraisonnable : les plaques étant d'épaisseur faible et les diamètres des pastilles petits devant la longueur d'onde, on peut considérer qu'on a une propagation analogue à celle d'une onde cylindrique émise par une source linéaire à la surface d'un milieu à trois dimensions.

Le pseudo-coefficient de Poisson du plexiglass en plaque étant connu ( $\sigma'$  voisin de 1/4; OLIVER, PRESS et EWING, 1954), nous connaissons d'après MILLER et PURSEY (1954) les diagrammes polaires des intensités du déplacement au niveau de l'émetteur E.

#### *Diagrammes polaires des ondes diffractées.*

Remarquons que non seulement l'amplitude mais encore la phase des ondes diffractées varient avec la direction. La détermination de l'amplitude est relativement commode par la méthode expérimentale mais celle de la phase est beaucoup plus délicate. On pourra néanmoins donner quelques indications sur cette dernière, en particulier au sujet des ondes de distorsion diffractées.

La détermination du diagramme polaire de l'onde diffractée longitudinale n'est possible que dans la zone d'ombre. Dans la zone de lumière, il y a interférence entre l'arrivée longitudinale directe

---

(1) Les symboles P et S désignent respectivement les ondes de dilatation (ou ondes longitudinales) et les ondes de distorsion (ou ondes transversales).

et l'arrivée longitudinale diffractée, et l'onde observée est le résultat de cette interférence.

Par contre la détermination du diagramme polaire de l'onde diffractée transversale est possible à la fois dans la zone d'ombre et dans la zone de lumière, car son arrivée est suffisamment bien séparée de l'arrivée longitudinale directe par suite de l'écart des vitesses de propagation longitudinale et transversale.

Pour déterminer le diagramme polaire des ondes P diffractées et S diffractées issues de I, tout en s'affranchissant de l'atténuation géométrique et de l'absorption dans le modèle, nous avons comparé la transmission des ondes diffractées issues de I à travers les 12,5 cm de plexiglass situés derrière l'écran diffracteur (fig. 5, 6, 7) à la transmission des ondes issues d'une source ordinaire E à travers une plaque rectangulaire de même largeur (fig. 8).

On s'affranchit ainsi non seulement de la variation de la réponse des récepteurs avec l'angle d'incidence sous lequel ils sont frappés, mais encore de l'amortissement dû à la géométrie et à l'absorption, à condition de supposer toutefois qu'il est le même pour les ondes issues d'une source ordinaire et pour les ondes issues d'une source de diffraction. Ceci implique que les spectres de fréquences des impulsions émises par les deux types de sources ne soient pas trop différents.

Le rayon vecteur  $r_{diff}$  du diagramme polaire de la source de diffraction I s'obtient à partir du rayon vecteur  $r$  du diagramme polaire connu de la source ordinaire  $E_1$  par la formule :

$$r_{diff} = r \frac{A_{diff}}{A}$$

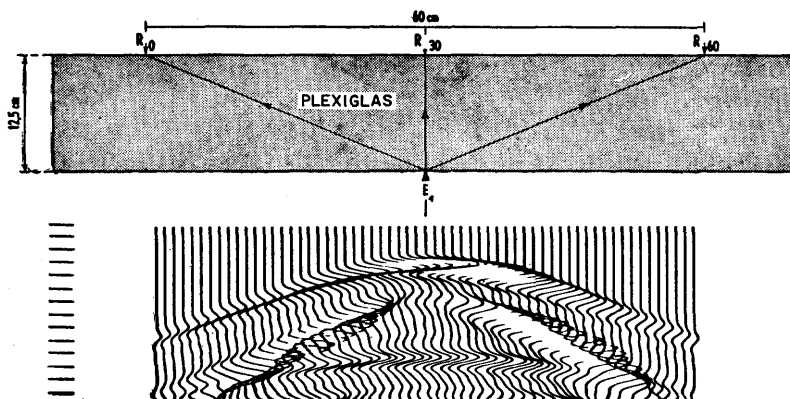


FIG. 8. — Transmission de l'onde longitudinale et de l'onde transversale à travers une plaque de plexiglass, et réflexions multiples.

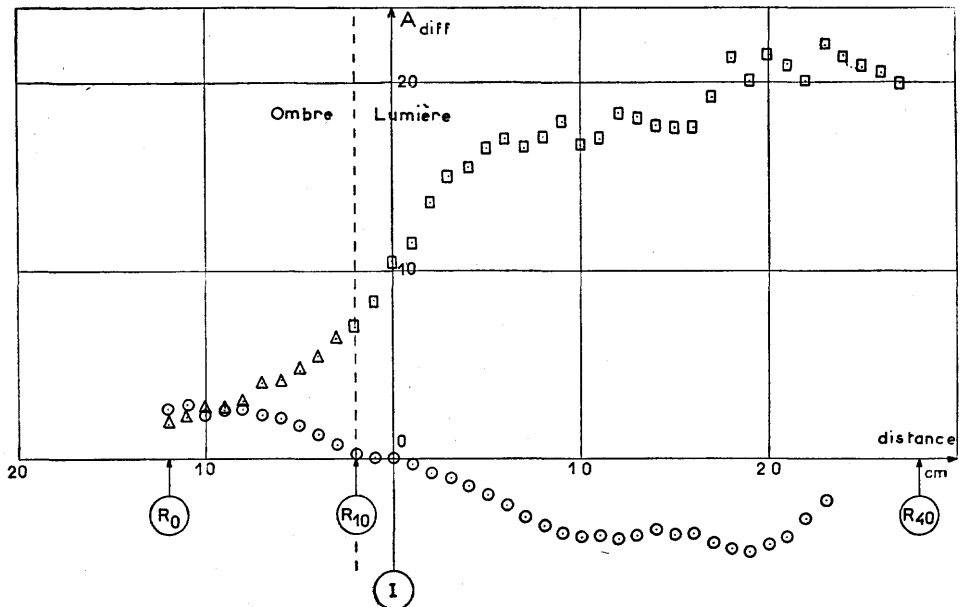


FIG. 9. — Amplitude des arrivées diffractées en fonction de la distance à la verticale de la source de diffraction. Incidence —  $9^\circ$  (1).

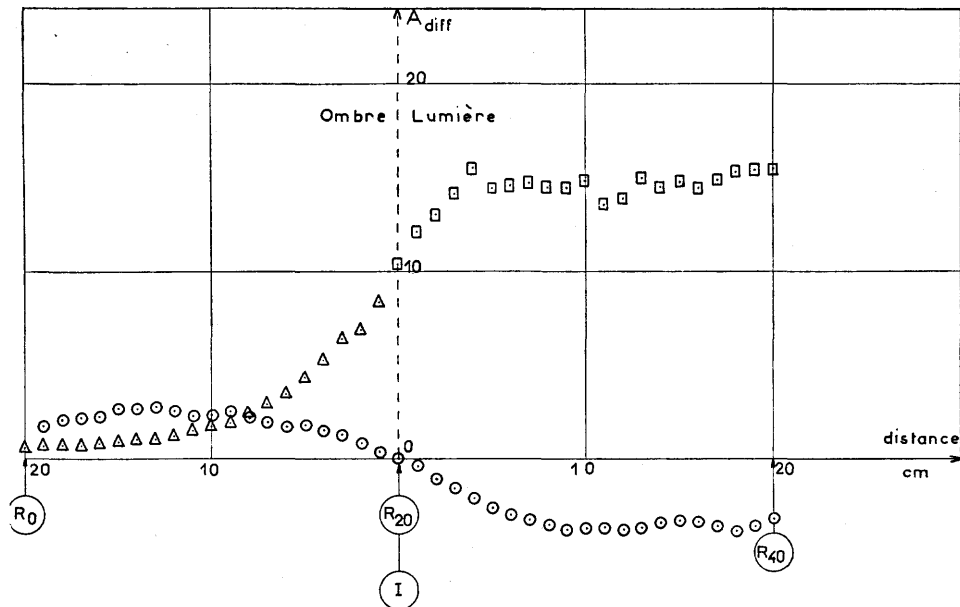


FIG. 10. — Amplitude des arrivées diffractées en fonction de la distance à la verticale de la source de diffraction. Incidence normale.  
○  $S_{\text{diffractée}}$      $\Delta P_{\text{diffractée}}$      $\square$  Interférence de  $P_{\text{diffractée}}$  et  $P_{\text{directe}}$ .

(1) Les ordonnées des figures 9, 10, 11 et 12 sont arbitraires mais cohérentes.

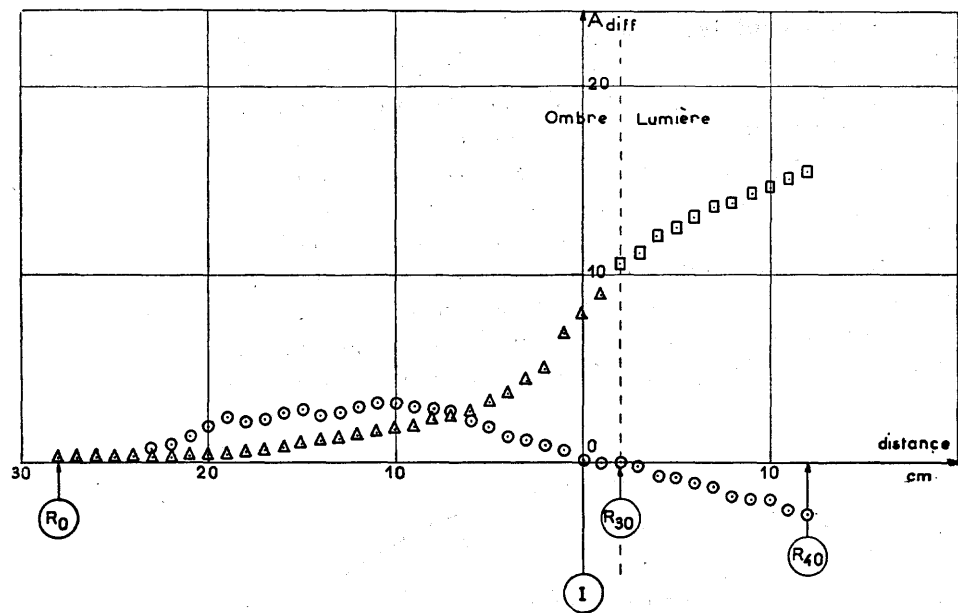


FIG. 11. — Amplitude des arrivées diffractées en fonction de la distance à la verticale de la source de diffraction. Incidence + 9°.

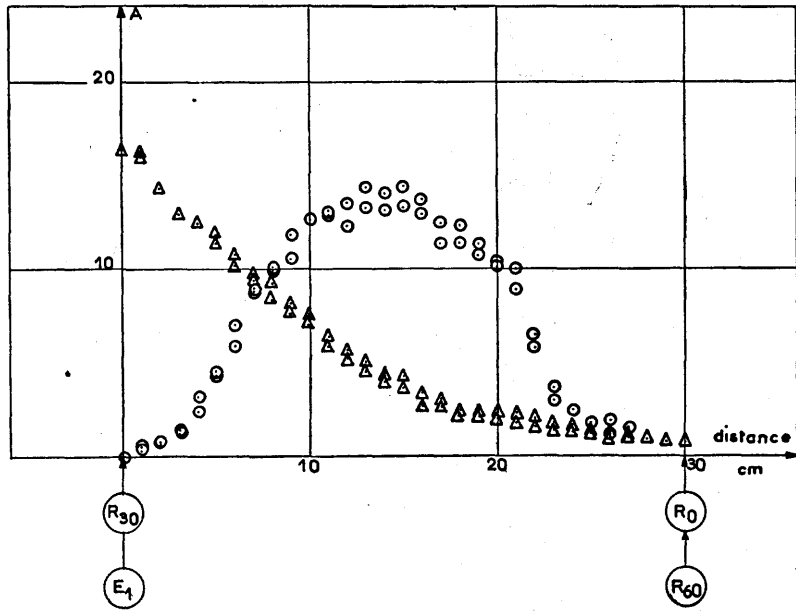


FIG. 12. — Amplitude des arrivées directes transmises à travers la plaque de plexiglass en fonction de la distance à la verticale de la source.  
○ S transmise    △ P transmise

où  $A_{diff}$  et  $A$  désignent les amplitudes des arrivées au récepteur, respectivement dans le cas de la source de diffraction I (fig. 5) et dans le cas de la source ordinaire  $E_1$  (fig. 8). Un raisonnement analogue peut s'appliquer aux cas des figures 6 et 7.

Les amplitudes  $A_{diff}$  des arrivées P et S diffractées observées aux différents récepteurs sont représentées sur les figures 9, 10, 11, pour les cas des figures 5, 6 et 7. Les amplitudes A des arrivées P et S ordinaires observées aux différents récepteurs sont données sur la figure 12 pour le cas de la source  $E_1$  de la figure 8.

Les diagrammes polaires des ondes diffractées longitudinales et transversales issues de I sont données sur les figures 13 a et b.

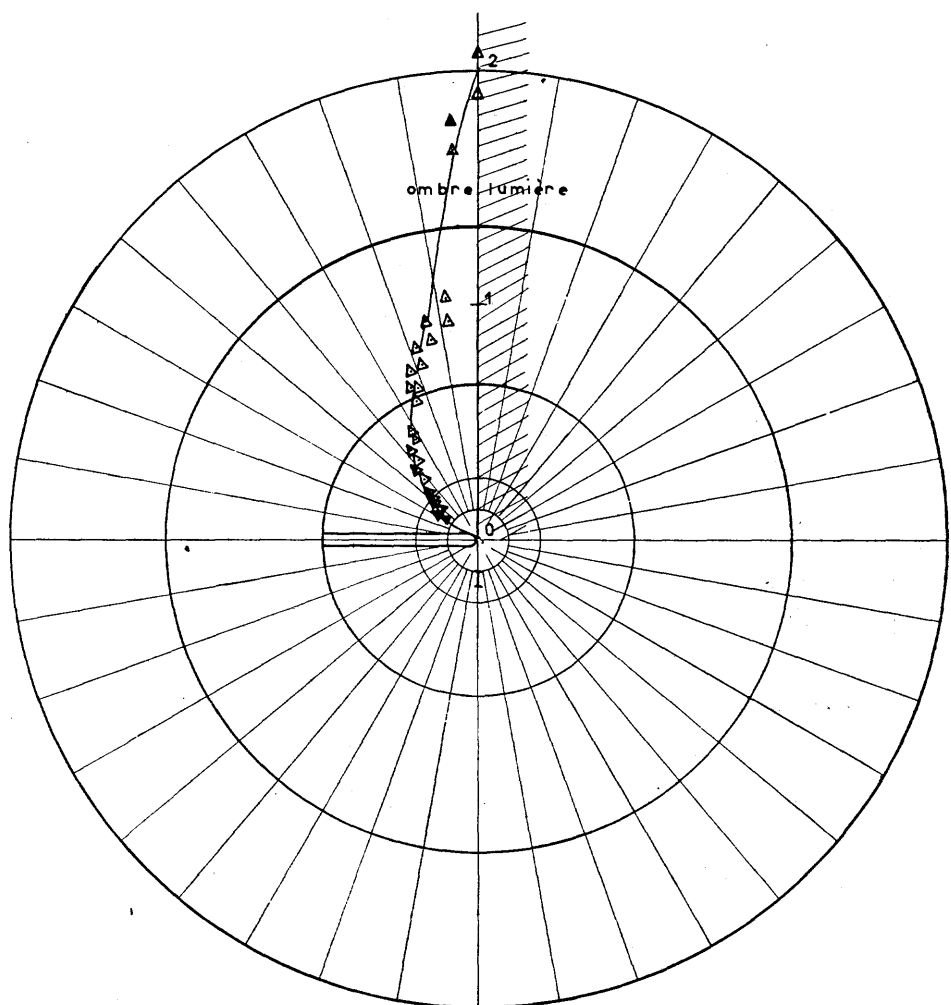


FIG. 13 a). — Diagramme polaire de l'onde de dilatation diffractée.

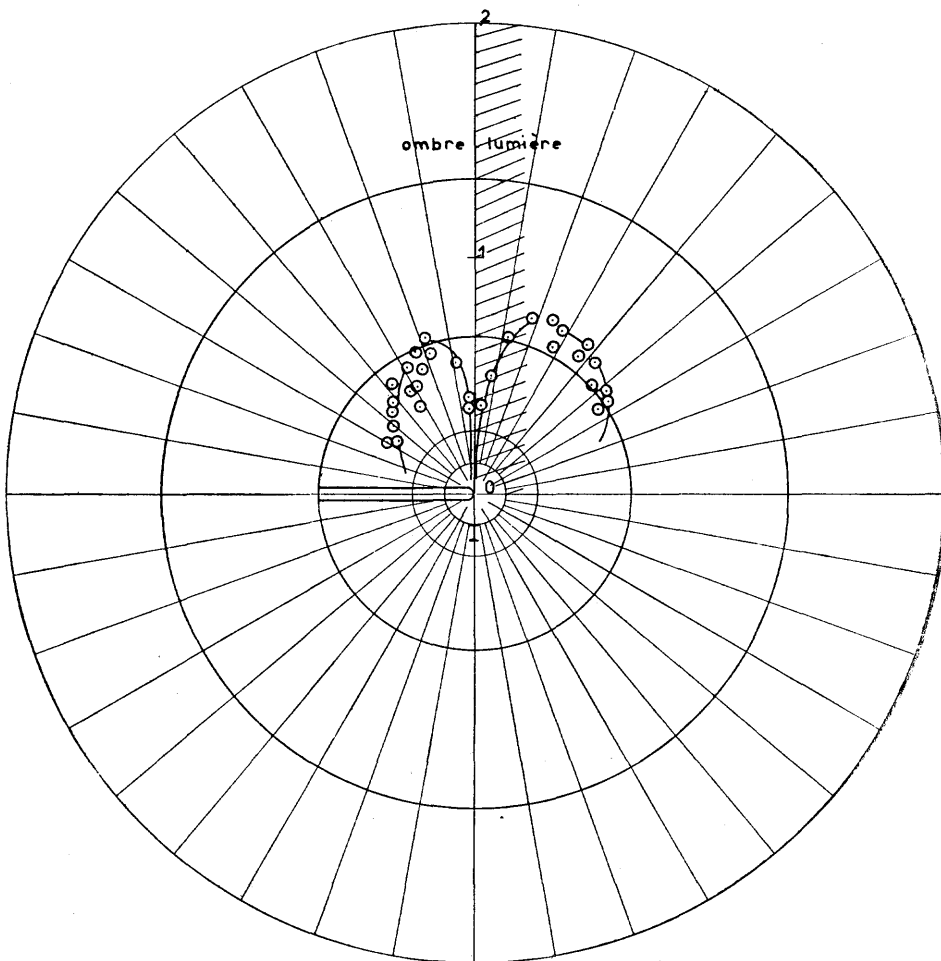


FIG. 13 b). — Diagramme polaire de l'onde de distortion diffractée.

*Effet de la largeur de l'écran diffracteur.*

Les formes des arrivées diffractées obtenues pour les fentes de 0,5 cm, 1 cm et 2 cm sont très voisines. En revanche on constate des déformations assez considérables pour la fente de 10 cm. La fente peut donc être considérée pratiquement comme un demi-plan tant que sa largeur ne dépasse pas une fraction notable de la longueur d'onde; la largeur maximale acceptable semble être voisine de  $\frac{\lambda}{4}$ .

### *Atténuation et déformation des ondes de dilatation et des ondes de distorsion diffractées.*

Les figures 5, 6, 7 et la figure 13 a montrent quelques propriétés des ondes de dilatation :

- le maximum d'amplitude de la première arrivée se produit dans la zone de lumière, par suite de l'intéférence de l'onde directe avec l'onde diffractée. On rapprochera ce résultat de ceux cités par MONK (1937) pour la diffraction de la lumière sur un écran opaque;
- les signaux correspondants aux arrivées diffractées sont atténus et déformés par rapport au signal de l'onde incidente, d'autant plus que l'on s'éloigne davantage de la limite des zones d'ombre et de lumière.

Les figures 5, 6, 7 et la figure 13 b montrent également quelques propriétés des ondes de distorsion :

- l'amplitude du signal de distorsion diffracté émis par la source I est nulle sur la limite des zones d'ombre et de lumière. Elle croît, passe par un maximum et finalement décroît, quand on s'éloigne progressivement de cette limite;
- dans le cas de l'incidence normale, les signaux de distorsion diffractés émis par la source I sont en opposition de phase en deux points symétriques par rapport à la droite de séparation des zones d'ombre et de lumière.

Des résultats analogues à ces deux dernières propriétés ont été établis par KNOPOFF (1959) pour une source de diffraction constituée par un obstacle sphérique.

### *Réflexions et diffractions multiples.*

Les temps d'arrivée des ondes 4 et 5 permettent de faire quelques hypothèses sur leur provenance :

- l'arrivée 4 semble être un multiple de l'onde P diffractée issue de I, qui parvient aux récepteurs après s'être réfléchie une première fois en surface et une deuxième fois sur l'écran diffracteur;
- l'arrivée 5 semble être une onde P diffractée issue de I au moment où ce point est excité par une onde provenant des parties supérieures de la plaque, et qui est due à la réflexion en surface de l'onde de dilatation issue de E.

### *Conclusion.*

Cette étude nous a montré que lorsqu'une onde incidente longitudinale frappe un écran semi-infini parfaitement réfléchissant

situé dans un solide homogène, l'extrémité de l'écran devient une source de diffraction et émet des vibrations longitudinales qui se propagent à la vitesse des ondes de dilatation et des vibrations transversales qui se propagent à la vitesse des ondes de distorsion.

L'écran peut pratiquement être assimilé à un demi-plan infiniment mince tant que son épaisseur reste inférieure au quart de la longueur d'onde du signal.

Les diagrammes polaires présentés donnent quelques indications sur la répartition directionnelle de l'énergie diffractée issue de l'extrémité de l'écran diffracteur pour les ondes de dilatation et pour les ondes de distorsion.

En particulier, les vibrations transversales diffractées sont en opposition de phase de part et d'autre de la limite des zones d'ombre et de lumière et elles s'annulent quand on traverse cette limite.

### III. ETUDE DES COUCHES MINCES EN SISMIQUE-RÉFRACTION.

L'étude théorique des ondes réfractées sous l'angle limite progressant le long d'une couche d'épaisseur limitée a été abordée par divers auteurs pour des cas particuliers relativement simples, souvent à l'occasion d'études sur la transmission à travers les plaques métalliques. REISSNER (1937) a établi les formules donnant la transmission du son à travers une plaque métallique plongée dans un fluide en fonction de l'angle d'incidence. CREMER (1942), SCHÖCH (1950), FAY et FORTIER (1951) ont repris le problème et donné des résultats plus directement accessibles au calcul. OSBORNE et HART (1945) étudient la propagation le long d'une plaque métallique plongée dans un liquide et assimilée à un guide d'onde.

D'après ces auteurs le maximum de transmission de l'énergie sismique à travers la plaque a lieu lorsque la plaque entre en résonance, et ce phénomène se produit pour des angles d'incidence tels que la vitesse apparente de l'onde incidente le long de la surface de la plaque soit précisément égale à l'une des vitesses de phase des ondes dispersives susceptibles de se propager dans la plaque. GOTZ (1943) montre que pour les angles d'incidence correspondant à un maximum de transmission à travers la plaque il y a également une propagation notable le long de la plaque, dont il détermine expérimentalement les lois d'atténuation.

La propagation d'une onde de Rayleigh généralisée le long d'une couche mince solide, baignant dans un fluide plus lent, est donc possible, et la vitesse de propagation semble obéir aux lois de dispersion dans les plaques, les équations donnant pour solution

limite aux fréquences élevées la vitesse de l'onde de Rayleigh à la surface de la plaque. La présence du fluide introduit un terme imaginaire dans l'expression de la vitesse, qui correspond à une perte d'énergie dans le fluide, perte d'autant plus grande que la vitesse de propagation dans le fluide est plus voisine de la vitesse de propagation dans la plaque (OSBORNE et HART, 1945).

La résolution théorique du problème de la naissance d'une onde réfractée sous l'angle limite, à l'interface d'une couche mince solide entourée de milieux solides, présente des difficultés certaines et c'est pourquoi nous avons utilisé les modèles pour aborder cette étude.

Une étude analogue sur modèles a déjà été faite par PRESS, OLIVER et EWING (1954) dans le cas où le milieu situé sous la couche mince est un milieu plus rapide ou le vide. Ces auteurs ont trouvé que l'onde longitudinale réfractée le long d'une couche mince ( $H = \frac{\Lambda}{8}$ , où  $\Lambda$  désigne la longueur d'onde dans la couche mince) a une vitesse de propagation inférieure de près de 5 % à celle de l'onde longitudinale réfractée le long d'une couche épaisse ( $H = 2\Lambda$ ).

Dans la présente étude, nous avons étudié le cas où les milieux sus-jacent et sous-jacent sont identiques (plexiglass), et nous avons réalisé les modèles schématisés sur la figure 14 pour un grand nombre de valeur de  $H$  ( $H = 2\Lambda, \frac{\Lambda}{3}, \frac{\Lambda}{5}, \frac{2\Lambda}{15}, \frac{\Lambda}{15}$ ,  $\Lambda$  désignant la longueur d'onde dans la couche de duralumin, d'épaisseur  $H$ ). Les longueurs d'onde de l'onde réfractée se propageant le long du marqueur sont voisines de 15 cm et les fréquences des arrivées correspondantes de l'ordre de 25 kc/s.

#### *Etude des premières arrivées.*

Le tracé des courbes de l'instant de la première arrivée, en fonction de l'éloignement du récepteur par rapport à l'émetteur (dromochroniques) donne, pour les distances comprises entre 0 et 40 cm environ, une pente de 2 330 m/s qui correspond à la vitesse de propagation d'une onde longitudinale de plaque le long de la tranche supérieure du plexiglass. Cette zone ne nous intéresse pas directement dans la présente étude et les arrivées correspondantes n'ont pas été représentées sur les films de la figure 14.

De 40 à 50 cm une zone où les vitesses sont assez difficiles à établir marque le passage de l'arrivée directe à l'arrivée réfractée. Notons que les arrivées réfléchies viennent également interférer

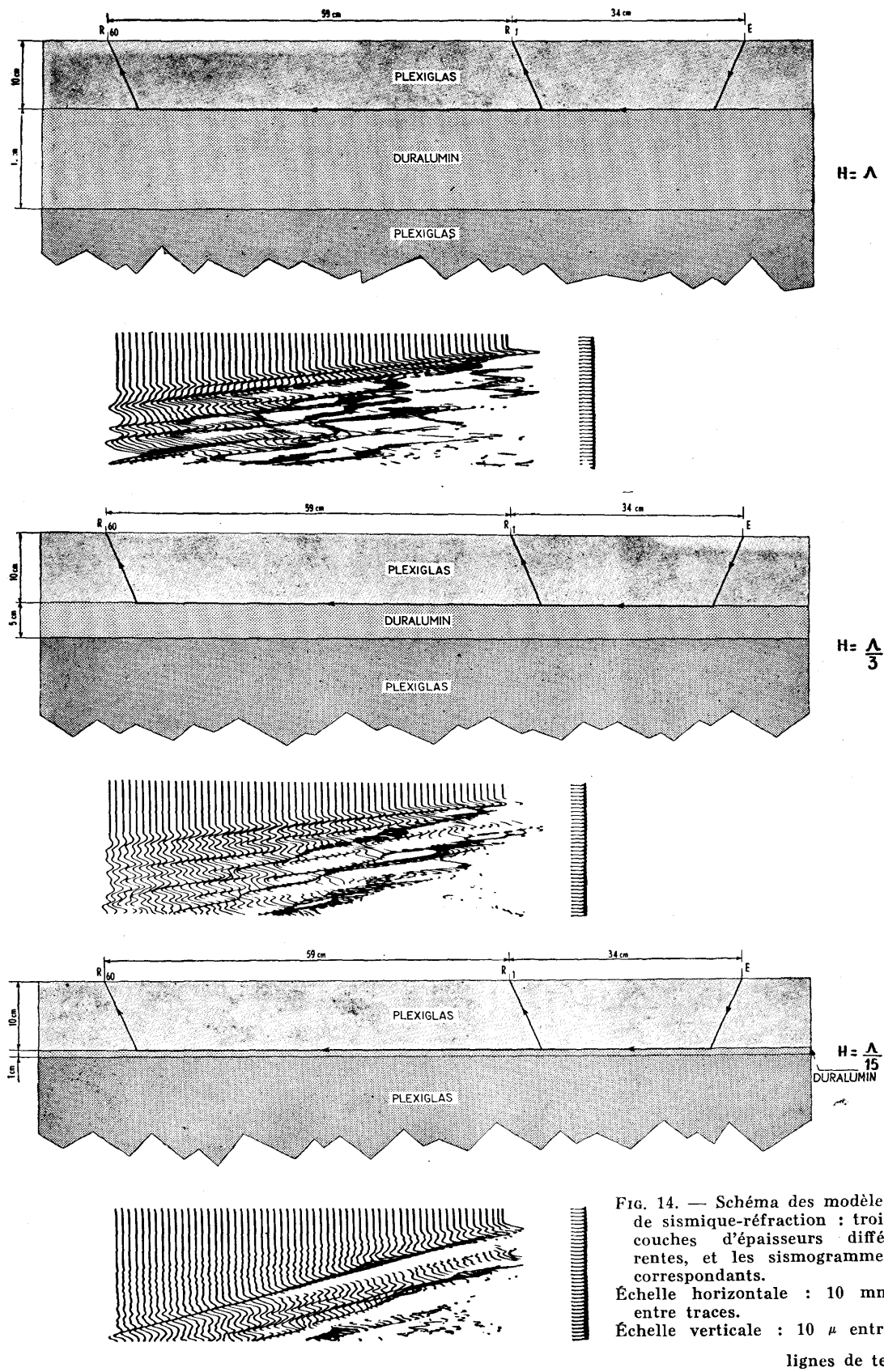


FIG. 14. — Schéma des modèles de sismique-réfraction : trois couches d'épaisseurs différentes, et les sismogrammes correspondants.

Échelle horizontale : 10 mm entre traces.

Échelle verticale : 10  $\mu$  entre lignes de temps.

avec les arrivées réfractées jusqu'à une distance assez éloignée de l'émetteur.

Au-delà de 50 cm, les premières arrivées correspondent à la propagation non perturbée de l'onde longitudinale réfractée le long du marqueur de duralumin; pour toutes les valeurs de  $H$  étudiées, les dromochroniques des arrivées réfractées sont sensiblement des droites au-delà de 50 cm.

En faisant une analyse par moindres carrés du temps des premières arrivées réfractées, on obtient la vitesse  $V$  à partir des temps d'arrivée  $t_0$  mesurés à la distance  $d$  par les formules de WORTHING et GEFFNER (1950).

Les moyennes des résultats obtenus pour les vitesses sont représentées sur la figure 15, avec les écarts types correspondants, en fonction de l'épaisseur  $H$  de la couche qui constitue le marqueur.

On constate (fig. 15) que les vitesses de l'onde réfractée varient

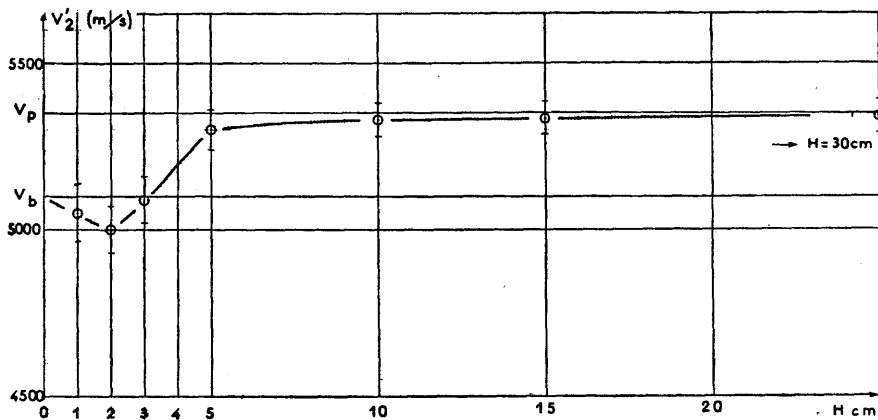


FIG. 15. — Vitesse de propagation de l'onde longitudinale réfractée le long du marqueur en fonction de l'épaisseur de la couche qui constitue le marqueur.

d'une façon continue suivant les valeurs de  $H$ , depuis des vitesses voisines de 5 350 m/s pour les fortes valeurs de  $H$ . Ceci semble indiquer que, si  $H \rightarrow 0$ , la vitesse tend vers la vitesse  $V_b$  de propagation le long d'une barre fine et, si  $H \rightarrow \infty$ , la vitesse tend vers la vitesse  $V_p$ , de propagation dans une plaque.

#### *Essai d'interprétation des phénomènes observés.*

Pour essayer de préciser la nature du phénomène de variation des vitesses avec l'épaisseur  $H$ , nous avons repris les mesures de vitesse en désolidarisant la couche  $H$  des milieux sus-jacent et sous-jacent et en disposant l'émetteur et le profil de récepteurs

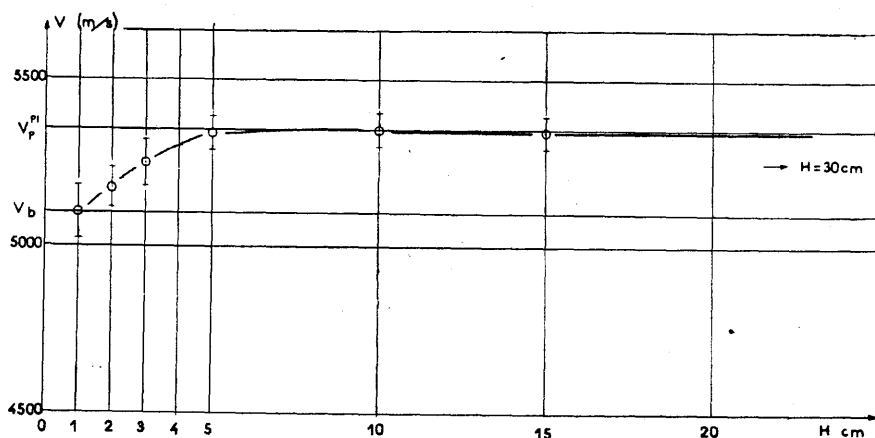


FIG. 16. — Vitesse de propagation de l'onde longitudinale à la surface de la couche isolée en fonction de l'épaisseur de cette couche.

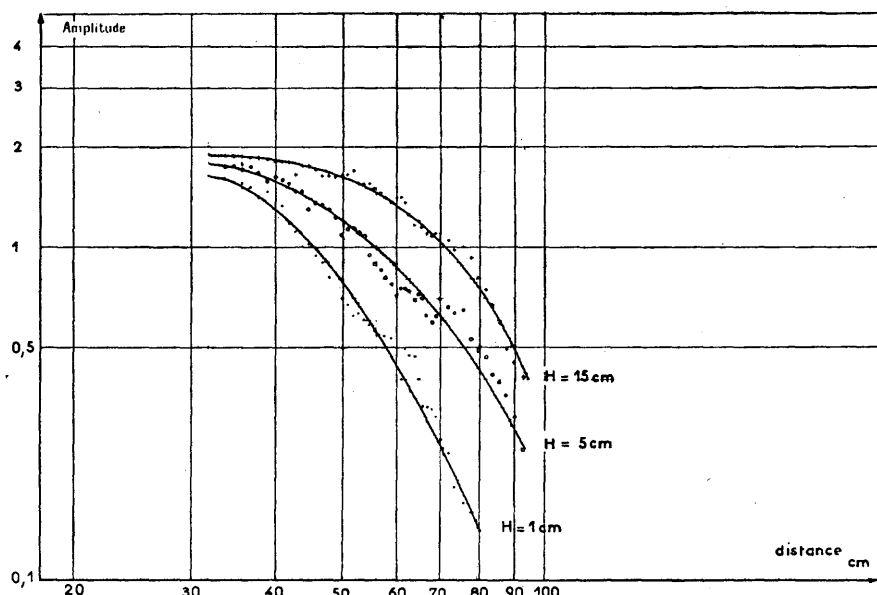


FIG. 17. — Amplitude de l'arrivée longitudinale réfractée, en fonction de la distance pour différentes épaisseurs de la couche qui constitue le marqueur.

directement au contact de la tranche de plaque qui constitue la couche  $H$ . Les vitesses observées sont représentées sur la figure 16. Notons que pour les valeurs de  $H$  inférieures à 15 cm, les arrivées des récepteurs situés au voisinage de l'émetteur ( $d < 10$  cm) n'ont pas été prises en considération, car elles donnent des vitesses systématiquement supérieures à la vitesse donnée par les arrivées suivantes.

tes, sans toutefois dépasser la vitesse limite de plaque (5 350 m/s).

On constate (*fig. 16*) que, pour les faibles valeurs de  $H$ , la vitesse de l'onde longitudinale le long de la tranche  $H$  est voisine de la vitesse limite de barre (5 100 m/s) et que, pour les grandes valeurs de  $H$ , elle est voisine de la vitesse limite de plaque (5 350 m/s).

Pour les épaisseurs intermédiaires, il y a, comme dans le cas de la réfraction, passage continu de la vitesse de plaque lorsque  $H$  croît. Mais pour les valeurs intermédiaires de  $H$ , les courbes des figures 15 et 16 diffèrent sensiblement, ce qui semble indiquer que la propagation d'une onde réfractée dans une couche mince n'obéit pas rigoureusement aux lois de propagation dans les plaques et les barres situées dans le vide.

Remarquons que le domaine où les épaisseurs sont sensiblement inférieures à la longueur d'onde est précisément celui où il serait légitime de s'attendre à une dispersion des vitesses avec la fréquence. L'utilisation d'impulsions voisines de celles de Dirac nous permettrait d'étudier plus commodément le phénomène, grâce à leur richesse en fréquences, mais on assisterait également à une dispersion dans la plaque indéfinie.

#### *Amortissement de l'arrivée réfractée avec la distance.*

L'amplitude de l'arrivée réfractée est représentée en fonction de la distance à l'émetteur en coordonnées bilogarithmiques sur la figure 17 pour trois valeurs de  $H$ . On constate que l'amortissement est sensiblement plus important pour les couches minces que pour les couches épaisses. Notons que, si l'amortissement consistait uniquement en une atténuation de la forme  $d^{-n}$ , nous obtiendrions des droites en coordonnées bilogarithmiques<sup>(1)</sup>. Le fait que les courbes obtenues ne sont pas rectilignes mais ont une concavité dirigée vers le bas indique que cette formule est insuffisante pour représenter le phénomène. Une absorption proportionnelle à  $e^{-kd}$ , où  $k$  est une constante due à l'inélasticité des milieux, combinée à l'atténuation  $d^{-n}$ , pourrait donner une interprétation convenable des courbes d'atténuation.

#### *Conclusion.*

L'étude sur modèles de plaques d'une couche mince en sismique-réfraction conduit aux résultats suivants :

— lorsque la couche est d'épaisseur voisine ou supérieure à la

---

(1) Dans le cas étudié, on devrait avoir  $n \sim 3/2$ . Dans le cas tridimensionnel,  $n = 2$ .

longueur d'onde du signal qui se propage le long de l'interface, la vitesse de l'onde longitudinale réfractée sous l'angle critique est égale à la vitesse de plaque. Dans les problèmes de prospection sur le terrain, elle serait égale à la vitesse du milieu;

— lorsque la couche est d'épaisseur faible devant la longueur d'onde du signal qui se propage le long de l'interface, la vitesse de l'onde longitudinale réfractée sous l'angle limite est voisine de la vitesse limite de barre. Dans les problèmes de prospection sur le terrain, elle serait égale à la vitesse limite de plaque;

— dans le domaine des épaisseurs intermédiaires, l'onde réfractée se propage suivant des vitesses qui ont été déterminées;

— l'amortissement avec la distance est sensiblement plus élevé pour les couches minces que pour les couches épaisses.

#### BIBLIOGRAPHIE

##### Première partie.

- BOIS (P.), CHAUVEAU (J.), GRAU (G.) et LAVERGNE (M.). — 1960. Sismogrammes synthétiques : Possibilités, Techniques de Réalisation et Limitations. *Geophysical Prospecting*, 8, 2, p. 260-314.
- CADY (W. G.). — 1946. Piezoelectricity. *Mc Graw Hill*, New York.
- CARABELLI (E.) et FOLICALDI (R.). — 1957. Seismic model experiments on thin layers. *Geophysical Prospecting*, 5, p. 317.
- CLAY (C. S.) et Mc NEIL (H.). — 1955. An amplitude study on a seismic model. *Geophysics*, 20, p. 766.
- EVANS (J. F.), HADLEY (C. F.), EISLER (J. D.) et SILVERMAN (D.). — 1954. A three dimensional seismic wave model with both electrical and visual observation of waves. *Geophysics*, 19, p. 220.
- HOWES (E. T.), TEJADA-FLORES (L. H.) et RANDOLPH (L.). — 1953. Seismic model Study. *Jour. of the Acoust. Soc. of Amer.*, 25, p. 915.
- KOEFOED (O.), VAN EWIJH (J. G.) et BAKKER (W. T.). — 1958. Seismic model experiments concerning reflected refractions. *Geophysical Prospecting*, 6, p. 382.
- LAVERGNE (M.) et CHAUVEAU (J.). — Fonction de transfert d'émetteurs et de capteurs piézoélectriques pour modèles sismiques, 1961. *Acústica*, 11, n° 2.
- LEVIN (F. K.) et HIBBARD (H. C.). — 1955. Three dimensional seismic model studies. *Geophysics*, 20, p. 19.
- MASON (W. P.). — 1948. Electromechanical Transducers and Wave Filters. *Van Nostrand*, New York.
- 1956. Piezoelectric Crystals and their Applications to Ultrasonics. *Van Nostrand*.
- NORTHWOOD (T. D.) et ANDERSON (D. V.). — 1953. Model Seismology. *Bull. Seis. Soc. of Amer.*, 43, p. 239.
- O'BRIEN (P. N. S.). — 1955. Model Seismology, the critical refraction of elastic waves. *Geophysics*, 20, p. 227.
- OLIVER (J.), PRESS (F.) et EWING (M.). — 1954. Two dimensional model Seismology. *Geophysics*, 19, p. 202.
- OLSON (H. F.). — 1958. Dynamical Analogies, 2<sup>e</sup> éd. *Van Nostrand*, New York.

OLSON (H. F.). — 1957. Acoustical Engineering. *Van Nostrand*, New York.  
ROCARD (Y.). — 1949. Dynamique générale des Vibrations, *Masson*.

*Deuxième partie.*

- ANGONA (F. A.). — 1960. Two-dimensional modeling and its application to seismic problems. *Geophysics*, **25**, 2, p. 468.  
CAGNIARD (L.). — 1935. Diffraction d'une onde progressive par un écran en forme de demi-plan. *Jour. de Phys.*, **6**, p. 310.  
FOX (E. N.). — 1948-1949. The diffraction of sound pulses by an infinitely long strip. *Phil. Trans. of the Roy. of London*, **241**, p. 71; **242**, p. 1.  
FRIEDLANDER (F. G.). — 1946. The diffraction of sound by a perfectly reflecting half plane. *Proc. Roy. Soc. of London*, A, **186**, p. 322.  
HEALY (J. H.), PRESS (F.). — 1959. Further model study of the radiation of elastic waves from a dipole source. *Bull. Seis. Soc. of Amer.*, **49**, 2, p. 193-198.  
KNOPOFF (L.). — 1959. The Scattering of compression waves by spherical obstacles. *Geophysics*, **24**, p. 30.  
KNOPOFF (L.). — 1959. The Scattering of shear waves by spherical obstacles. *Geophysics*, **24**, p. 209.  
LAMBS (G. L.). — 1959. Diffraction of a plane sound wave by a semi-infinite thin elastic plate. *Jour. of the Acoust. Soc. of Amer.*, **31**, p. 929.  
MAGNUS (W.). — 1941. Über die Beugung elektromagnetischer Wellen an einer Halbebene. *Zeitschrift f. Phys.*, **117**, p. 168.  
MILLER (G. F.) et PURSEY (U.). — 1954. The field and radiation impedance of mechanical radiators on the free surface of a semi-infinite isotropic solid. *Proc. Roy. Soc. of London*, **223**, A, p. 521.  
MINTZ (M. D.) et INGARD (U.). — 1959. Experiments on scattering of sound by turbulence. *Jour. of the Acoust. Soc. of Amer.*, **31**, p. 115.  
MONK (G. S.). — 1937. Light. *Mc Graw Hill*, New York.  
NUSSENZVEIG (H. M.). — 1959. Solution of a diffraction problem : I. The wide double Wedge, II. The narrow double Wedge. *Phil. Trans. Roy. Soc. of London*, Série A, **252**, p. 1.  
OFFICER (C. B.). — 1958. Introduction to the theory of Sound Transmission. *Mc Graw Hill*, New York.  
SECKLER (B. D.) et KELLER (J. B.). — 1959. Geometrical theory of diffraction in inhomogeneous media. *Jour. of the Acoust. Soc. of Amer.*, **31**, p. 192.  
SECKLER (B. D.) et KELLER (J. B.). — 1959. Asymptotic theory of diffraction in inhomogeneous media. *Jour. of the Acoust. Soc. of Amer.*, **31**, p. 206.  
SKUDRZYK (E.). — 1959. Sound scattering in a homogeneous medium in the case of a Kolmogorov distribution of patch sizes. *Jour. of the Acoust. Soc. of Amer.*, **31**, p. 845.  
SOMMERFELD (A.). — 1895. Matematische theorie der Diffraktion. *Math. Ann.*, **47**, p. 317.  
WHITE (R. M.). — 1958. Elastic wave scattering at a cylindrical discontinuity in a solid. *Jour. of the Acoust. Soc. of Amer.*, **30**, p. 771.

*Troisième partie.*

- BRUNE (J. N.), NAFE (J. E.) et OLIVER (J. E.). — 1960. A simplified method for the analysis and synthesis of dispersed wave trains. *Geophysical Research*, **65**, 1, p. 287.  
CAGNIARD (L.). — 1939. Réflexion et réfraction des ondes sismiques progressives. *Gauthiers-Villars*, Paris.

- CREMER (L.). — 1942. Theorie der Schalldämmung dünner Wände bei schrägem Einfall, *Akust. Zeitschrift*, 7, p. 81.
- EWING (W. M.), JARDETZKY (W. S.) et PRESS (F.). — 1957. Elastic Waves in layered Media. *Mc Graw Hill*, New York.
- FAY (R. D.) et FORTIER (O. V.). — 1951. Transmission of sound through steel plates immersed in water. *Jour. of the Acoust. Soc. of Amer.*, 23, 3, p. 339.
- GÖTZ (J.). — 1943. Über den Schalldurchgang durch Metall platten in Flüssigkeiten bei schrägem Einfall einer ebenen Welle. *Akust. Zeitschrift*, 8, p. 145.
- OSBORNE (M. F.) et HART (S. D.). — 1945. Transmission, reflection and guiding of an exponential pulse by a steel plate in water. *Jour. of the Acoust. Soc. of Amer.*, 17, p. 1.
- PRESS (F.), OLIVER (J.) et EWING (M.). — 1954. Seismic Model study of refractions from a layer of finite thickness. *Geophysics*, 19, p. 388.
- REDWOOD (M.). — 1959. Velocity and attenuation of a narrow band high frequency compressional pulse in a solid wave guide. *Jour. of the Acoust. Soc. of Amer.*, 31, p. 442.
- REISSNER (H.). — 1937. Der senkrechte und schräge Durchtritt einer in einem flüssigen Medium erzeugten ebenen Dilatations-Longitudinal-Welle durch eine in diesem Medium befindliche plan parallele feste Platte. *Helv. Phys. Acta*, 11, p. 140.
- SCHOCHE (A.). — 1950. Der Durchgang Ultraschall durch Platten. *Nuovo cimento*, ser. 9, 7 (suppl.), p. 302.
- SEZAWA (K.) et NISHIMURA (G.). — 1928. Rayleigh-type waves propagated along an inner stratum of a body. *Bull. Earthquake Research Inst. (Tokio)*, 5, p. 85.
- TOLSTOY (I.) et USDIN (E.). — 1953. Dispersive properties of stratified elastic and liquid media : a ray theory. *Geophysics*, 18, p. 844.
- WORTHING (A. G.) et GEFFNER (J.). — 1950. Treatment of Experimental Data. 6<sup>e</sup> éd., *Wiley*, New York.



---

**TOULOUSE. — IMPRIMERIE ÉDOUARD PRIVAT.— 6963-6-61**  
**PRINTED IN FRANCE.**

---

